Ka-band Radio characterisation for SatCom services in arctic and high latitude regions

Final report

ESA Contract ESA Contract No. 4000106010/12/NL/CLP

Prepared by
Terje Tjelta
Lars Erling Bråten
Jan Erik Håkegård
Per Arne Grotthing
Martin Rytir
Michael Cheffena
Knut Grythe

ESA Technical Officer
Dr. Antonio Martellucci

Table of Contents

1 Revision history ... 3
2 Introduction ... 3
3 Objective ... 3
4 History of the campaign ... 4
5 Propagation experiment ... 4
5.1 Measurement set-up ... 4
5.1.1 Overview ... 4
5.1.2 Measurement requirements and parameters ... 5
5.1.3 Measurement equipment ... 6
5.1.4 Detailed description of equipment ... 7
5.1.5 Environmental protection and shielding equipment ... 9
5.1.6 Beacon receivers ... 11
5.1.7 Meteorological equipment ... 15
5.1.8 Power supply ... 16
5.1.9 Data collection ... 16
5.1.10 Link budgets ... 17
5.1.11 Example measured time series data ... 19
5.1.12 Experience ... 23
5.2 Propagation data analyses ... 23
5.2.1 First order statistics of attenuation and rain ... 24
5.2.2 Second order statistics of rain attenuation ... 40
5.2.3 Scintillation ... 49
6 Telecom experiment ... 58
6.1 Experiment set-up ... 58
6.2 Experiment data analyses ... 60
6.2.1 Measurements ... 60
6.2.2 Pre-processing of the data ... 61
6.2.3 Frequency flat fading ... 63
6.2.4 Frequency selective fading ... 65
6.2.5 Modem effects ... 66
6.3 Summary ... 66
6.4 Further work ... 66
7 Conclusion and recommendation ... 66
8 Future work ... 67
Acknowledgements ... 67
References ... 67
Appendix A: Abbreviations ... 68

1 Revision history

Revision	Date	Section	Changes/Comments
0.1	3 July 2016	All	Draft submitted to ESA for initial evaluation for the final milestone
0.2	8 October 2016	All	Revised taking ESA comment into account
0.3	31 October 2016	All	Revised taking ESA comments into account
0.4	27 June 2017	All	Added new stations with one year results, and a third year results to the other stations
2.0	30 July 2017	All	Final version submitted to ESA

2 Introduction

The High-North European area is of increasing importance due to natural resources such as fishing industry and oil/gas exploration. The arctic is of crucial importance as the potential climate effects opens up frozen sea parts for longer periods of the year. Reliable communication systems to cover these regions can only realistically be delivered by satellites. Svalbard has already proven to be a highly suitable location for downloading data from polar orbiting Earth observations satellites.

A SatCom Ka-band system is particularly attractive for broadband communication. Both Telenor Satellite (TS) and Norwegian Defence Logistic (NDLO) organisation are investing in satellite capabilities serving civilian commercial users and defence and governmental users, respectively. In 2015 TS launched Thor 7, a satellite with a Ka-Band transponder.

At high latitudes the propagation conditions change significantly from low latitude locations, particularly for geostationary satellite systems that all get very low elevation angle paths. The rain attenuation effects are of particular interest as the current version of the ITU-R rainfall intensity maps indicates significantly higher rainfall rates over some coastal high latitude areas compared observed overland long-term Norwegian maps. Low elevation radio links are affected by atmospheric propagation mechanisms that are much more severe than the ones experienced at lower frequencies at lower latitudes and higher elevation angles. In particular, due to the longer path in the atmosphere, not only rain attenuation but also other propagation effects, such as gaseous attenuation, cloud attenuation, scintillation, and ducting effects must be considered.

Maritime radio links at low elevation angles are challenging to dimension correctly. Lower prediction accuracy is due to the lack of ground meteorological measurements, in particular for rain.

The experimental campaign was set up to define the radio channel characteristics relevant for the design and the performance assessment of a radio link [1]. The campaign includes five stations, where three are in the High North maritime environment.

The stations were equipped with metrological instruments and other inputs such as location information. Two years of data have been collected and six months data for the telecom measurements.

The participants in the study include operators, industry, research institutes and academia.

3 Objective

The project's first objective is to aid GEO satellite system dimensioning by performing long-term study of Ka-band propagation effects within the designated coverage areas at High North locations. The outcome of the study will be used to refine and enhance relevant ITU-R radio wave propagation models and prediction methods for geostationary orbiting satellites serving high latitude low elevation angle locations on land, coastal areas, and at sea. Results will also become important for other orbits.

A second objective is to perform telecom measurements involving traffic data for a Ka Band satellite. It involves analyses to what degree telecom data relates to propagation information.

A third objective is to gain experience with Ka-band band system operated at High North locations, normally in more challenging conditions that lower latitude locations.

4 History of the campaign

The project proposal was submitted in response to the invitation to Tender AO/1-7049/12/NL/CLP KA-BAND RADIO CHARACTERISATION FOR SATCOM SERVICES IN ARCTIC AND HIGH LATITUDE REGIONS published on EMITS 12 January 2012.

Date	Comment
2012.09	Project kick-off meeting
2013.08	Propagation measurement start first station Nittedal
2013.10	Propagation measurement start last station Røst
2015.07	Telecom measurement start
2015.10	Two-year propagation data completed
2015.12	Telecom measurement end
2016.04	Measurement at Bjørnøya started
2016.09	Three-years of data collected at most stations
2017.02	Three-years of scintillation data collected at Røst
2017.04	One-year of data collected at Bjørnøya

Table 4-1. History of the campaign.

5 Propagation experiment

5.1 Measurement set-up

5.1.1 Overview

Five measurement sites have been chosen. Three of the most northern are in maritime climates, Røst, on a small island surrounded by water, then Vadsø and Isfjord Radio, see Figure 5-1. There are two stations in Southern Norway, Nittedal and Eggemoen. The station at Bjørnøya (Bear Island), between Vadsø and Isfjord Radio, was added after about two years of data had been collected. The key station data are listed in Table 5-1.

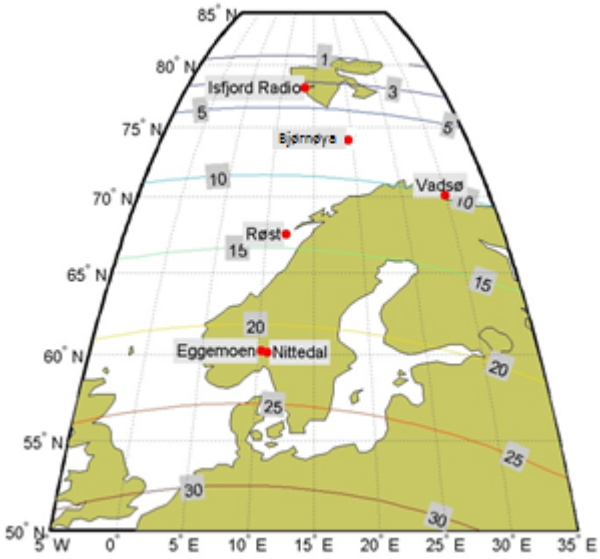

Figure 5-1. ***Map with elevation angle contours for Ka-Sat and measurement sites indicating the most Northern stations are located in maritime climates.***

At each site measurements are carried out and automatically saved to a local disk. A dedicated program runs continuously to collect data and emits alarms according to defined criteria. Pre-processing of the data is carried out automatically enabling visual inspections.

5.1.1.1 Description of measurement locations

The measurement at Røst is located at Store Glea, which is part of Røst municipality in the Lofoten region of Norway. It is approximately 115 km north of the Arctic Circle. The annual average rain intensity of 15.6 mm/h at 0.01 % of the time, as indicated by the new Norwegian rainfall rate maps [2], for a location in Lofoten close to Røst. The maps do not cover the area dominated by the sea including Røst, only land, but values as suggested by the nearest land are used.

Location	Latitude (°N)	Longitude (°E)	Altitude (m)	Elevation angle (°)*
Nittedal	60.1	10.8	200	21.8
Eggemoen	60.2	10.3	200	21.7
Røst	67.5	12.1	10	14.1
Vadsø	70.1	29.7	30	10.1
Bjørnøya	74.5	19.0	10	6.6
Isfjord Radio	78.1	13.6	5	3.2

*: Elevation angles are the geometrical ones

Table 5-1. Measurement locations key location data end elevation angel towards Ka-Sat.

The Vadsø measurement site is located on the Varanger peninsula close to sea level. The Earth-space path crosses a fjord, enabling costal climate measurements with a variety of precipitation forms and possible atmospheric anomalies. The maximum monthly temperature may well be above zero C also during the winter months, while minimum temperatures typically are below 0 °C for all months except June and July. An annual average rain intensity of 12.7 mm/h is predicted for 0.01% of time [3].

Bjørnøya is an approximately 17x19 km^2 large triangular island located half-way between Svalbard and the Norwegian mainland. The path crosses the island approximately along the longest north-south axis. The climate on the island is rather warm with small temperature changes. Normal average temperature is -8.8 ºC for January and 4.4 ºC for August.

Isfjord Radio is located at Svalbard, close to the Sea level. The location is representative for typical maritime users far north, representing the practical limit for stations communicating via geostationary satellites. Svalbard is a major download site for polar orbiting Earth observation satellites. An annual average rain intensity of 14 mm/h is predicted for 0.01 % of time [3].

The two sites at 60^0N latitudes, Nittedal and Eggemoen, are forming a diversity pair separated by 29 km in an almost East to West direction.

5.1.2 Measurement requirements and parameters

The parameters measured at each location are as follows:

- Rainfall rate [mm/h]
- Hail [Hits/cm^2]
- Air temperature [°C]
- Air relative humidity [%]
- Atmospheric total pressure [hPa]
- Wind speed [m/s]
- Wind direction [°]
- Signal plus noise power within the noise bandwidth [W]
- Noise floor (W/Hz)

The parameters in Table 5-2 were used as design criteria for the technical design and selection of equipment.

Parameter	Sampling rate	Accuracy/resolution
Rainfall rate [mm/h]	1 minute	Range: (0 ... 200 mm/h), Accuracy: 1 % (at 25 mm/h)
Hail [Hits/cm^2]	1 minute	Accuracy: 0.1 hits/cm^2
Air temperature [C]	1 minute	Range: -52 ... +60, Accuracy for sensor at +20 °C ±0.3 C
Air relative humidity [%]	1 minute	Range: 0 ... 100 %, Accuracy: ±3 %RH within 0 ... 90 %RH, ±5 %RH within 90 ... 100%RH
Atmospheric total pressure [hPa]	1 minute	Range: 600 ... 1100 hPa, Accuracy: ±0.5 hPa at 0 ... +30 C, ±1 hPa at -52 ... +60 C
Wind speed [m/s]	1 minute	Range: 0 ... 60 m/s, Accuracy: 0 ... 35 m/s ±0.3 m/s or ±3%, whichever is greater 35 m/s ... 60 m/s ±5%
Wind direction [Deg.]	1 minute	Range: 0 ... 360°, Accuracy: ±3°
Signal plus noise level [W]	10 Hz	Accuracy 0.48 dB RMS error
Noise floor [W/Hz]	10 Hz	Time and frequency averaged

Table 5-2. Parameters measured.

The accuracy of the beacon measurements is described in Section 5.1.6.

5.1.3 Measurement equipment

Details on the measurement equipment are provided in project Deliverable DD2 *Ka-band Arctic Experiment design document*. The operational experience obtained during the campaign is given in this section. An external publication describing the campaign is given in [4].

Figure 5-2 shows the propagation terminals with a block diagram for the signal strength receiver, an indication of how meteorological data are included, and the connection to the data collection network. All hardware items have been procured from vendors: the key radio frequency components are low noise block converter (LNB) and 10 MHz reference signal oscillator from Orbital, and Prodelin antennas. There is heating on the antennas (lower half part of the reflector and the horn) except at Vadsø and Eggemoen. The interior of the waveguides is kept dry using dehydrators, and plastic shields cover the horns to reduce rain and snow accumulation on the feed windows.

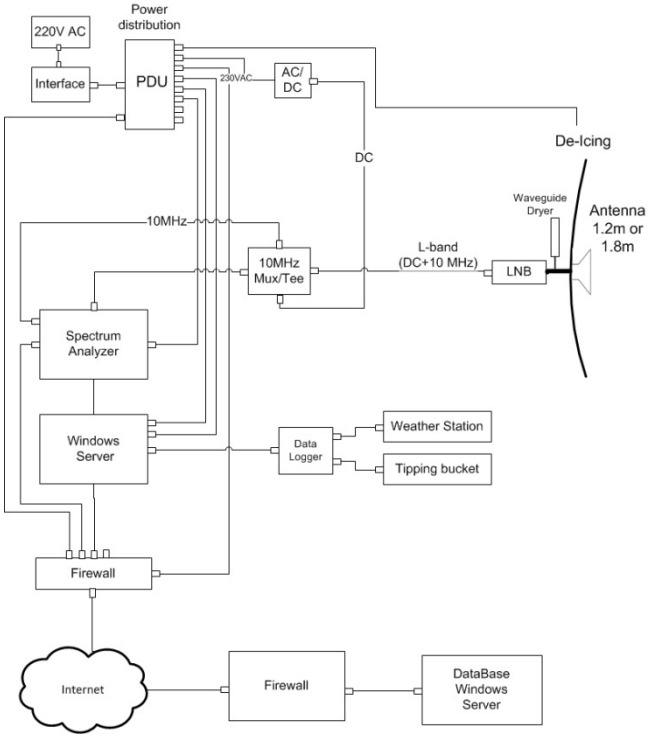

Figure 5-2. Propagation measurement terminal.

The software analysing the spectrum analyser has been developed by FFI [5]. The data collecting solution and surveillance are also delivered by vendor, although adapted to the project purpose. It is part of the surveillance Telenor Satellite (TS) uses for commercial services and hence the project as a 24/7 facility, Dataminer, to ensure high data collecting period.

At each site measurements are carried out and automatically saved to a local disk. This includes data from the beacon receiver as well as meteorological data combined in the data logger from the compact and the tipping bucket rain gauges, see Table 5-3. The meteorological sensors are heated, such that also winter precipitation will be recorded in the form of liquid water.

Parameter	Range	Sampling period	Equipment
Signal strength	-110 to -50 dBm or -120 to -60 dBm	~0.1 s	Spectrum analyzer Agilent EXA
Rainfall rate: Acoustic/electrical Tipping bucket	 0 - 200 mm/h 0 - 600 mm/h	 10 s Time (ms) between tips	 Vaisala WXT 520 Lambrecht 1518H3
Hail	Count	10 s	Vaisala WXT 520
Air pressure	600 - 1100 hPa	10 s	Vaisala WXT 520
Air temperature	-52 - 60 °C	10 s	Vaisala WXT 520
Air relative humidity	0 - 100 %	10 s	Vaisala WXT 520
Wind speed	0 - 60 m/s	10 s	Vaisala WXT 520
Wind direction	0 - 360 °	10 s	Vaisala WXT 520

Table 5-3. Measurement parameters.

5.1.4 Detailed description of equipment

Figure 5-3 shows an overview of how each receive-only site for the propagation measurements is equipped. The main components are as follows:

- A stationary receive-only K-band antenna receiving the beacon signal.
- A temperature stable low noise RF-frontend amplifying the received K-band signal and converting it to L-band.
- A beacon receiver receiving and detecting the signal.
- Weather stations measure rain intensity and accumulation.
- A PC with logging software for the received signal data. Network time protocol is utilised for timing reference.

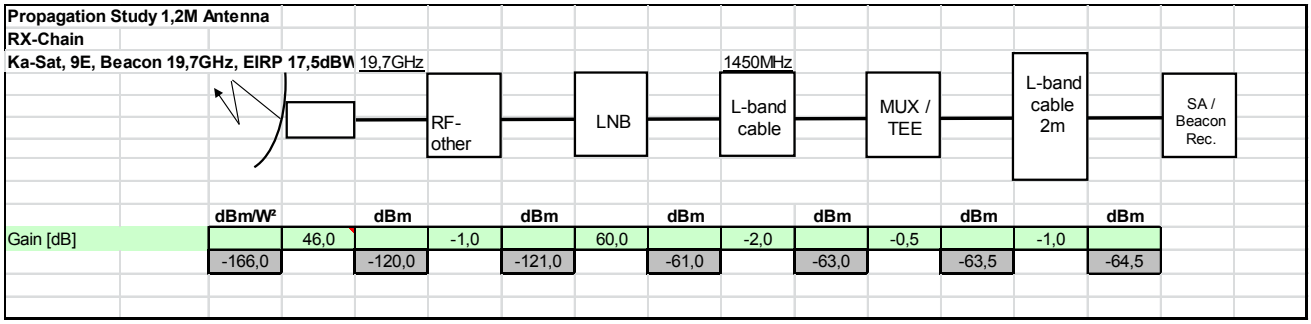

Figure 5-3. Main principles of the setup for the propagation measurements, frequencies and levels.

5.1.4.1 Antennas

The size and thereby the gain of the K-band antenna and the receiver RF noise factor is to a large extent determining the requirements on the L-band beacon receiver SNR. A reasonable compromise that fulfils link budget calculations and also taking into account the antenna cost is an antenna diameter of about 1.2 m. For

the measurements the Prodelin 3120 and 3180 Ka-band antennas are used. Figure 5-4 shows one of the selected antennas. The performance numbers of the antennas are given in Table 5-4.

.

Figure 5-4. Ka-band antenna Prodelin 1.2 m.

Diameter (m)	Gain (dBi)		Opening (HPBW at -3 dB)		X-polarisation (dB)
	Rx	Tx	Rx	Tx	
1.2	45.8	49	0.84˚	0.54˚	26
1.8	49.2	52.4	0.58°	0.4°	26

Table 5-4. Performance numbers for the Prodelin Ka band antennas.

5.1.4.2 Optical intermediate frequency and cables

For the locations Vadsø and Eggemoen, the distance between the antenna and the receiver indoor location necessitates optical transfer of the signal from LNB to the beacon receiver, and transmission from a modem to the BUC. Converter equipment from the company Pulse Power and Measurement have been installed by FFI on these two locations.

5.1.4.3 Low noise block down converter (LNB)

The requirements for the LNB are as follows:

- It shall cover the Ka-Sat beacon frequency at 19.7 GHz.
- The gain should be at least 50 dB.
- The noise figure should be better than 1.3 dB.
- The gain variation shall be max ±0.5 dB over a temperature range of -35 to +55°C.
- The gain variation shall not be larger than 0.2 dB peak to peak within any 10°C range.
- A certificate of the gain as a function of temperature within the required temperature range is required to be issued by the LNB manufacturer.

A LNB version from Orbital Research that fulfils the requirement is available and represents an example component. It is designed to have a temperature stable gain suitable for Nordic climates such as in Norway and Canada. The LNB requires an external stable 10 MHz reference and has a noise figure of maximum 1.2 dB at 23°C. A photo of the LNB is shown in Figure 5-5.

Figure 5-5. *Orbital Research LNB 694XA Series.*

Typical gain is 60 dB, with the selected temperature stabilisation the resulting gain stability is ±0.5 dB max over temperature range of -35 to +55°C.

5.1.4.4 Reference oscillator

The LNBs require a stable 10 MHz reference to obtain minimum phase noise. Also, the beacon receiver requires a 10 MHz reference, preferably a common oscillator. The requirements for the reference oscillator are as follows:

- Phase noise spectrum should be better than -160 dBc/Hz at 1 kHz and -120 dBc/Hz at 10 Hz off the centre frequency.
- Temperature drift should be less than 0.05 ppm between -30 and 50°C.
- Drift with time is within ±1 x 10^{-9} per day after 30 days.
- It shall be able to operate down to at least -30 degrees Celsius.
- Output power should be between -10 and 0 dBm.

At some of the installations the reference oscillators were positioned outdoors. It was therefore decided to select a double oven stabilised crystal oscillators (OCXOs) with two outputs able to operate down to at least -30 degrees Celsius. An example component from Orbital Research is shown in Figure 5-6.

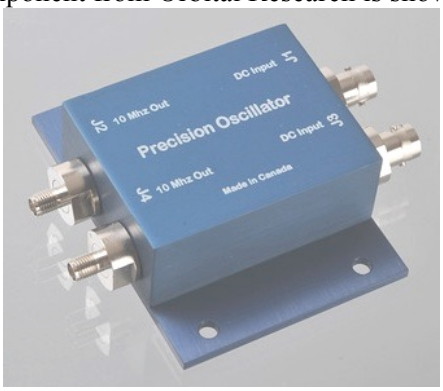

Figure 5-6. Orbital Research double oven crystal oscillator.

Phase noise spectrum specified is -160 dBc/Hz at 1 kHz and -120 dBc/Hz at 10 Hz off the centre frequency. Temperature drift is less than 0.05 ppm between -30 and 50°C (double oven version). Drift with time is within ±1 x 10-9 per day after 30 days. Input DC voltage between 15 and 20 V supplied via DC input connector.

5.1.4.5 Computers

One computer at each measurement site is required. They have the following specifications:

- One rack unit or tower cabinet (depending on physical environment).
- Redundant and hot-swap fans, disks and power supplies.
- Intel Xeon quad core E5-2603 processor.
- 16GB RAM DDR3.
- Integrated hardware of redundant array of independent disks (RAID) controller.
- 4 x Disks (300GB 2.5"15K rpm 6Gbps SAS) in RAID 1 (mirrored).
    - This disk setup provides 600GB safe high-performance storage space.

For the central storage server, the specifications are the same, except from double number of disks, i.e., 8 disks and 1200 GB safe high performance storage space.

5.1.5 Environmental protection and shielding equipment

5.1.5.1 Feed window shield

Snow accumulating on the antenna reflector or feed horn can significantly degrade the antenna performance. Similarly, raindrops or wet snow on the feed window will lead to unwanted signal attenuation. Shielding of

antenna from snow and rain may therefore improve the measurement precision. Antenna pointing stability during windy conditions is also expected to be improved with a shelter.

As a first measure, each site will have a plastic shield mounted over the horn to reduce snow and rain on the feed window, see Figure 5-7.

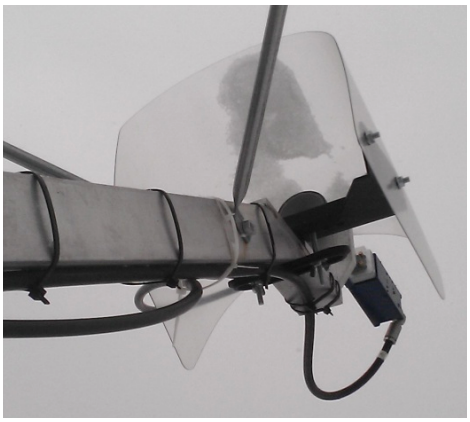

Figure 5-7. Protection of the feed window.

Ice on the window with high humidity and below zero degrees Celsius air temperature is a concern. Such cases are probably best avoided by using a hot air blower.

5.1.5.2 Waveguide dehydration

It is important to avoid condensation inside the waveguide and keep it absolutely dry in all weather conditions. There are two different types of this device considered in the project, air pressure and drying salt. One solution is to pressurise the waveguide and employ a unit removing water vapour from the air. Such air dehydrators are available at Eggemoen and Vadsø and have been used in the project.

The other solution is to utilize static desiccators with periodic replacement of drying salt. For both solutions a waveguide unit with an air nipple, inserted between the OMT and LNB, is required. The additional loss is relatively small, and taken into account in the link budgets. The desiccator solution is less costly and selected for the sites Nittedal, Røst and Isfjord Radio. The most relevant device is SD-003 Static Desiccator from Andrew.

5.1.5.3 Feed horn heater

Feed horn heater will do the drying process even more reliable. This device is often a part of the antenna dish de-icing system and all sites except Eggemoen and Vadsø were equipped with de-icing. During the experiment it was noted that the heating produced gain variations in order of up to 0.6 dB.

The RF frontend for the beacon experiment is shown in Figure 4-10. In this implementation an automatic air dehydrator and a pressure waveguide unit is utilised to avoid condensation inside the waveguide. A plastic LNB-shield is mounted over the horn to reduce rain and snow on the feed window.

Figure 5-8. LNB mount with pressurisation waveguide unit and horn shielding.

5.1.6 Beacon receivers

The beacon receiver is required to have:

- Sampling rate of 10 Hz.
- Acquisition threshold C/N_0 of 10 dBHz or better.
- Measure carrier power C and noise spectral density N_0.

There are a number of commercially available beacon receivers on the market. The possibility for using these is to a large extent dependent on the required dynamic range of the equipment, their ability to lock onto a weak attenuated signal and sampling rate. Noise floor estimation is also of interest in the current measurement campaign. In a similar campaign, three different approaches for implementing a beacon receiver were considered:

1. A low-cost software defined beacon receiver.
2. Identifying and testing commercially available receivers
3. To explore the use of medium to low end spectrum analysers based designs.

The investigation of commercially available receivers showed that they typically have a phase-locked loop (PLL) bandwidth of 2 kHz, while the detection bandwidth used in the current project is about 30 Hz, resulting in a difference in dynamic range exceeding 18 dB in favour of the design based on spectral approaches.

A software designed beacon receiver based on the Ettus DBSRX2 card was developed, covering a frequency range of 800 MHz to 2.4 GHz with a 3-5 dB noise figure. During tests with a stable carrier wave (CW) and additive white Gaussian noise (AWGN) it was found that the amplifier chain signal gain varied with temperature, making power measurements difficult to calibrate. It was therefore decided to investigate the use of spectrum analysers as beacon receiver.

The spectrum analyser based beacon receiver was developed to enable measurements of signal attenuation, signal scintillation and relative sky noise temperature, all at the same frequency utilizing a common antenna. The main issues for the design are a low noise bandwidth as well as oscillators with low phase noise.

Spectrum analysers able to perform FFT filtering at IF are, together with a PC, able to provide much of the same functionality as a software defined beacon receiver based on the spectral approach. Lab trials showed that relatively low-end analysers were able to zoom on to the signal with 20-30 Hz resolution bandwidth and with a sweep time of less than 100 ms, depending on the instrument used. The developed software routine controls the instrument, periodically locating the maximum signal power for frequency adjustment. Markers are utilised to read out measured noise and carrier power. The implementation at Kjeller provides about 7 samples per second; an alternative instrument provides 11 samples per second. This set-up has a significantly better sensitivity than commercial receivers and is expected to track the signals down to about C/N_0 of

10 dBHz. This is considered a major improvement was found interesting, enabling reasonably sized receive antennas (~1 m) obtaining sufficient attenuation margin to cope with most expected degradation events.

We have utilised Agilent EXA spectrum analysers or equivalent, fulfilling the goal of 10 samples per second with a relatively good price/performance ratio. The EXA analysers are operational at a related beacon measurement campaign and works well as beacon receivers.

The main issues for the design are low noise bandwidth and low phase noise oscillators.

The developed software routine controls the instrument, periodically locating the maximum signal power for frequency adjustment. A flow chart of the algorithm is shown in Figure 3.9.

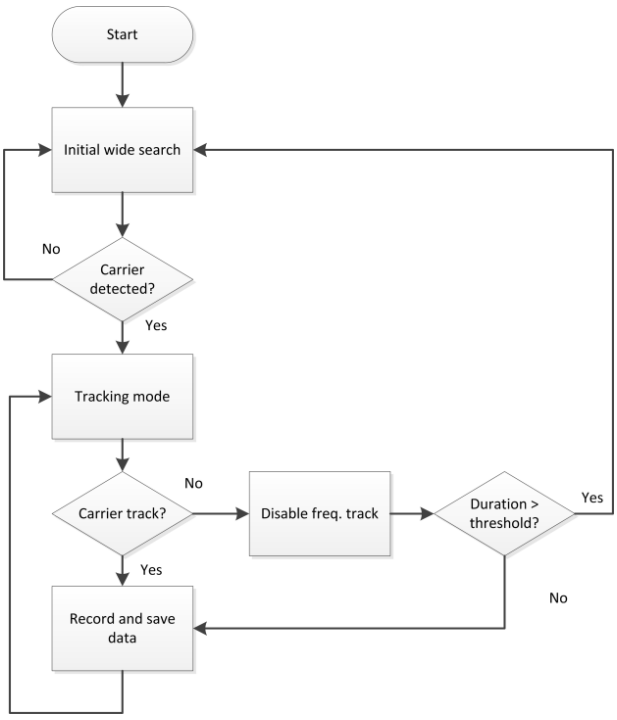

Figure 5-9. Flow chart receiver software.

During the initial wide search, the GPIB interface is selected, and a number of parameters initialised. This includes initial search centre frequency, frequency span, resolution bandwidth, and power threshold level. Two traces are set up; the first is a clear/write trace without time averaging and the second a trace averaging the last 40 traces. Both traces currently employ sample detectors. A marker located on the averaged trace is positioned utilising a peak search function.

The carrier observed on the analyser drifts slowly in frequency over time. The centre frequency is adjusted periodically according to the maximum power within the frequency span. If the carrier drifts towards one of the neighbouring bins in the FFT in between frequency adjustments, a dip in received power is registered. In the current implementation the power a few Hertz on each side of the assumed carrier frequency is measured to avoid this. The marker with the registered largest power is then selected as the carrier power estimate.

If the marker power value exceeds the initial signal plus noise threshold, the initial search is declared successful, the centre frequency is adjusted to the peak frequency, and the tracking mode is entered.

In the tracking mode the span is reduced to 1 kHz with a 30 Hz resolution bandwidth, depending on the analyser used. Three additional markers are positioned along the sample detector trace. The main marker is located at the centre frequency (peak) and is used to read out estimated carrier plus noise power. Two additional markers are located 300 Hz on each side and is used to estimate the noise floor. While the signal plus noise marker exceeds the tracking threshold, the markers are continuously read out and their values and frequencies saved to an hourly time stamped ASCII file.

The tracking threshold is set tentatively to 10 dB below the initial search threshold and a few dB above the actual noise floor observed on the spectrum analyser. Every five seconds, the peak search routine is applied to the averaged trace and the centre frequency adjusted. This is to cater for frequency drift in the oscillators as well as Doppler frequency drift. Complete traces are saved every 30 minutes to enable later inspection of the spectrum surrounding the carrier.

If the estimated carrier plus noise power density decrease below the tracking threshold, the measurement continues for 20 minutes before the initial acquisition routine is entered. During this time, no frequency adjustment is employed. During laboratory test with noise and signal sources the signal plus noise standard deviation for a similar instrument was below 0.1 dB at 40 dBHz, 0.3 dB at 30 dBHz and 0.8 dB at 20 dBHz.

An example of a significant attenuation event is given in Figure 3-10, where the attenuation reached about 50 dB. At the same period of time, high intensity rain was registered.

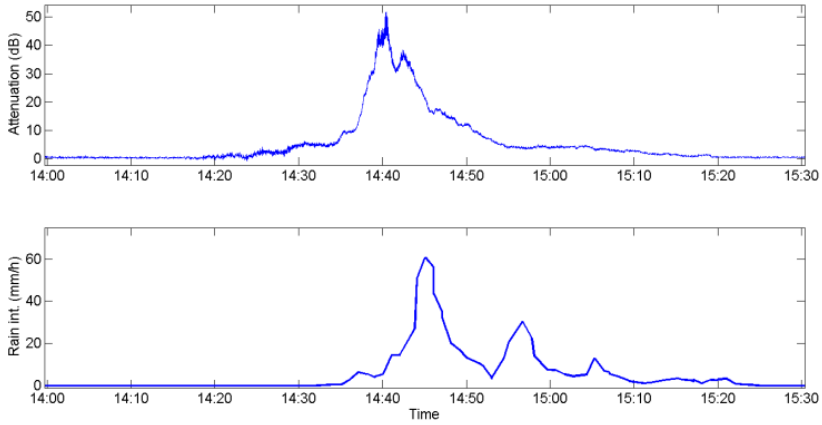

Figure 5-10. Attenuation event and rain rate 5 August 2012, Eggemoen.

The main characteristics of the beacon receivers utilised are summarised in Table 5-5.

Equipment	Agilent EXA
Resulting sampling rate (samples/s)	10
Noise bandwidth (Hz)	30
C/N threshold (dB)	5
Measurement accuracy	0.1 dB at 40 dBHz 0.3 dB at 30 dBHz 0.8 dB at 20 dBHz

Table 5-5. Main characteristics of the beacon receiver.

5.1.6.1 Software processing

The Matlab script controlling the spectrum analyser generates two binary Matlab ".mat" files:

- Signal file containing various signal measurements at a sampling rate exceeding 10 per s
- Spectrum file each 30 minute

The measured signal and noise floor binary file from the spectrum analyser contains columns:

1. Marker 1 (M1) value on trace 1 (carrier plus noise)
2. Marker 2 (M2) value relative to M1 (delta) on trace 1 (noise)
3. Marker 3 (M3) value relative to M1 (delta) on trace 1 (noise)
4. Marker 1 frequency (F1)

5. Marker 2 frequency (F2)
6. Marker 3 frequency (F3)
7. UTC time hour in (decimal format)
8. UTC time minute in (decimal format)
9. UTC time second in (decimal format)
10. Marker 4 on trace 2 (carrier pus noise)
11. Number of trace 1 used to produce averaged trace 2
12. Marker 7 on trace 2 relative to marker 4 (noise)
13. Marker 8 on trace 2 relative to marker 4 (noise)

One example row is:

-63.704 -40.851 -52.816 1429999076.667 1429998776.667 1429999376.667 23 38 5.709 -63.905 -44.644 -45,361
The spectrum file contains frequencies, and traces 1 and 2. Trace 1 is a clear write trace without averaging, and Trace 2 is an averaged trace. The Spectrum file columns are:

1. Trace 1
2. Trace 2
3. Frequency

This file may be used to investigate the conditions around the carrier with respect to for example interference and phase noise to identify possible anomalies during the post processing.

Beacon and noise data is retrieved from binary files generated by the beacon receiver. The recorded data is processed to extract the variables required in the post-processing. The fields represented in the daily file structure include:

- Carrier (Estimated carrier power in dBm)
- N_0 dB (Estimated noise floor in dBm/Hz)
- Nint dB (Noise interference indicator dBm/Hz)
- Timestamp (Matlab datenum format)
- Invalid (index to values marked as invalid)
- Frequency (carrier frequency in Hz, Marker 1)

5.1.6.1.1 Noise processing

As mentioned above our noise markers are recorded during the data collection. **Markers 2 and 3** are instant values as given by the continuously updated (clear/write) trace of the spectrum analyser at a rate of approximately 10 samples per second. These are located 600 Hz below and above the current frequency of the beacon. **Markers 7 and 8** are located 250 Hz below and above the current frequency record the value as given by the "average" trace of the spectrum analyser. This average trace uses a moving average of 30 values. With 10 samples per second this gives an averaging window of approximately 3 seconds. This averaged trace gets reset every time the centre frequency of the spectrum analyser is changed.

During pre-processing (combining the data files into a single file per day) the procedure for noise estimation is as follows:

1. Instant Markers 2 and 3 are averaged using a 30-sample moving average window to get values comparable with the other set of markers.
2. All 4 markers are filtered using a median filter with a length of 99 samples. This removes spikes due to "averaging reset" of Markers 7 and 8.
3. **Nint** value is calculated as the maximum of these 4 values to indicate possible interference/tracking issues with the receiver.
4. **N_0** noise floor value is calculated as a moving average of 300 samples (10 seconds) of the median calculated from the 4 values.

Note that both these values are given in dBm/Hz, as their value is normalized to the equivalent noise

bandwidth of the 30 Hz Gaussian RBW filter which is exactly 15 dB.

5.1.6.2 Measurement accuracy

The EXA spectrum analyser feature auto align maintains the instrument in warranted operation across varying temperature and over time. The total absolute amplitude accuracy is specified as ±0.5 dB at the 95th percentile for the relevant frequency range. The frequency response accuracy is ±0.55 dB at the 95th percentile without internal preamplifier engaged. Both numbers are given for 10 MHz bandwidth. The specified LNB gain temperature stability is maximum ±0.5 dB over a relatively wide temperature range. For the random errors we assume a uniform distribution. The measurement error standard deviation, or the root mean square (RMS) error, is thus about 0.48 dB. The LNB error values for the gain stability at one frequency is not specified, nor the analyser performance for a bandwidth of 1 kHz. Thus, the actual measurement RMS error is expected to be below the specified value of 0.48 dB. During testing of the measurement setup, it is possible to extract the errors from measurements with a signal generator and a noise source. The connection between the measurement error budget and the requirements in Deliverable DD1 is that 0.48 dB applies to total attenuation measurements. The implementation of the post processing routines may impact the resulting relative accuracy. Signal levels may for example be normalized before and after attenuation events. The total attenuation is understood as the absolute (actual) value of the attenuation.

5.1.7 Meteorological equipment

Precipitation is the most important parameter to measure, followed by air pressure, temperature, and humidity. The wind strength and direction also provide useful information for discussing propagation effects. It is difficult to find one instrument accurately estimating precipitation intensity, accumulation and type. Thus, it may be necessary to measure precipitation intensity with an additional sensor, such as tipping bucket.

5.1.7.1 Weather station

The Vaisala WXT 520 metrological measurement station meets most of the requirements and is possible to employ in the experiment, see Figure 5-11.

Figure 5-11. Vaisala WXT 520 metrological measurement station.

The WXT instrument enables measurements of barometric pressure, humidity, precipitation, temperature, and wind speed and direction. In addition, accumulated rainfall, rain intensity and duration of the rain are measured.

5.1.7.2 Tipping bucket

Figure 5-12. Lambrecht 1518 H3 rain gauge.

Each station is equipped with a tipping bucket instrument with heating and of 0.1 mm bucket size, see picture in Figure 5-12.

5.1.8 Power supply

Each site had a backup power supply or an uninterruptible power supply (UPS). Power supply at Nittedal and Eggemoen is considered stable enough and no additional UPS are required. At Vadsø, the indoor equipment is connected to a UPS while the outdoor installations are not.

5.1.9 Data collection

Most of the equipment is interconnected via Internet as shown in Figure 5-13 except for the sites at Eggemoen and Vadsø which are connected to a separate and closed network. This network is connected to FFI, Kjeller, where control, monitoring and data collection are performed for those two stations. The data collected at Kjeller will be transferred to the main storage server at Nittedal.

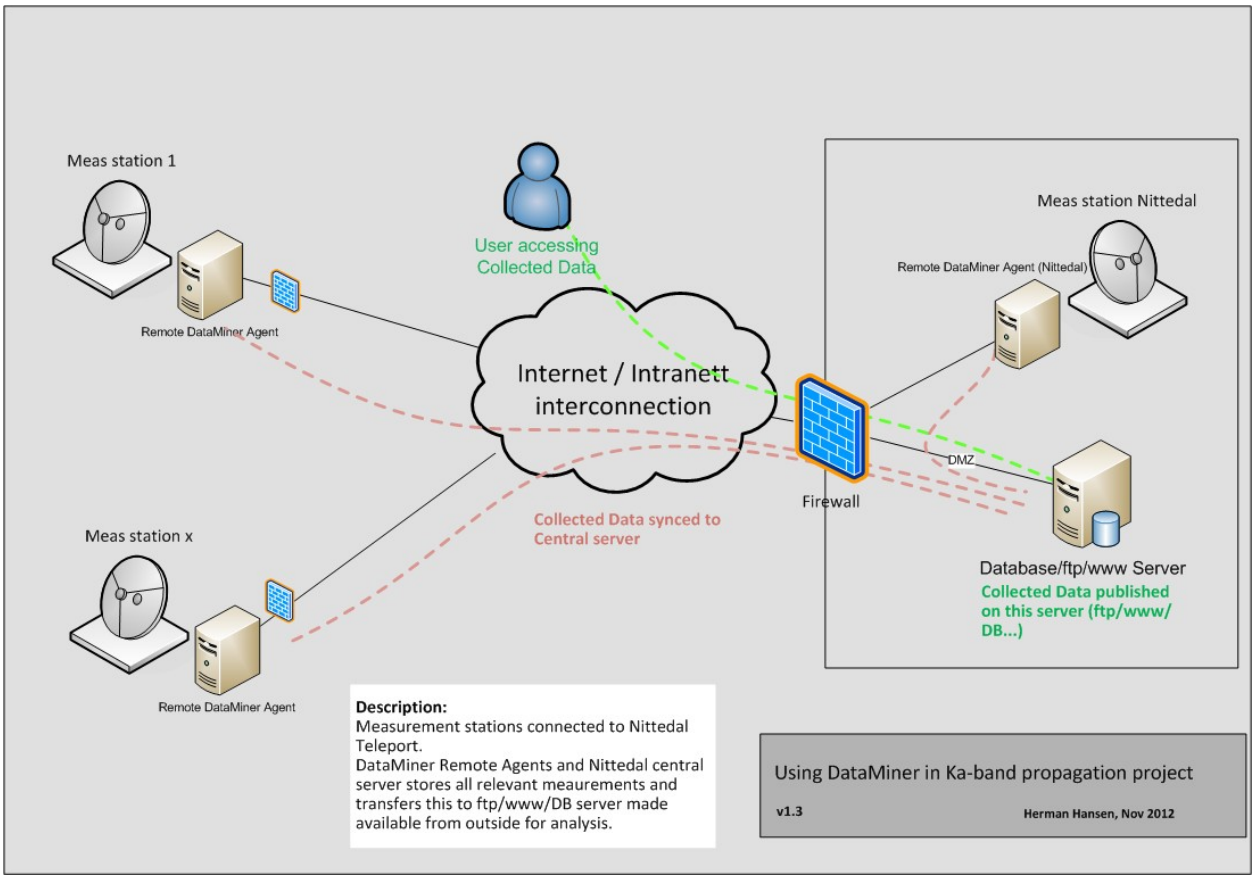

Figure 5-13. Connection of sites for collecting measurement data.

Thus, two instances of a data collection and monitor software, *DataMiner*, is running continuously to collect data to two storage servers and to emit alarm e-mails according to defined criteria. Pre-processing of the data is carried out automatically, and daily plots e-mailed for visual inspection during the campaign. Results are transferred semi-automatically from Kjeller to Nittedal to create a common set of data in the project.

5.1.10 Link budgets

The measurement campaign used two satellites: Ka-Sat for the propagation measurements and Thor 7 for the telecom measurements. The sub-sections below give a summary of the most important and relevant properties of Ka-Sat.

Ka-Sat was launched in Q4 2010 and became operational from Q2 2011. The spacecraft is a multi Ka-band spot beam satellite with coverage from Scandinavia to Middle East. The satellite is located at 9.1 ° East.

Ka-Sat is equipped with beacon signals in the K/Ka-band uplink and downlink bands. The effective isotopically radiated power (EIRP) footprint is shown in Figure 5-14.

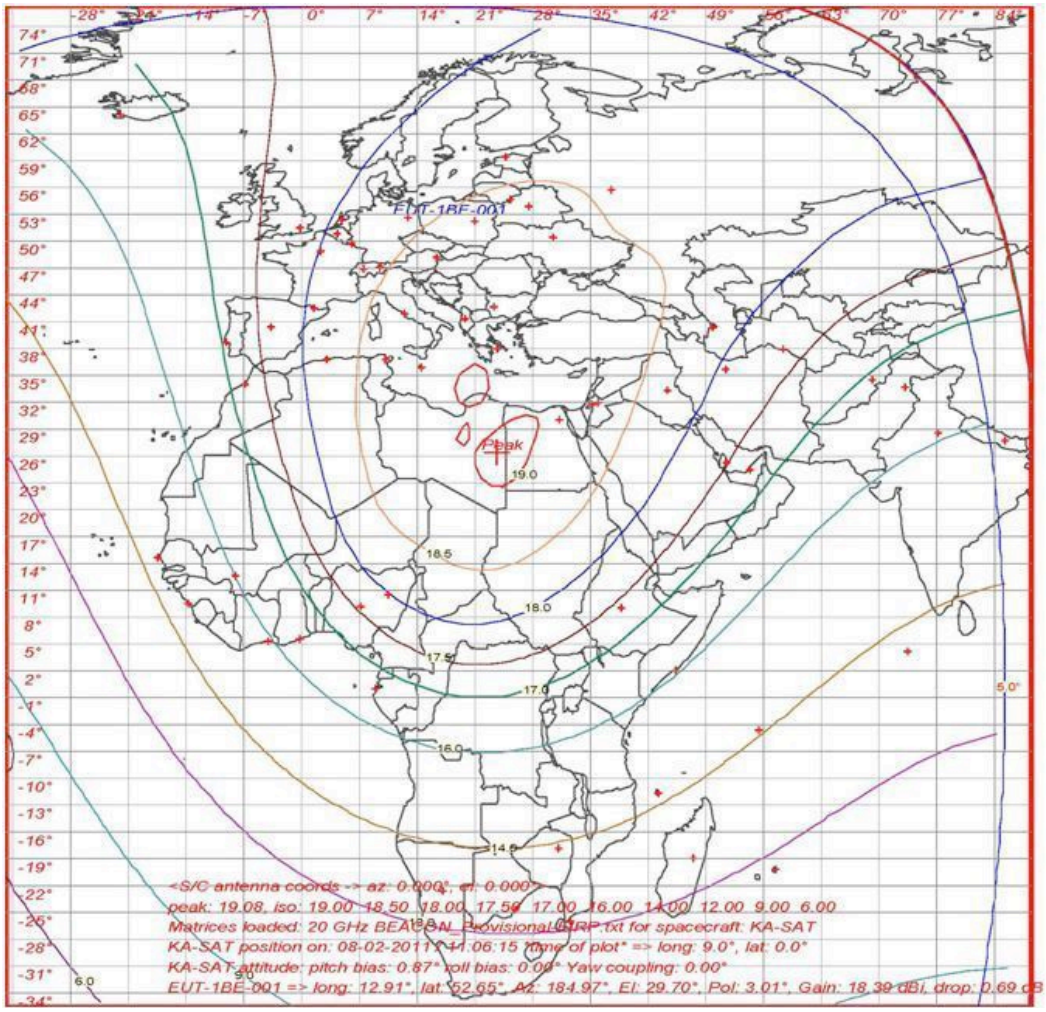

Figure 5-14. Ka-Sat beacon coverage.

The beacon in the downlink band is used for the propagation measurements. The EIRP of the beacon signal is 17.5 dBW or higher for all measurement sites, polarisation is horizontal, and the frequency is 19.68 GHz.

Link budgets for 1.2 m antennas receiving Eutelsat Ka-Sat at 19.68 GHz beacon in Vadsø, Svalbard, Nittedal, Eggemoen and Røst are displayed in Table 5-6 - **Error! Reference source not found.**. The assumptions taken regarding the transmitted beacon and the receiver key figures are based on the following sections. We have utilised the 2010 version of the CNES Propagation dynamic link library software to estimate propagation degradations according to ITU-R recommendations:

- Atmospheric gases: ITU-R Rec. P.676-8 Annex 2
- Rain attenuation: ITU-R Rec. P.618-9
- Clouds attenuation: ITU-R Rec. P. 840-4
- Scintillation: ITU-R Rec. P.618-9

The digital maps for rain intensity, rain height, temperature, water vapour content, wet term of refraction co-index and total columnar content were applied. The software provides a convenient way of implementing the recommendations when the expected increased accuracy of the latest recommendations is not required. We have selected to calculate the propagation impairments at two availability time percentages, 99.9 and 80.0 %. The first value may represent a typical link availability requirement corresponding to 8h 33m outage per year while the latter is used to estimate the measurement dynamic range.

Availability	%	99,9	80,0
EIRP	dBW	18,0	18,0
Free space loss	dB	210,5	210,5
Gas attenuation	dB	0,8	0,8
Rain attenuation	dB	5,8	0,0
Cloud attenuation	dB	1,1	1,1
Scintillation	dB	1,3	0,2
Total attenuation	dB	218,3	212,4
Terminal G/T	dB/K	20,4	21,8
C/N0	dBHz	48,7	56,0

a)

Availability	%	99,9	80,0
EIRP	dBW	17,5	17,5
Free space loss	dB	210,6	210,6
Gas attenuation	dB	2,2	2,2
Rain attenuation	dB	7,0	0,0
Cloud attenuation	dB	2,4	2,4
Scintillation	dB	4,5	0,7
Total attenuation	dB	223,3	215,3
Terminal G/T	dB/K	20,3	21,8
C/N0	dBHz	43,2	52,6

b)

Table 5-6. Power link budget for Ka-Sat beacon received in Vadsø (a) and Svalbard (b).

Availability	%	99,9	80,0
EIRP	dBW	18,0	18,0
Free space loss	dB	210,2	210,2
Gas attenuation	dB	0,4	0,4
Rain attenuation	dB	5,0	0,0
Cloud attenuation	dB	0,5	0,5
Scintillation	dB	0,5	0,1
Total attenuation	dB	216,2	211,1
Terminal G/T	dB/K	20,5	21,8
C/N0	dBHz	51,0	57,3

a)

Availability	%	99,9	80,0
EIRP	dBW	18,0	18,0
Free space loss	dB	210,2	210,2
Gas attenuation	dB	0,4	0,4
Rain attenuation	dB	5,1	0,0
Cloud attenuation	dB	0,4	0,4
Scintillation	dB	0,5	0,1
Total attenuation	dB	216,2	211,1
Terminal G/T	dB/K	20,5	21,8
C/N0	dBHz	50,9	57,3

b)

Table 5-7. Power link budget for Ka-Sat beacon received in Nittedal (a) and Eggemoen (b).

Availability	%	99,9	80,0
EIRP	dBW	17,8	17,8
Free space loss	dB	210,4	210,4
Gas attenuation	dB	0,7	0,7
Rain attenuation	dB	4,9	0,0
Cloud attenuation	dB	0,7	0,7
Scintillation	dB	1,0	0,2
Total attenuation	dB	216,9	211,9
Terminal G/T	dB/K	20,5	21,8
C/N0	dBHz	50,0	56,3

a)

Availability	%	99,9	80,0
EIRP	dBW	17,8	17,8
Free space loss	dB	210,6	210,6
Gas attenuation	dB	1,3	1,3
Rain attenuation	dB	4,7	0,0
Cloud attenuation	dB	1,5	1,5
Scintillation	dB	2,3	0,4
Total attenuation	dB	218,5	213,4
Terminal G/T	dB/K	20,6	21,8
C/N0	dBHz	48,4	54,7

b)

Table 5-8. Power link budget for Ka-Sat beacon received in Røst (a) and Bjørnøya (b).

Typical commercial beacon receivers have a C/N_0 threshold of 43 dBHz. As seen in the last row in the link budgets the margins for such a receiver are in the range 10 to 14 dB. With a receiver C/N_0 threshold of about 10 dBHz a calculated dynamic range exceeding 40 dB is obtainable at all sites. This was considered satisfactory for the beacon propagation campaign and motivates use of alternative receiver techniques with improved sensitivity.

5.1.11 Example measured time series data

Figure 5-15 to Figure 5- show measured examples of data from all six stations.

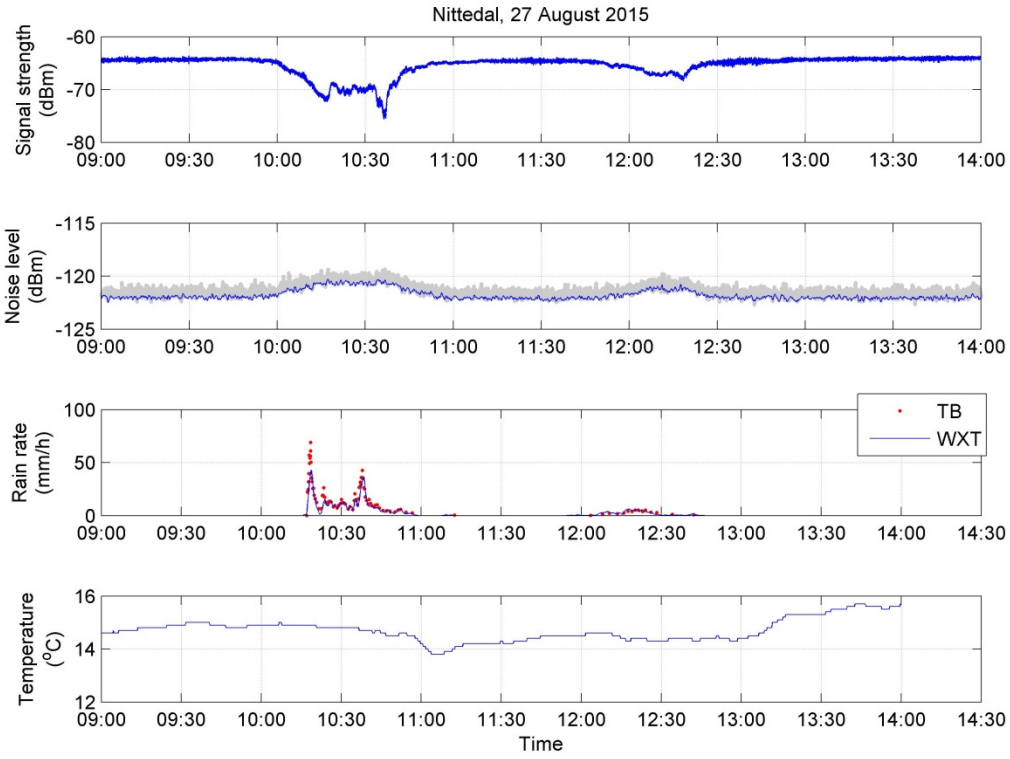

Figure 5-15. Measurement example Nittedal.

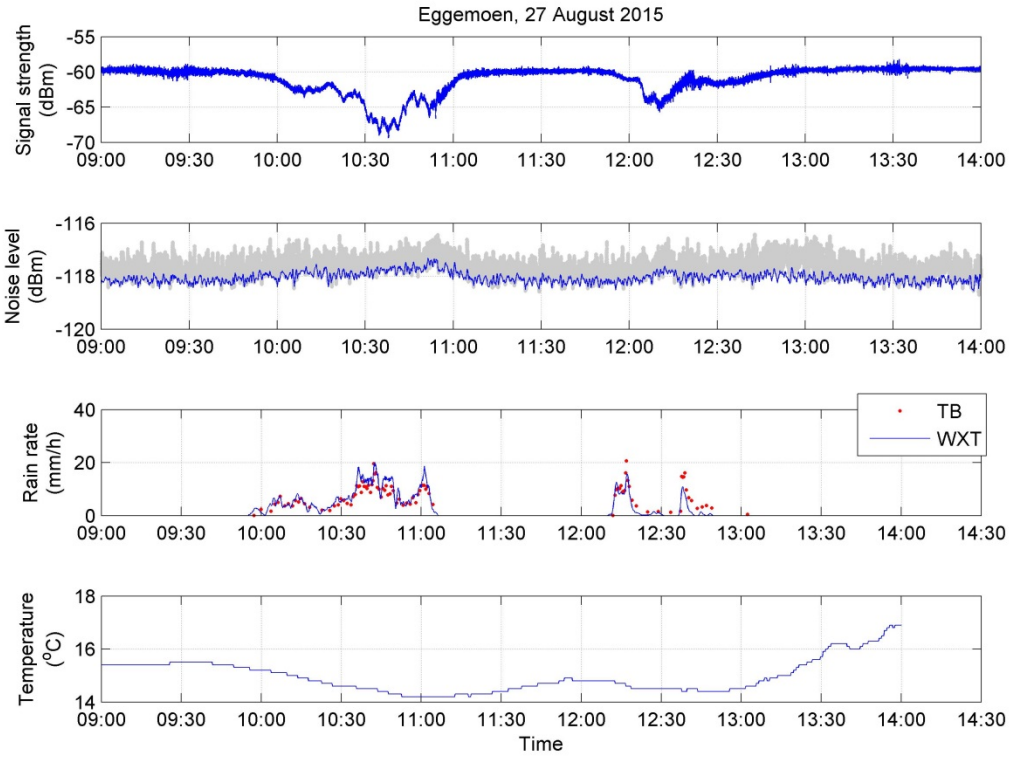

Figure 5-16. Measurement example Eggemoen.

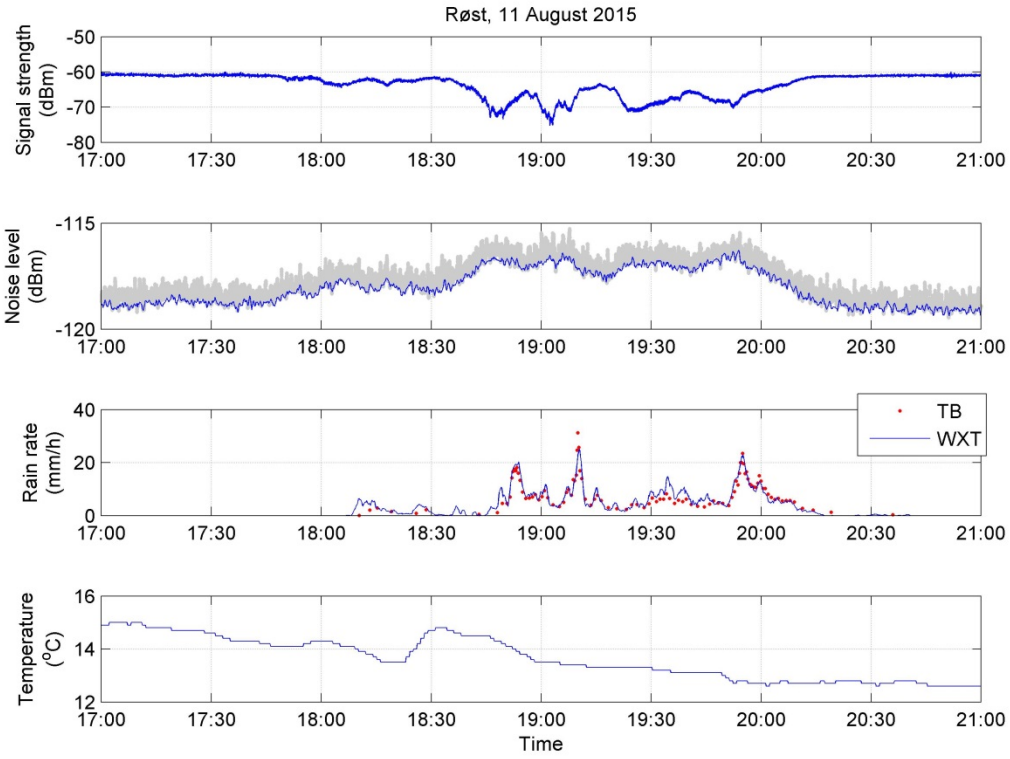

Figure 5-17. Measurement example Røst.

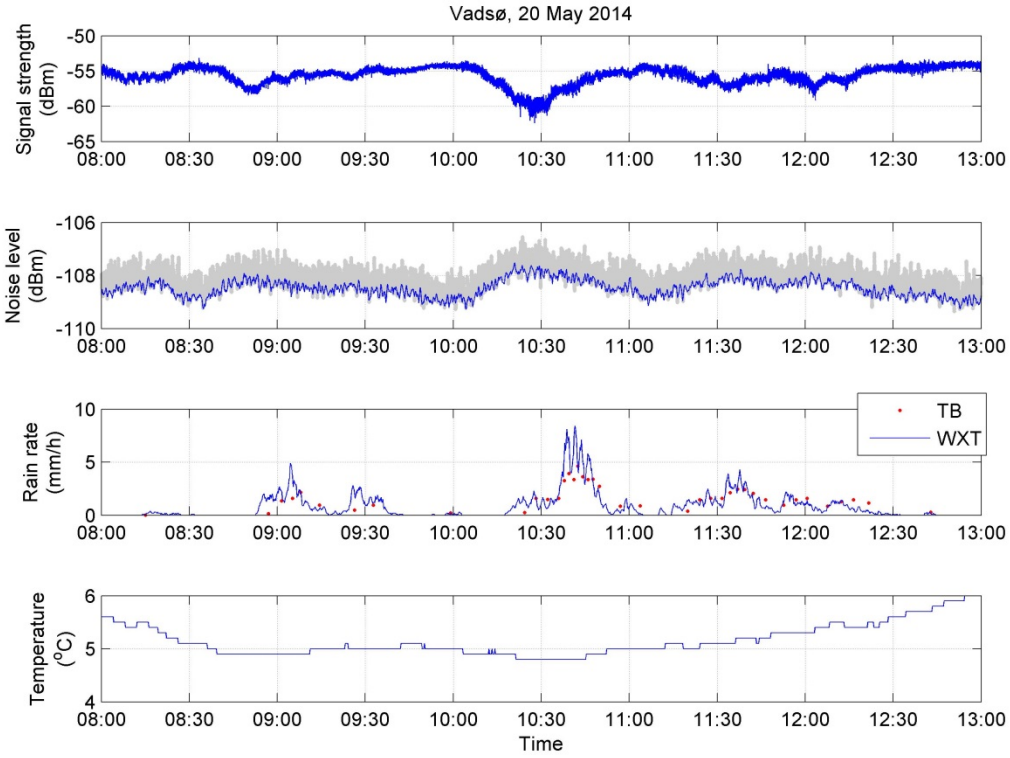

Figure 5-18. Measurement example Vadsø.

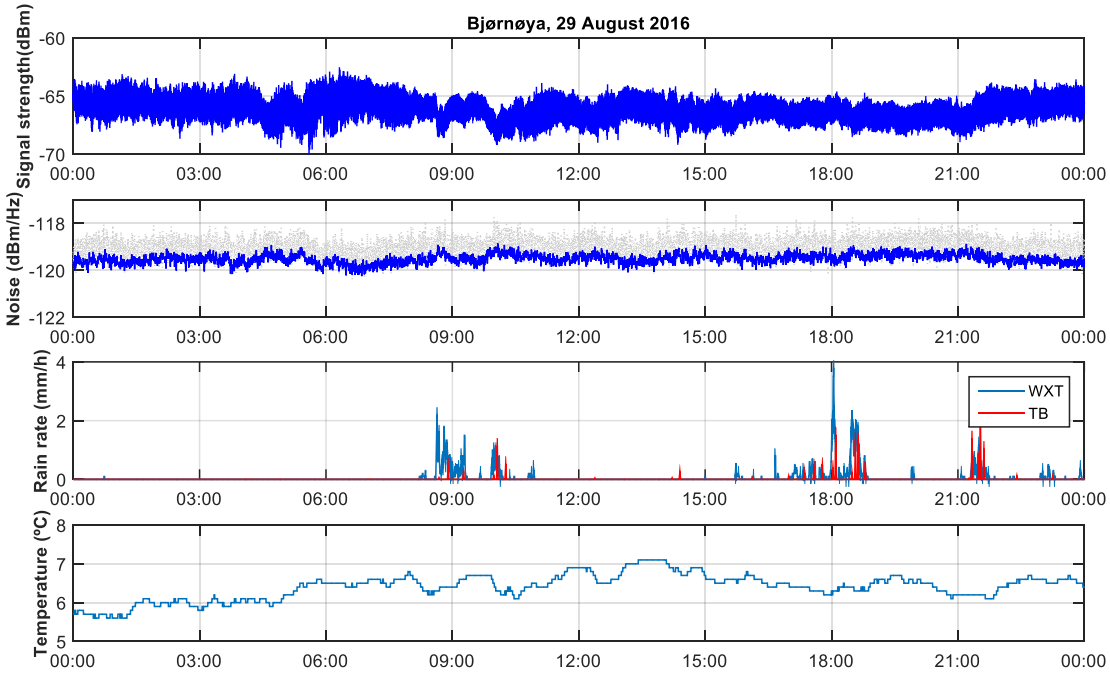

Figure 5-19. Measurement example Bjørnøya.

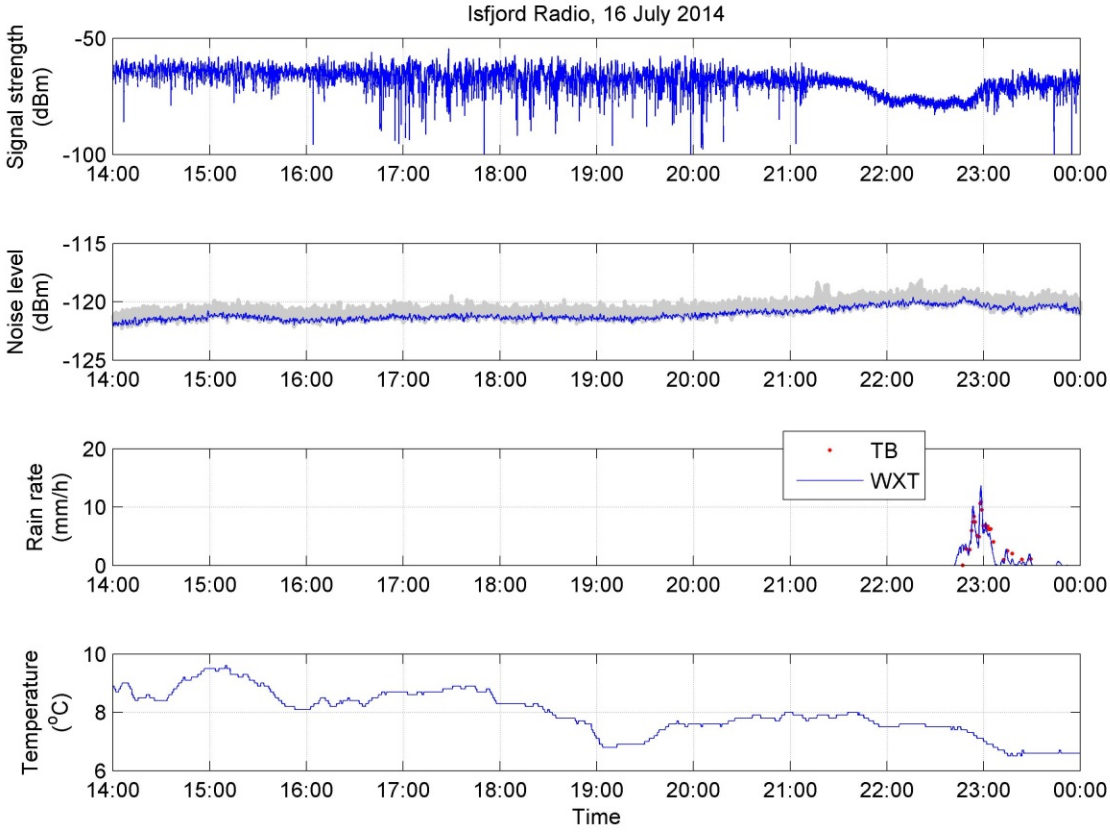

Figure 5-20. Measurement example Isfjord Radio.

5.1.12 Experience

The measurement setup is considered stable however, a few cases of front-end hardware failures have occurred. This applies to both the LNB and the local oscillator, where equipment has been replaced as described in project DD7 *Experiment log-book in electronic format*. One instance of spectrum analyser problem was also observed at Isfjord Radio; a spare analyser provided by FFI was taken into use to resolve the problem. The beacon receiver is sensitive to phase noise. Coaxial connectors with good connections proved to be important to obtain stable measurements at Røst. At Vadsø it was necessary to stabilise the antenna due to wind load to avoid gain antenna variations influencing the measurements. The weather logger has also experienced some challenges; usually a manual restart solved the problems. The ability to tailor the DataMiner alarm triggering specification is somewhat limited, sometimes causing more alarms than necessary.

The resulting experiment availability is well within the required 80 per cent of time and more than two years of data has been collected.

The availability of an additional PhD student resource has facilitated continuous analysis and dissemination of results during the campaign. Results from each site have been analysed on a monthly basis. The post processing includes validation and marking of invalid data, event classification and extraction of the required statistical results.

Two methods have been implemented to establish the zero-attenuation level: event based and automatically. The results include diversity studies for the pair Nittedal-Eggemoen as well as scintillation studies with focus on Isfjord Radio. These results are of importance in general, and specifically for the project partners including Telenor and the Norwegian Armed Forces.

5.2 Propagation data analyses

The following subsections show detailed statistics of two years measured attenuation, rain and scintillation effects. Figure 5-19 and Figure 5-20 show two examples of measure beacon data (top panel). The low-pass filtered signal shown in red is extracted from the signal and the remaining is the scintillation shown in the bottom panel. For Nittedal in middle panel of Figure 5-19 is the excess attenuation shown per event where it refers to a straight line through the levels in dB from before to after with scintillation included in between events. For Isfjord Radio the middle panel of Figure 5-20 shows the attenuation referred to a fixed level obtained a clear sky day.

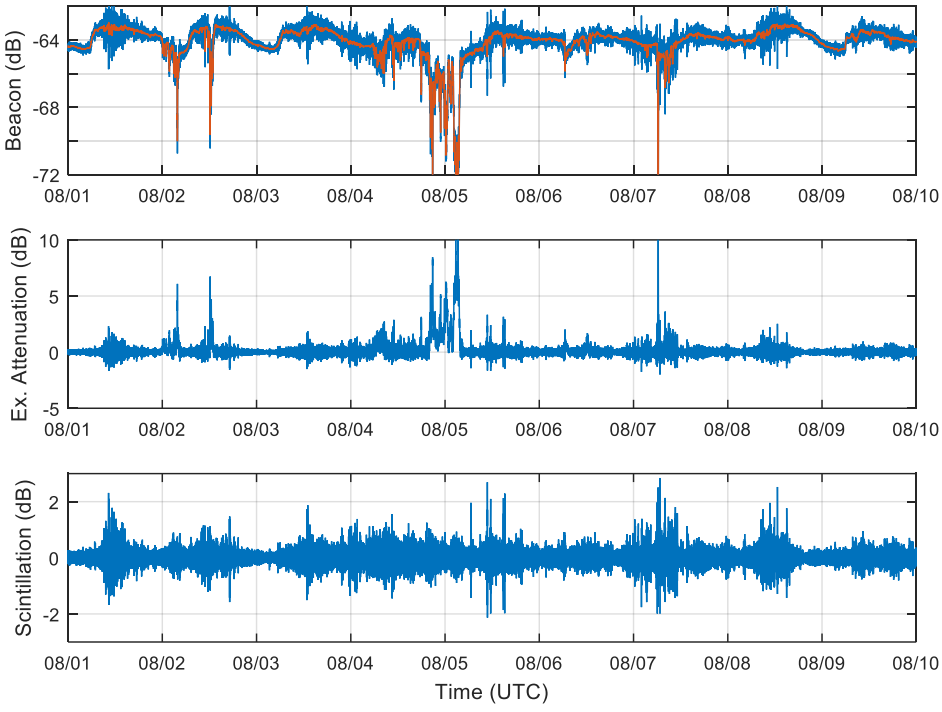

Figure 5-19. Measurement example from Nittedal 2015 showing beacon (top), excess attenuation (middle) and scintillation (bottom).

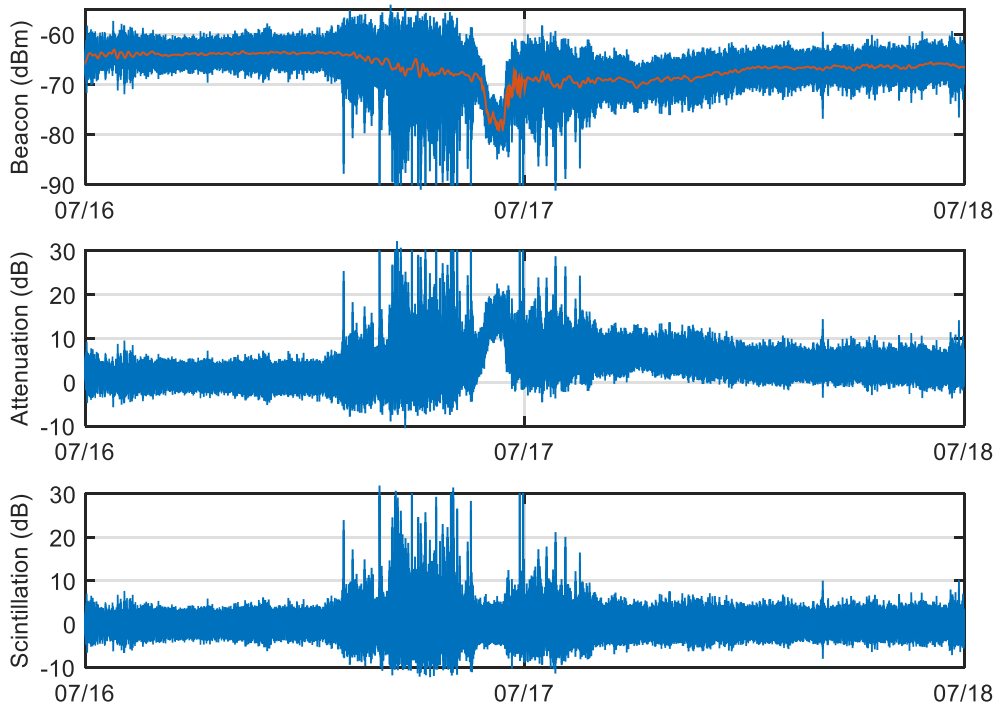

Figure 5-20. Measurement example from Isfjord Radio in 2014 showing beacon (top), attenuation (middle) and scintillation (bottom).

A few longer continuous periods of data are missing, namely February 2014 at Nittedal, August 2014 at Eggemoen and most of October 2015 at Isfjord Radio. An issue during installation at Røst resulted in significantly reduced dynamic range for the first 2.5 months of measurements, therefore these data are excluded from second order statistics and scintillation studies and two partly overlapping periods of a year each are used instead. However, even with these missing the data for both years appear consistent and give good indication of the measured effects.

5.2.1 First order statistics of attenuation and rain

The procedure chosen for setting 0 dB attenuation reference level for the 4 southernmost stations used manual identification of all attenuation events and automatic calculation of the 0 dB level from the signal power before and after each event.

However, for Isfjord Radio this procedure does not give good results. Probably, due to the long path through the atmosphere there were a large number of long-duration events (from 6 hours to a few days) without any clear beginning and end and without a clear indication of their possible origin. The location has cloud cover about 80% of the year (based on satellite images) so cloud attenuation can be one of the causes. Furthermore, during the warm months the water vapour content in the atmosphere increases dramatically and at this very low elevation angle causes significant attenuation on the link. Water vapour content can also change at a rate comparable to cloud cover. Since attenuation from these sources cannot be separated from rain attenuation using the measurement setup and since it will have significant effect on the performance of a communication link a fixed 0 dB level based on a period of clear and dry air during winter was used instead for the 0 dB reference. Alternative methods based on detailed weather models are being investigated, but these may well introduce additional errors due to non-perfect modelling. At Bjørnøya slow long-term 2-3 dB decrease of measured signal level in the course of 1 year prevented the use of constant reference level for whole year, instead monthly reference levels based on a few clear-sky days in each month were utilized.

Events related to wet snow/icing on the antenna parts were observed a few times per year on all stations and removed from the valid data. Investigations are underway to closely determine their origin and see how they can be avoided.

Since two independent sensors were used for rain rate measurement, results from both are plotted. During normal conditions they give very similar results especially for the percentage of time of most interest in propagation modelling (0.01 %). The tipping bucket gives very different values during low intensity rain, likely due to evaporation. Some differences were also observed during very high rain intensity events.
The biggest differences were observed during high winds (> 15 m/s) at the two stations located closes to the seacoast. Both Røst and Isfjord Radio are within 100 meters of the seafront and only a few meters above the sea level. Vadsø while relatively close to the sea is on a small hill some 30 meters above the sea surface. During the mentioned high winds, the WXT sensor often measured long periods of low intensity rain while no data came from the Tipping Bucket. It is likely that there were water droplets in the air at that time and hit the WXT sensor nearly vertically resulting in the recorded values while at the same time they did not enter the Tipping Bucket due to turbulence at the opening. These droplets could be sea spray but could as well be rain showers so neither WXT nor TB is expected to give the correct values. In any case the effect of these droplets on the attenuation on the link should be limited.

All data in this section is scaled relative to the total measurement period.

5.2.1.1 Attenuation and rain Nittedal

Nittedal has inland climate with high-intensity convective rain events during the summer months that results in high attenuation. Limited attenuation was recording outside of the few months.

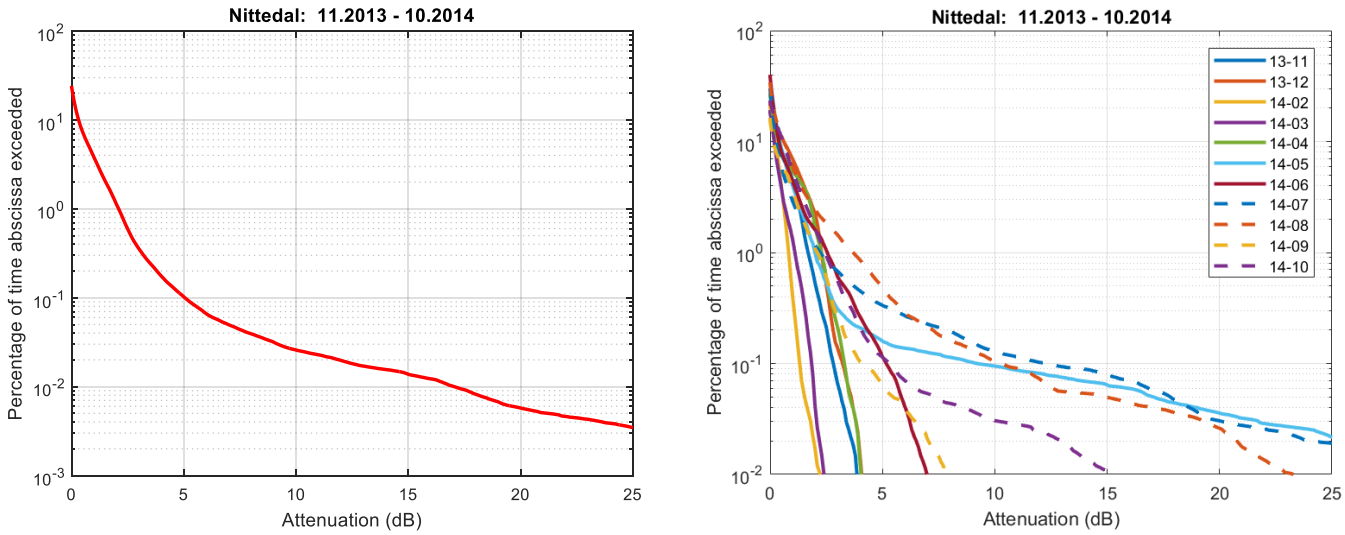

Figure 5-21. ***CCDF of attenuation for the period 11.2013 – 10.2014 and for each month with valid measurements during the period.***

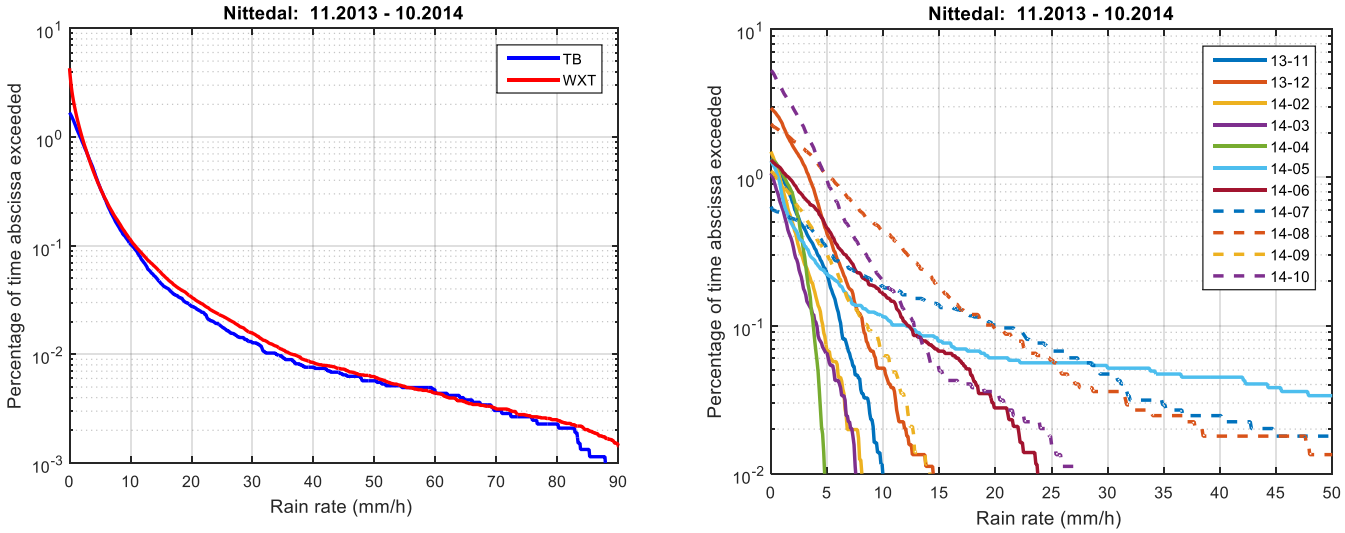

Figure 5-22. ***CCDF of rain rate for the period 11.2013 – 10.2014 and for each month with valid measurements during the period. Monthly data are from tipping bucket only.***

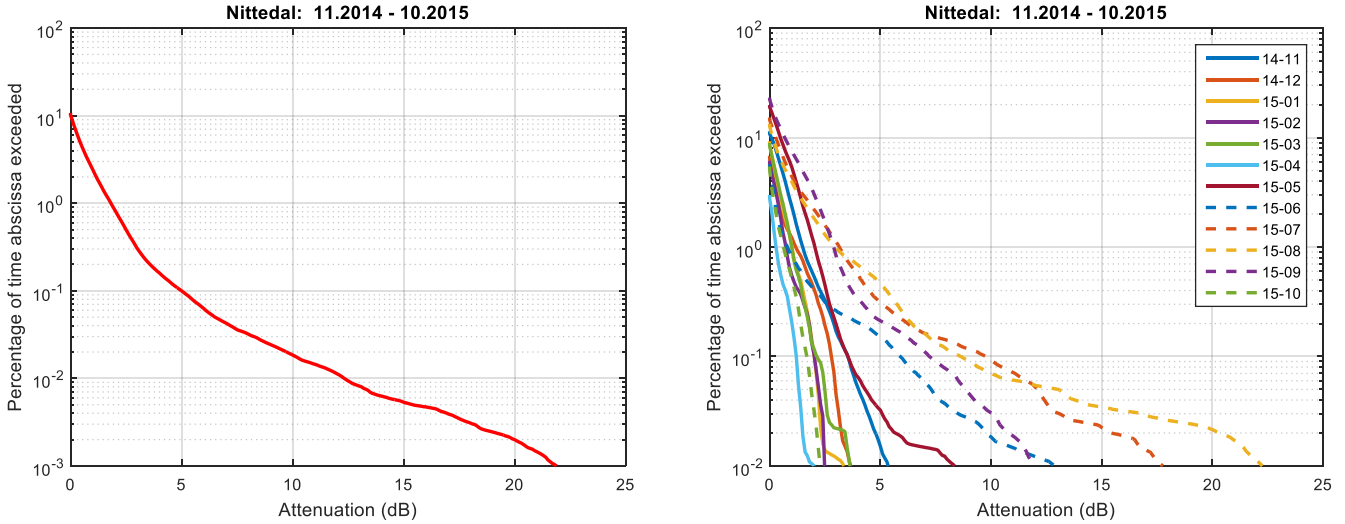

Figure 5-23. ***CCDF of attenuation for the period 11.2014 – 10.2015 and for each month with valid measurements during the period.***

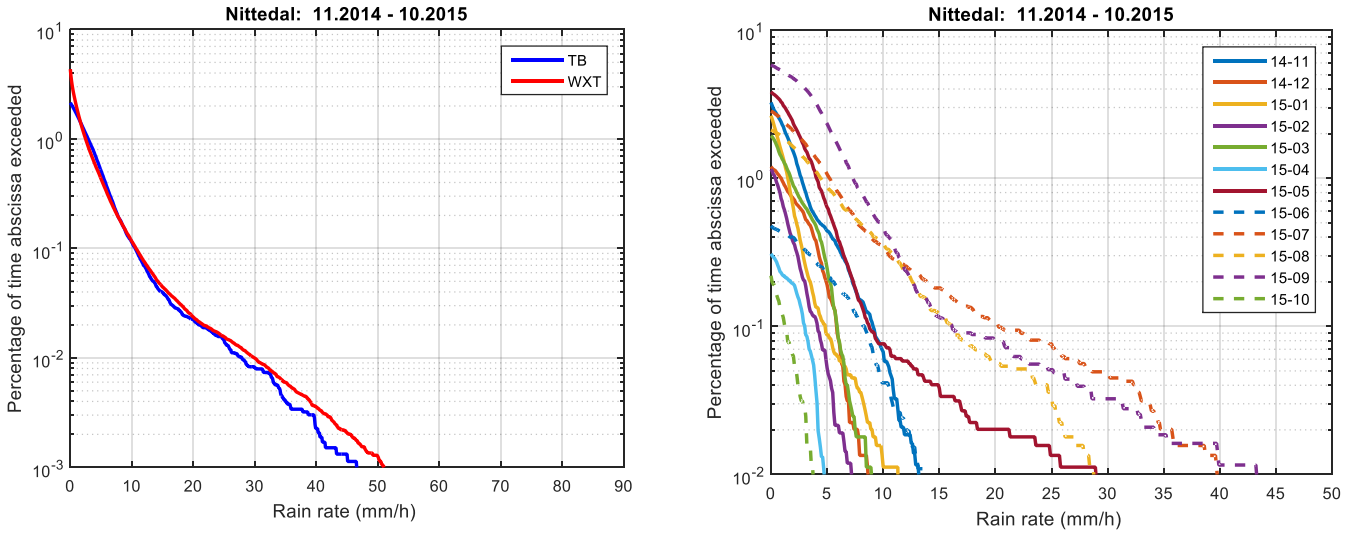

Figure 5-24. ***CCDF of rain for the period 11.2014 – 10.2015 and for each month with valid measurements during the period. Monthly data are from tipping bucket only.***

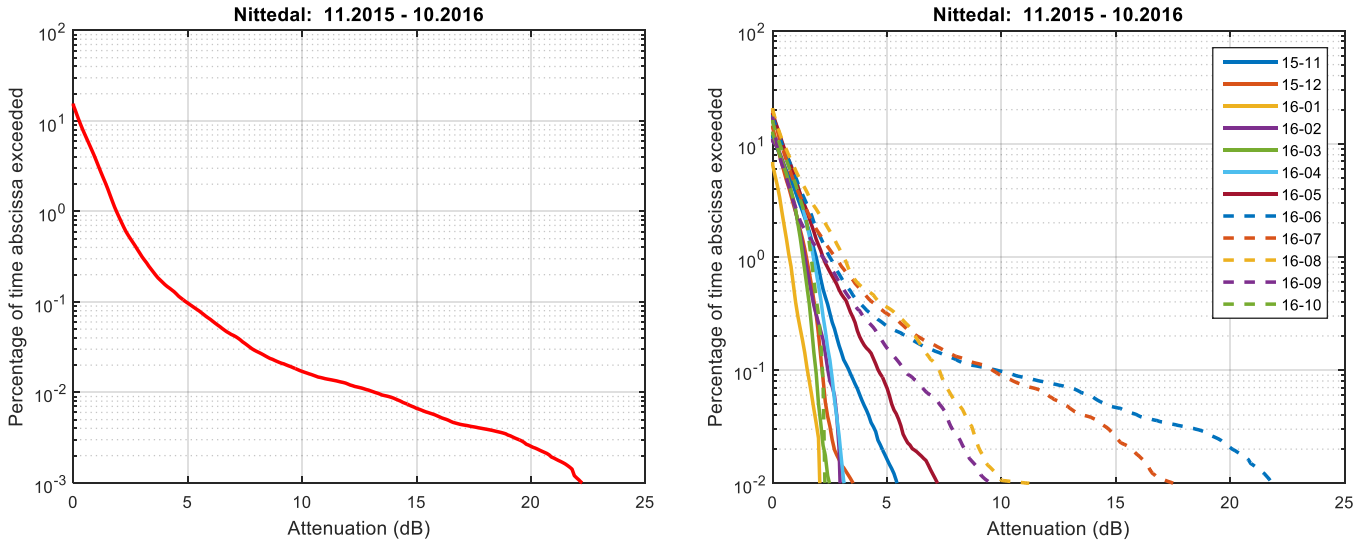

Figure 5-256. ***CCDF of attenuation for the period 11.2015 – 10.2016 and for each month with valid measurements during the period.***

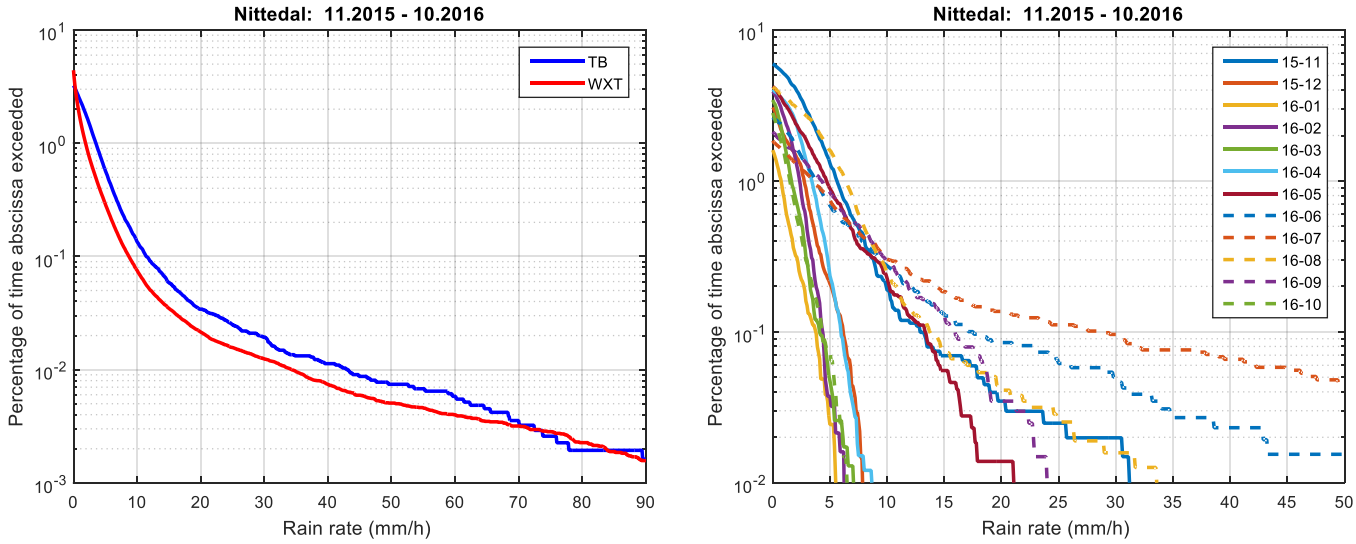

Figure 5-26. ***CCDF of rain for the period 11.2015 – 10.2016 and for each month with valid measurements during the period. Monthly data are from tipping bucket only.***

5.2.1.2 Attenuation and rain Eggemoen

Being located 29.7 km from Nittedal the attenuation characteristics are also similar with a few high intensity events during the summer but relatively low attenuation otherwise. Overall the attenuation is slightly lower. The rain rate from WXT and Tipping Bucket did not match during high intensity rain in the first year of measurements while following each other closely during the second year.

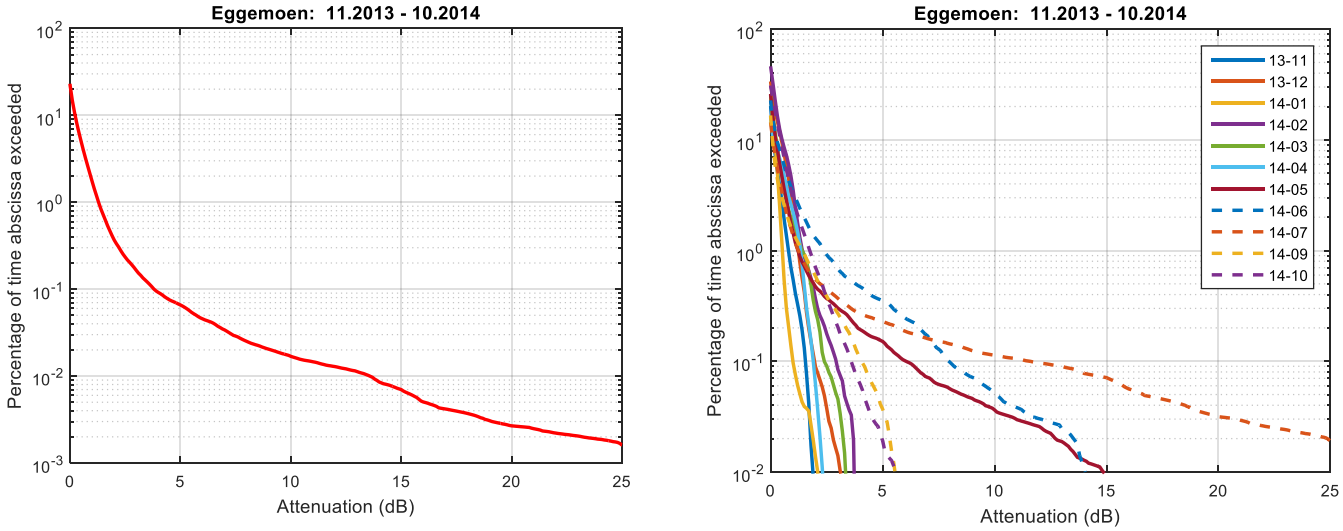

Figure 5-27. ***CCDF of attenuation for the period 11.2013 – 10.2014 and for each month with valid measurements during the period.***

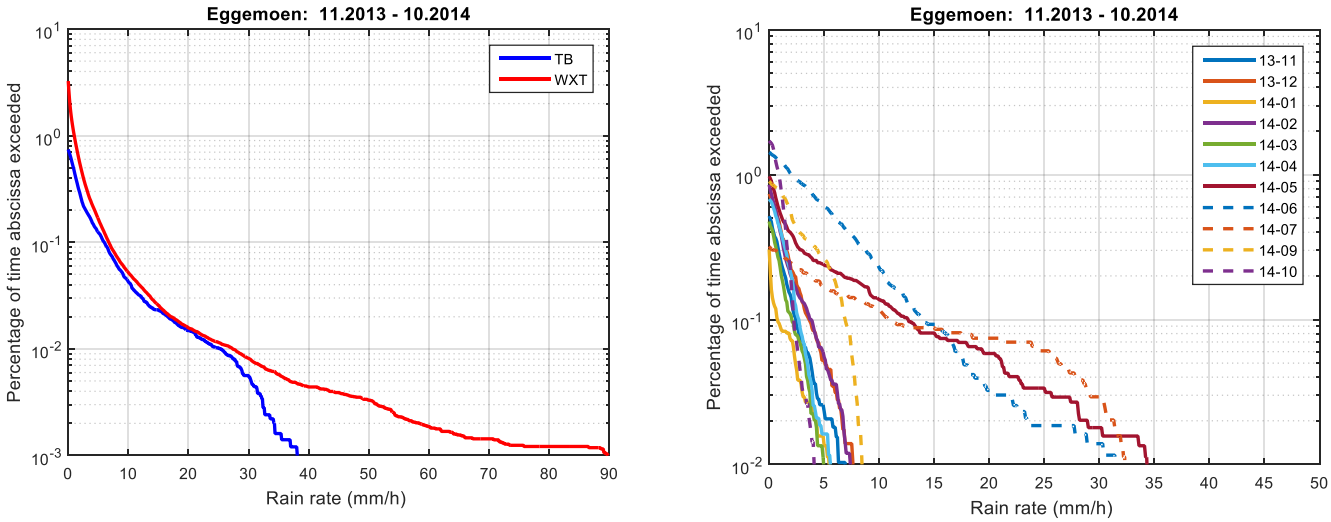

Figure 5-28. ***CCDF of rain rate for the period 11.2013 – 10.2014 and for each month with valid measurements during the period. Monthly data are from tipping bucket only.***

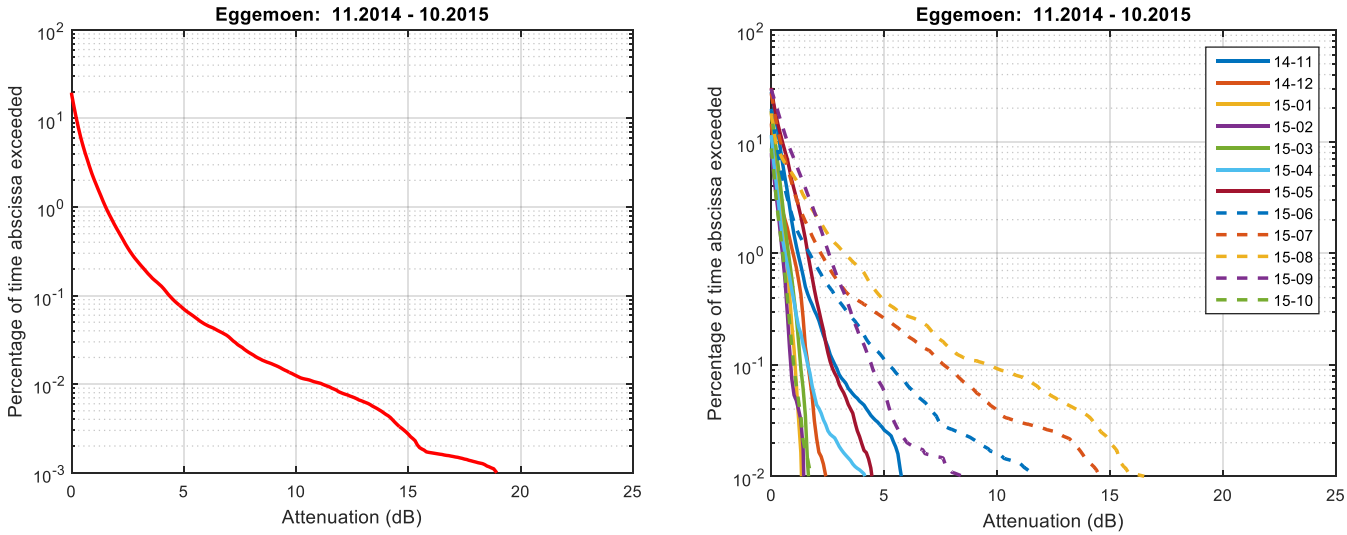

Figure 5-29. ***CCDF of attenuation for the period 11.2014 – 10.2015 and for each month with valid measurements during the period.***

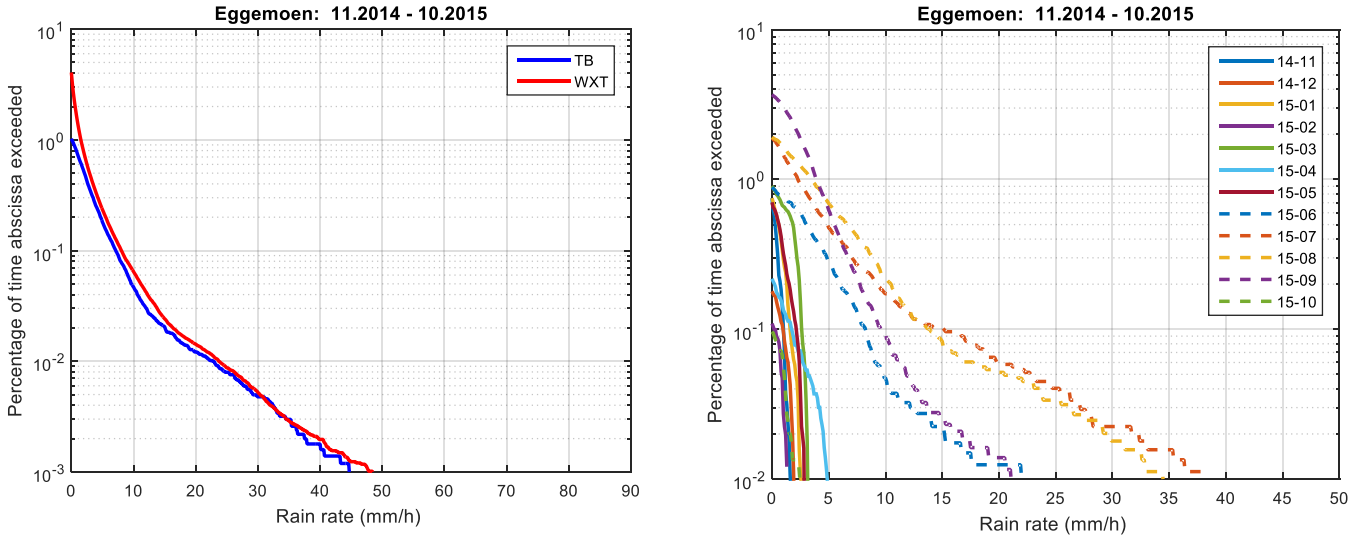

Figure 5-30. ***CCDF of rain for the period 11.2014 – 10.2015 and for each month with valid measurements during the period. Monthly data are from tipping bucket only.***

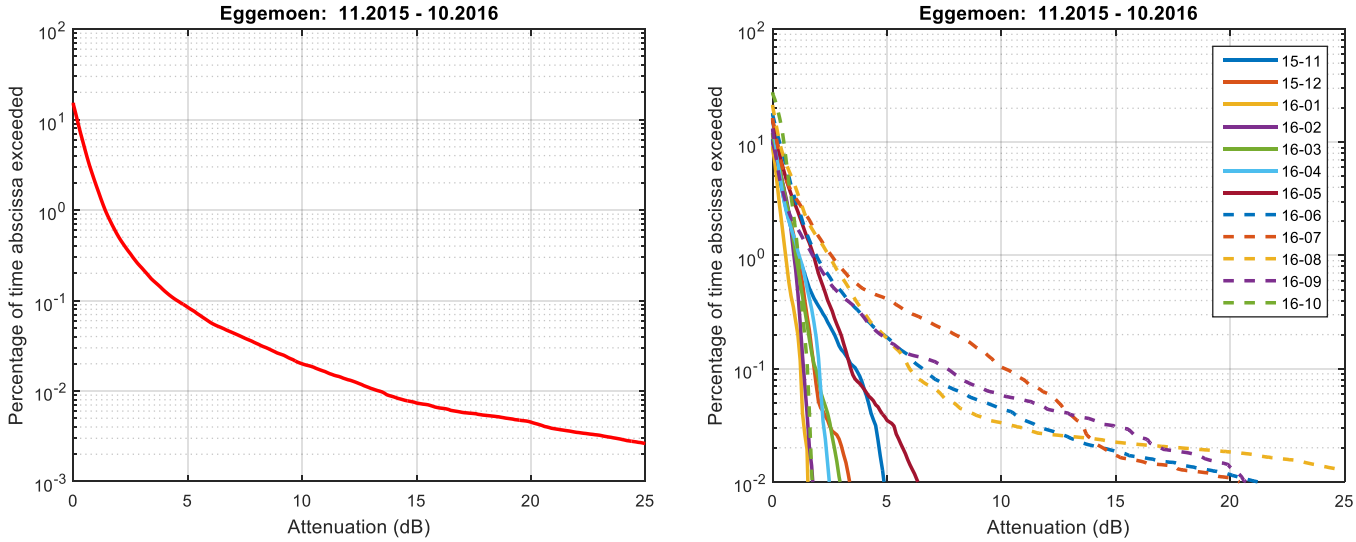

Figure 5-31. ***CCDF of attenuation for the period 11.2015 – 10.2016 and for each month with valid measurements during the period.***

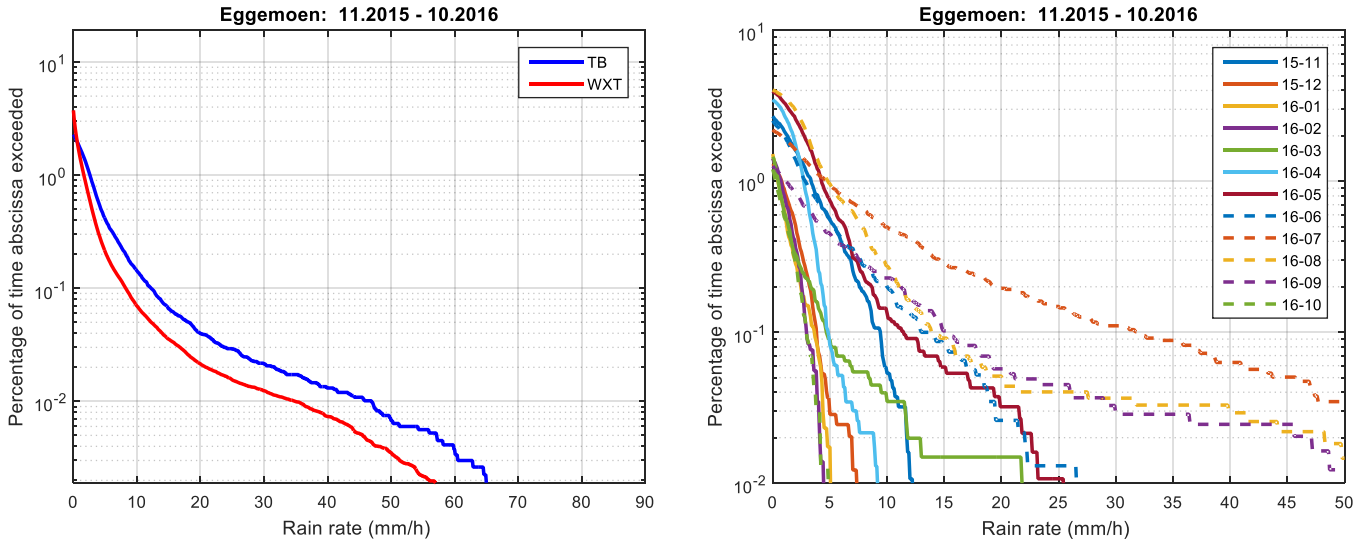

Figure 5-32. ***CCDF of rain for the period 11.2015 – 10.2016 and for each month with valid measurements during the period. Monthly data are from tipping bucket only.***

5.2.1.3 Attenuation and rain Røst

At Røst, being a small island in the middle of the sea, the temperature and rain rate changes very little during the year. Convective rain is almost totally absent while low intensity stratiform rain occurs often. Therefore there is a high percentage of low amplitude attenuation and almost no monthly variation. As mentioned at the start of the chapter the WXT and Tipping Bucket rain rate values do not agree for this station.

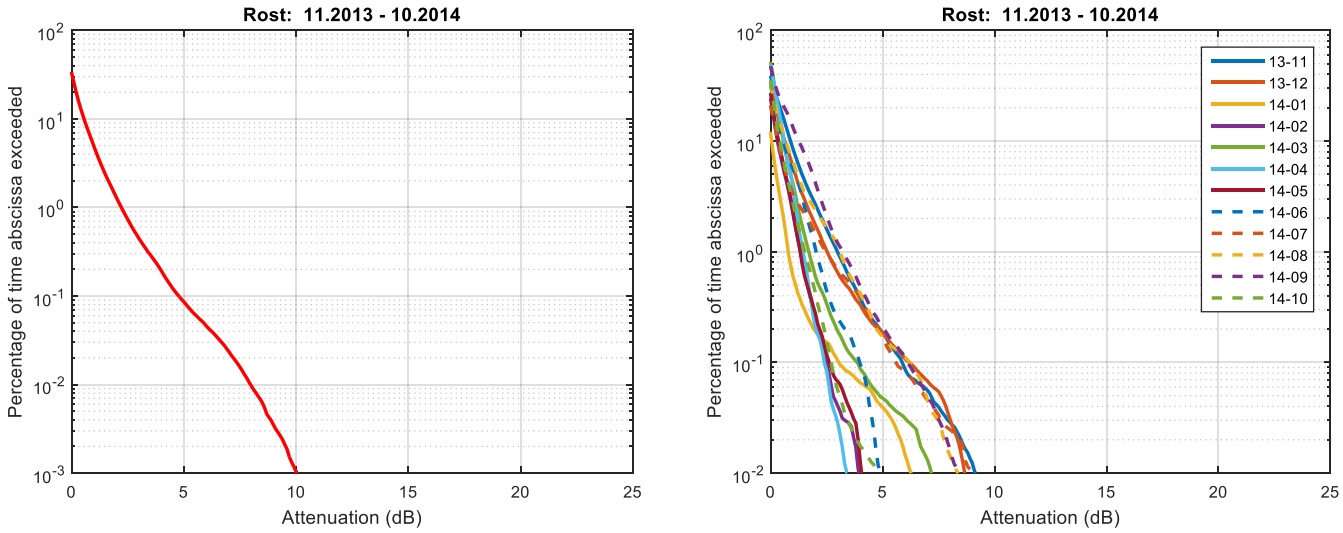

Figure 5-33. ***CCDF of attenuation for the period 11.2013 – 10.2014 and for each month with valid measurements during the period.***

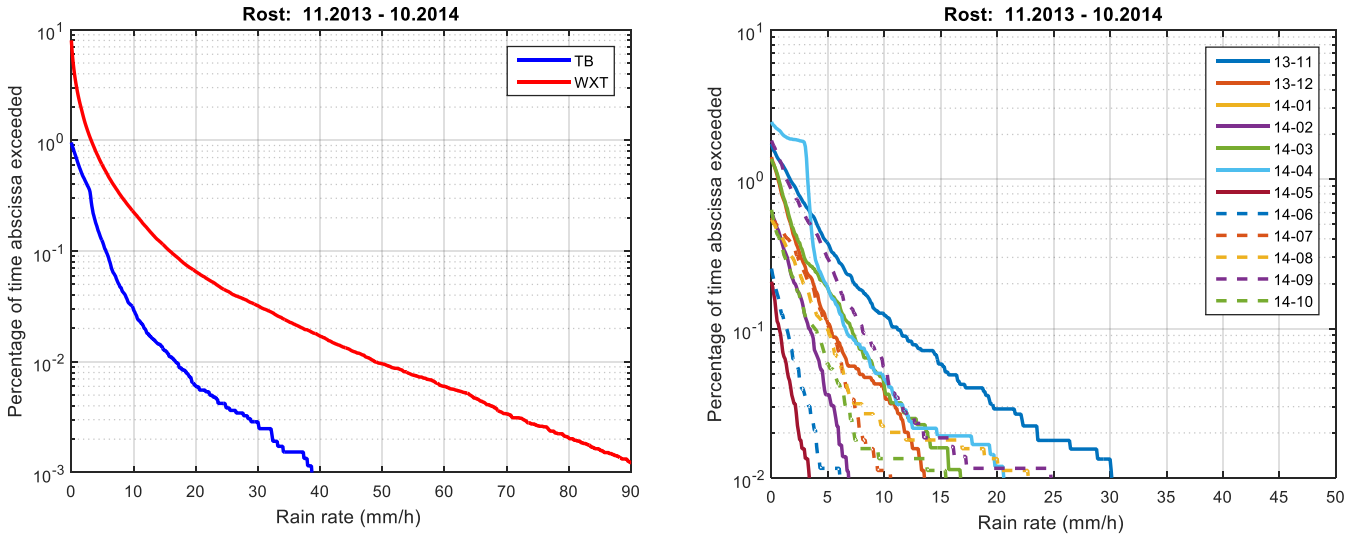

Figure 5-34. ***CCDF of rain rate for the period 11.2013 – 10.2014 and for each month with valid measurements during the period. Monthly data are from tipping bucket only.***

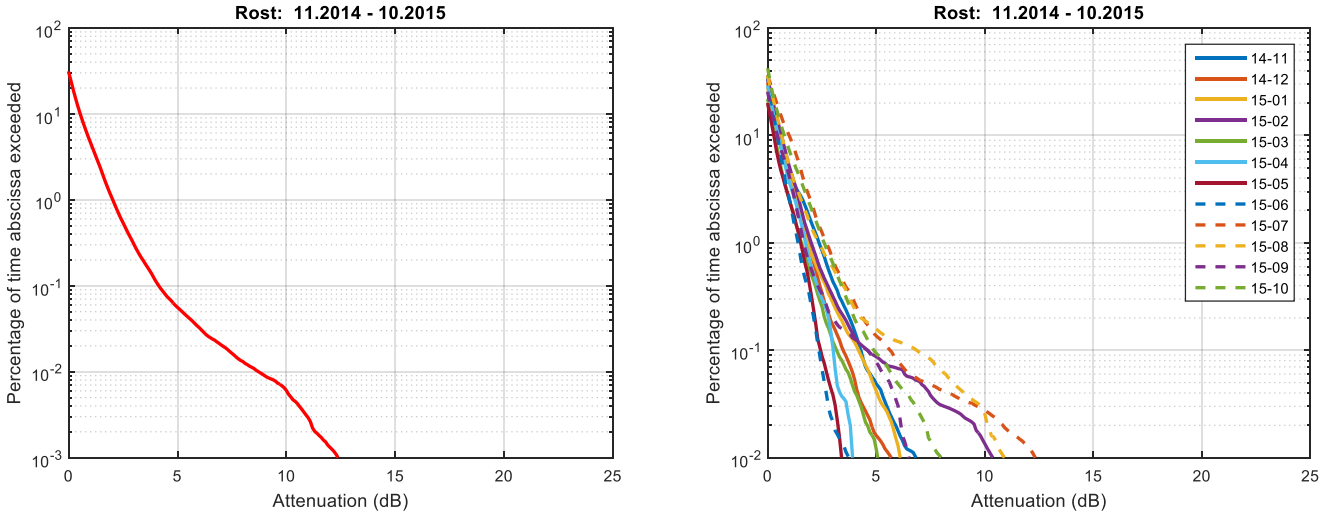

Figure 5-35. ***CCDF of attenuation for the period 11.2014 – 10.2015 and for each month with valid measurements during the period.***

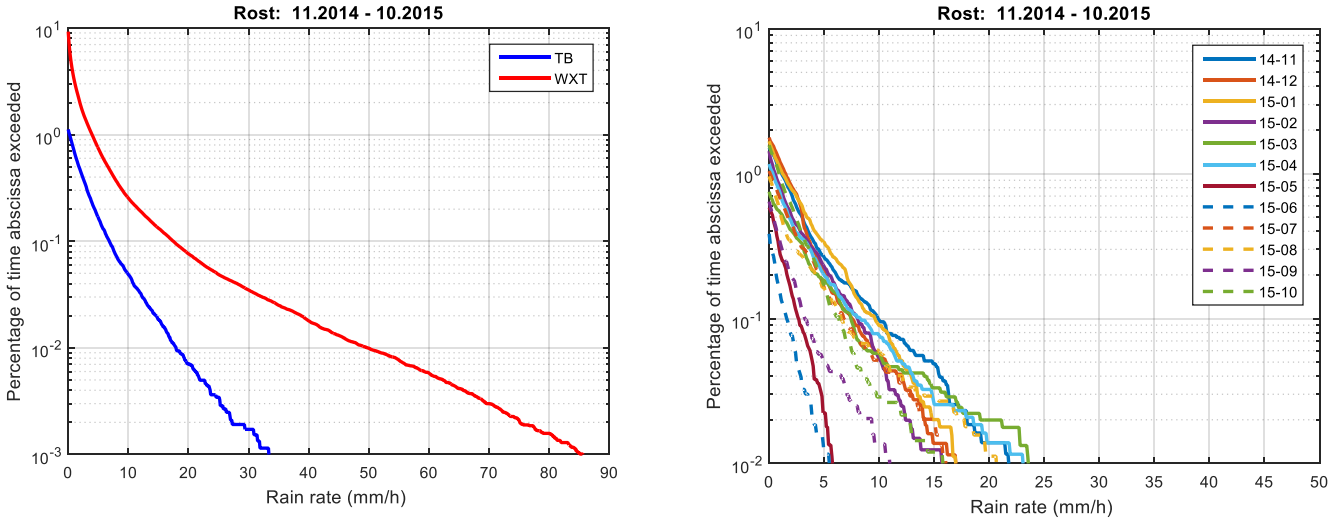

Figure 5-36. ***CCDF of rain for the period 11.2014 – 10.2015 and for each month with valid measurements during the period. Monthly data are from tipping bucket only.***

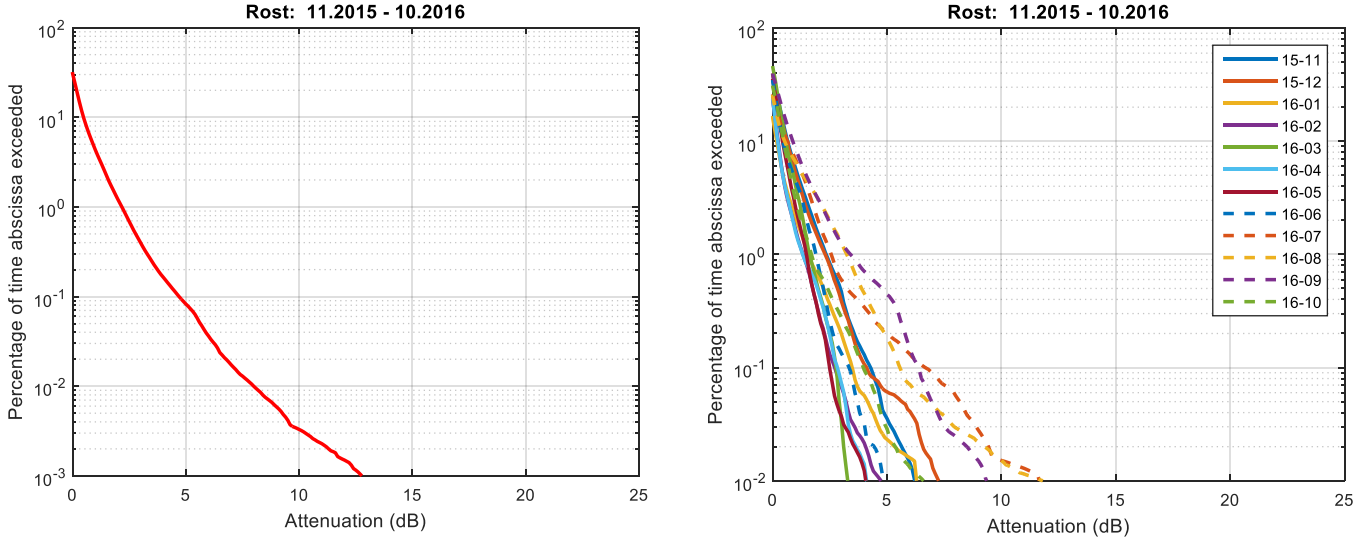

Figure 5-37. ***CCDF of attenuation for the period 11.2015 – 10.2016 and for each month with valid measurements during the period.***

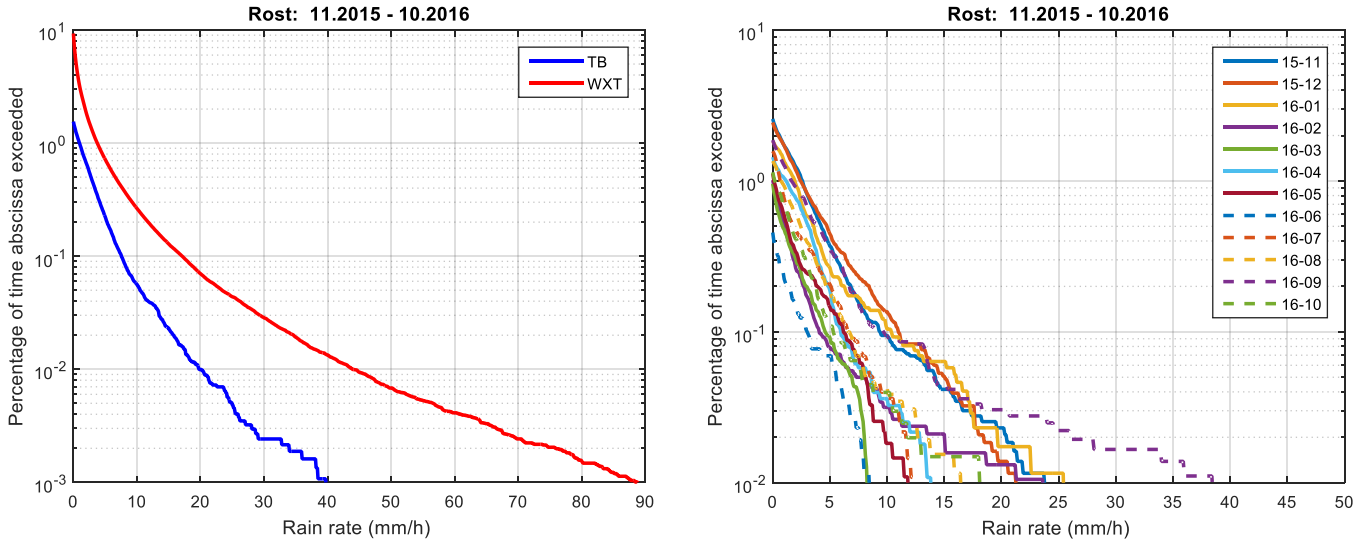

Figure 5-38. ***CCDF of rain for the period 11.2015 – 10.2016 and for each month with valid measurements during the period. Monthly data are from tipping bucket only.***

5.2.1.4 Attenuation and rain Vadsø

Due to low elevation angle at Vadsø, even the medium-intensity rain recorded causes relatively large attenuation. Furthermore, even though the station is at the coast of a small fjord it is surrounded by significant landmass. Therefore, there are convective high-intensity rain events during the summer that cause large attenuation.

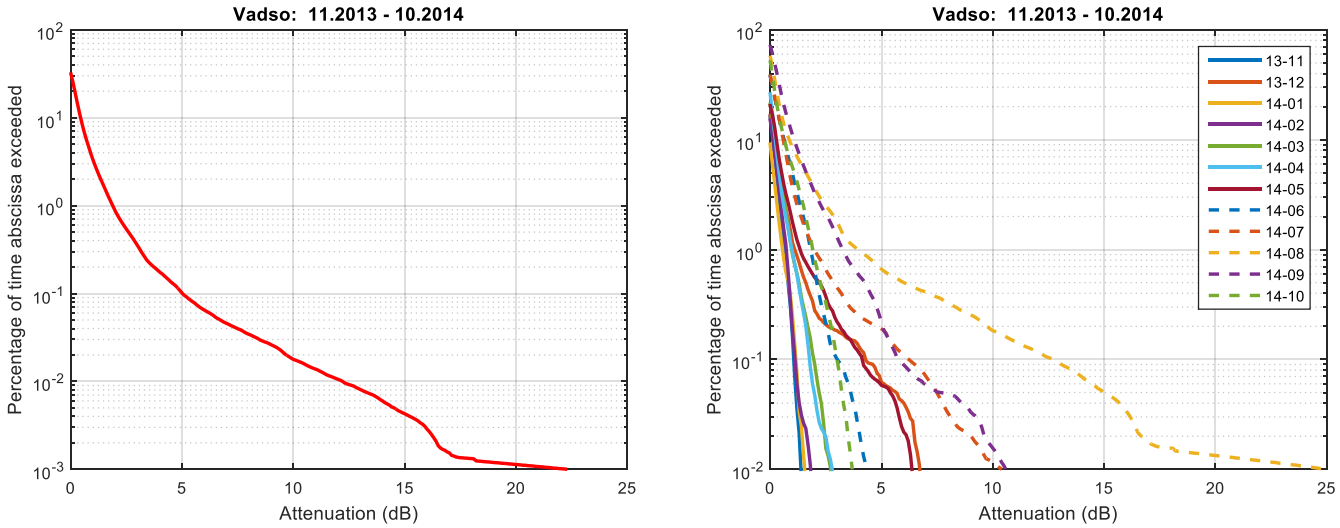

Figure 5-39. ***CCDF of attenuation for the period 11.2013 – 10.2014 and for each month with valid measurements during the period.***

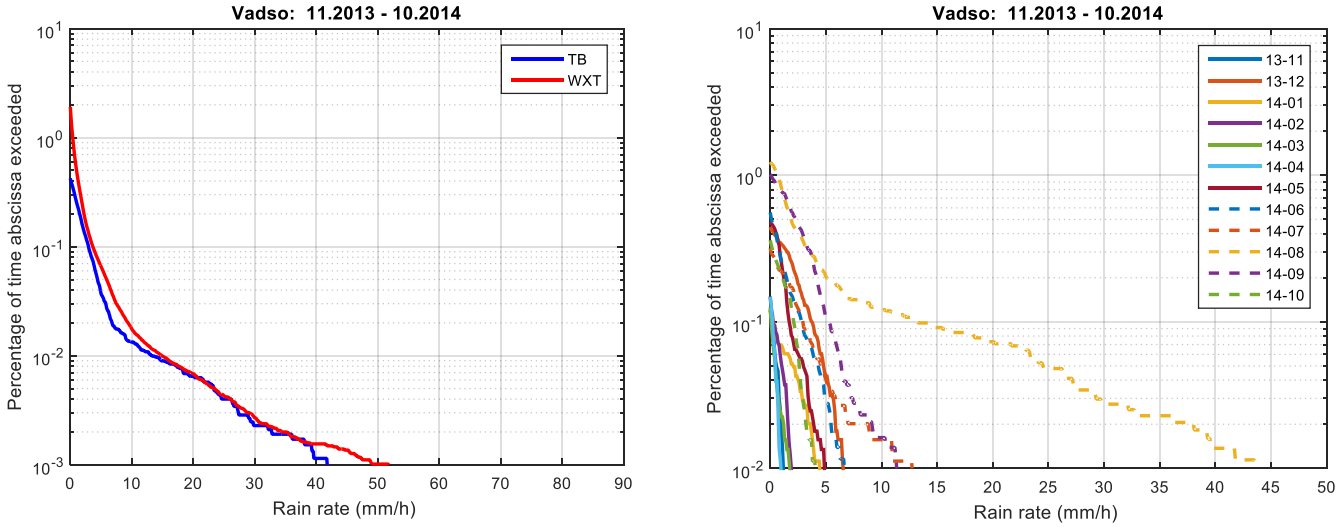

Figure 5-40. ***CCDF of rain rate for the period 11.2013 – 10.2014 and for each month with valid measurements during the period. Monthly data are from tipping bucket only.***

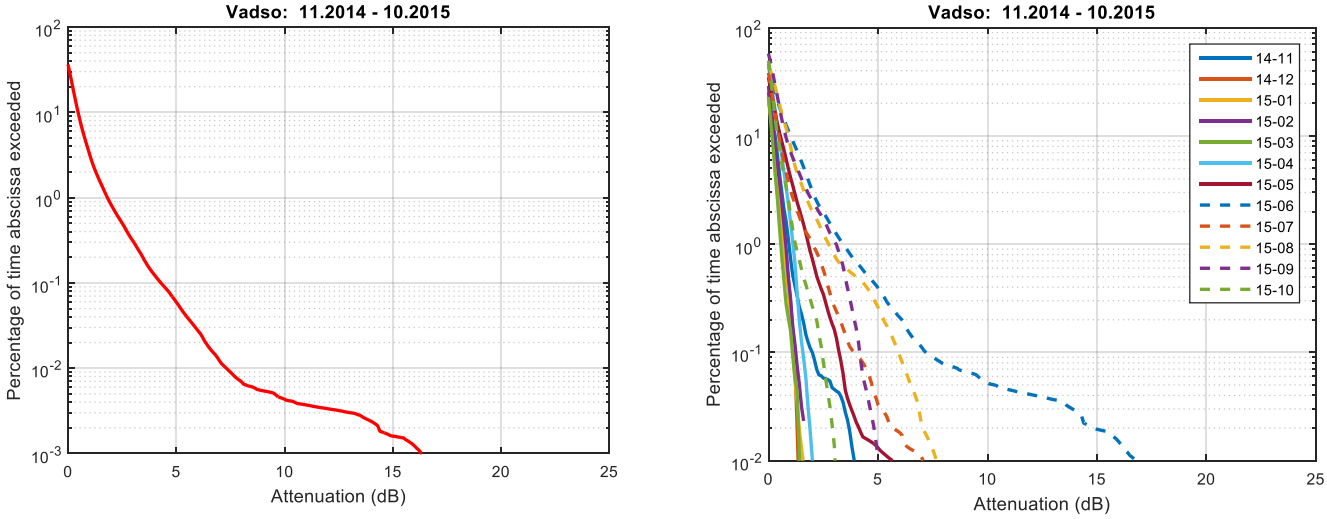

Figure 5-41. ***CCDF of attenuation for the period 11.2014 – 10.2015 and for each month with valid measurements during the period.***

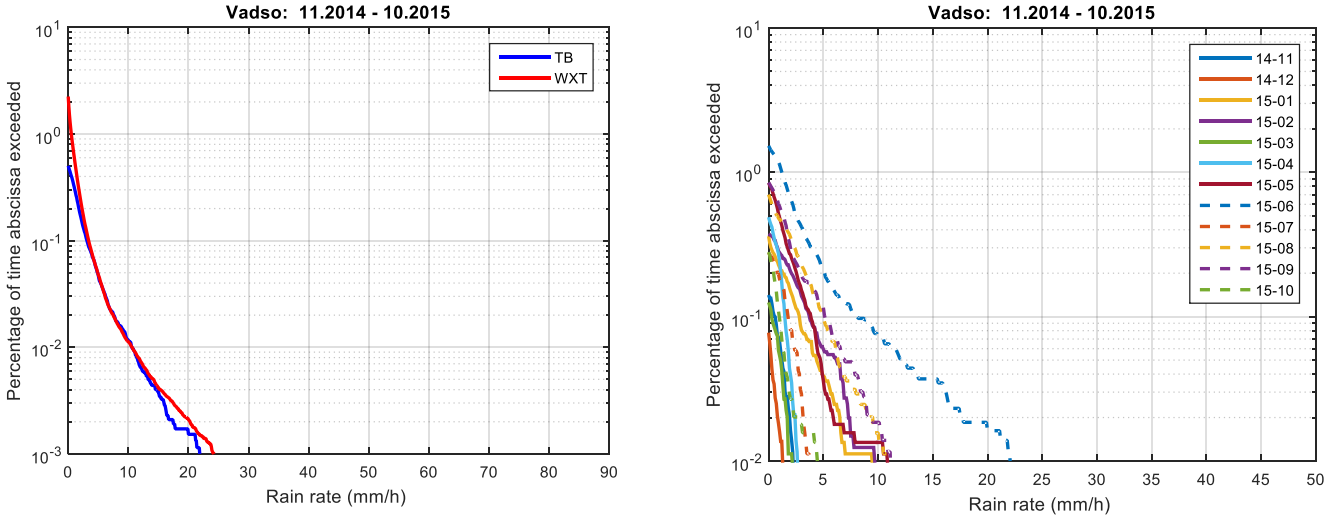

Figure 5-42. ***CCDF of rain for the period 11.2014 – 10.2015 and for each month with valid measurements during the period. Monthly data are from tipping bucket only.***

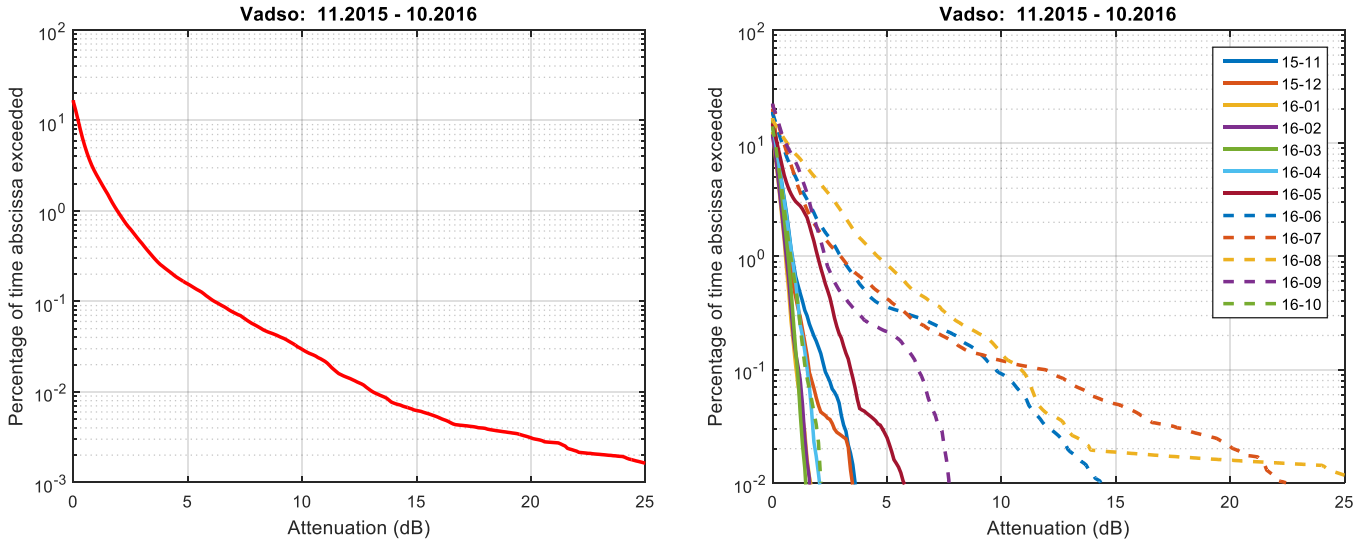

Figure 5-43. ***CCDF of attenuation for the period 11.2015 – 10.2016 and for each month with valid measurements during the period.***

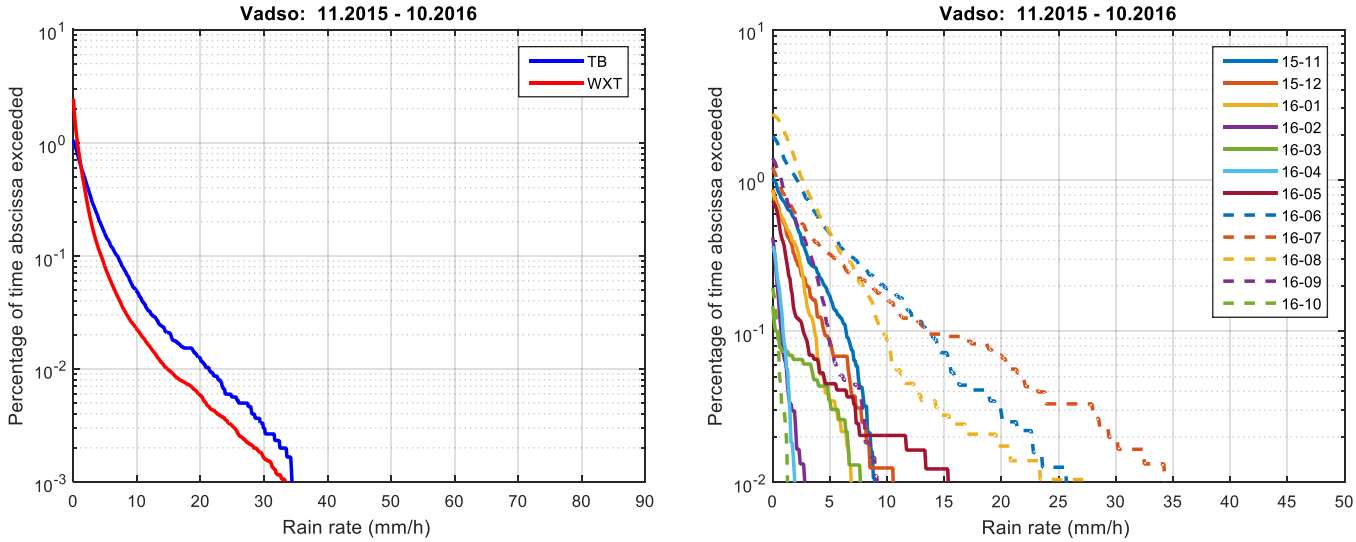

Figure 5-44. ***CCDF of rain for the period 11.2015 – 10.2016 and for each month with valid measurements during the period. Monthly data are from tipping bucket only.***

5.2.1.5 Attenuation and rain Isfjord Radio

The attenuation plots in this section show combined water vapour, cloud and rain attenuation as mentioned at the start of the chapter. The actual amount and intensity of precipitation are very low, with little variation through the year. But due to the very low elevation angle the total attenuation from all sources is very high.

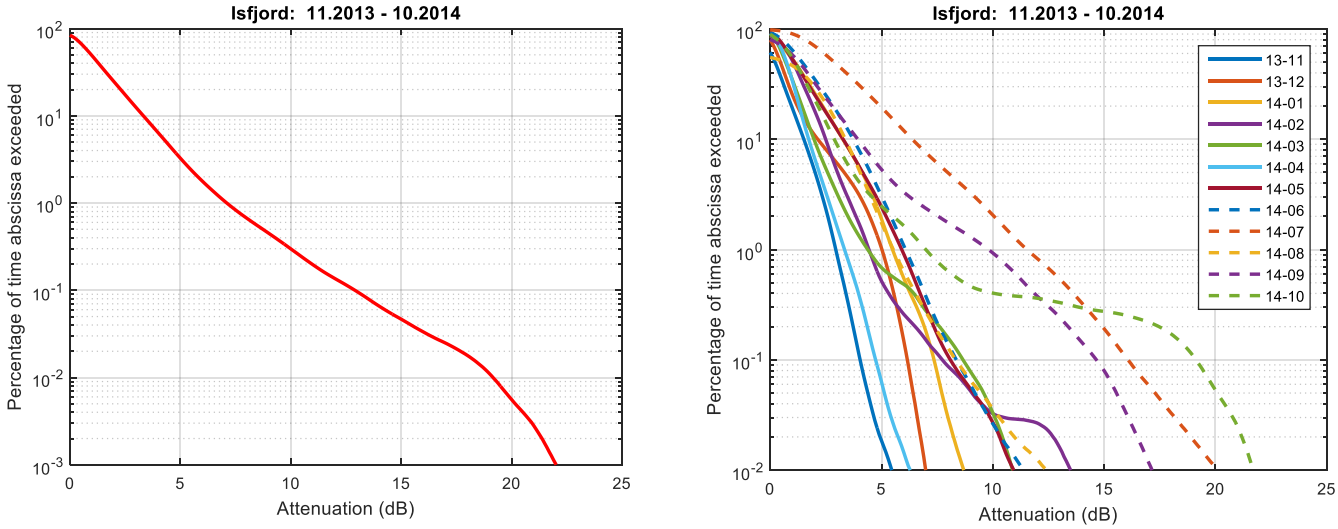

Figure 5-45. ***CCDF of attenuation for the period 11.2013 – 10.2014 and for each month with valid measurements during the period.***

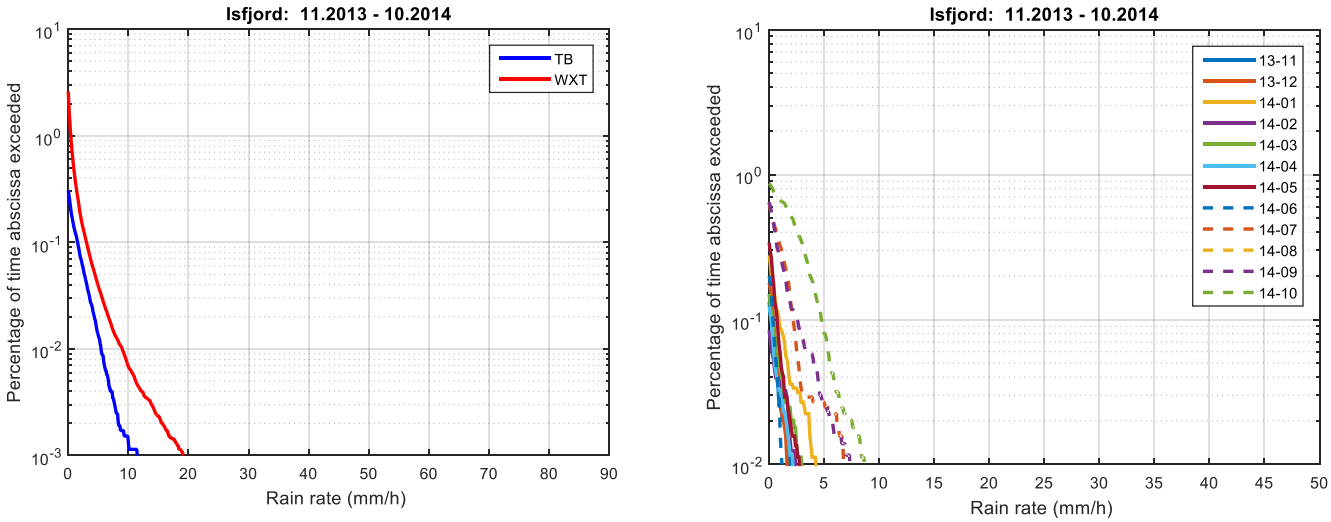

Figure 5-46. ***CCDF of rain rate for the period 11.2013 – 10.2014 and for each month with valid measurements during the period. monthly data is from Tipping bucket only.***

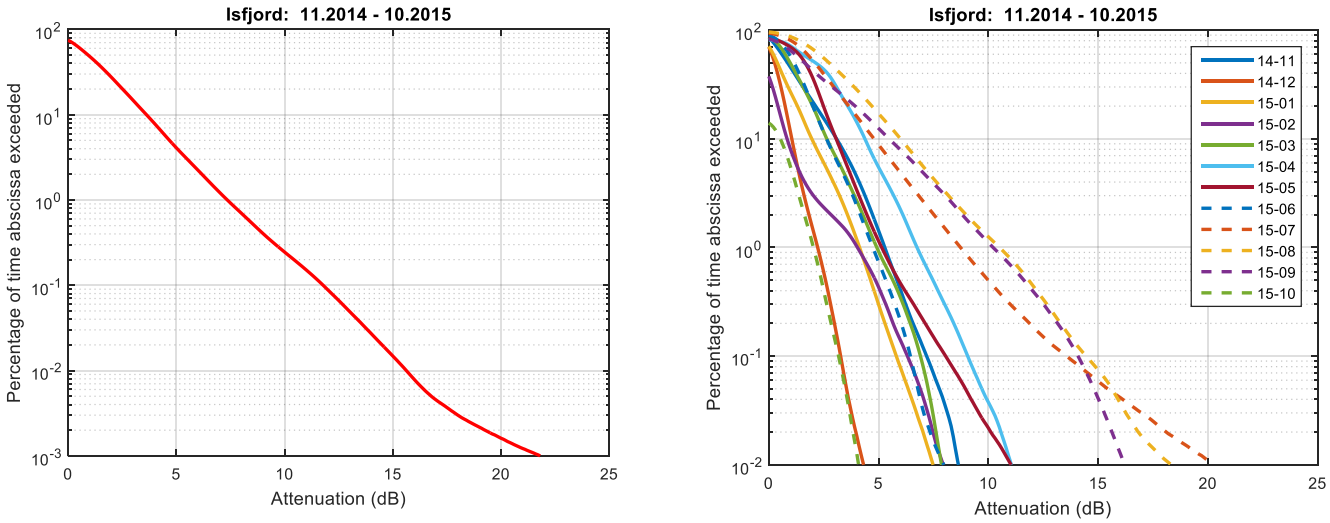

Figure 5-47. ***CCDF of attenuation for the period 11.2014 – 10.2015 and for each month with valid measurements during the period.***

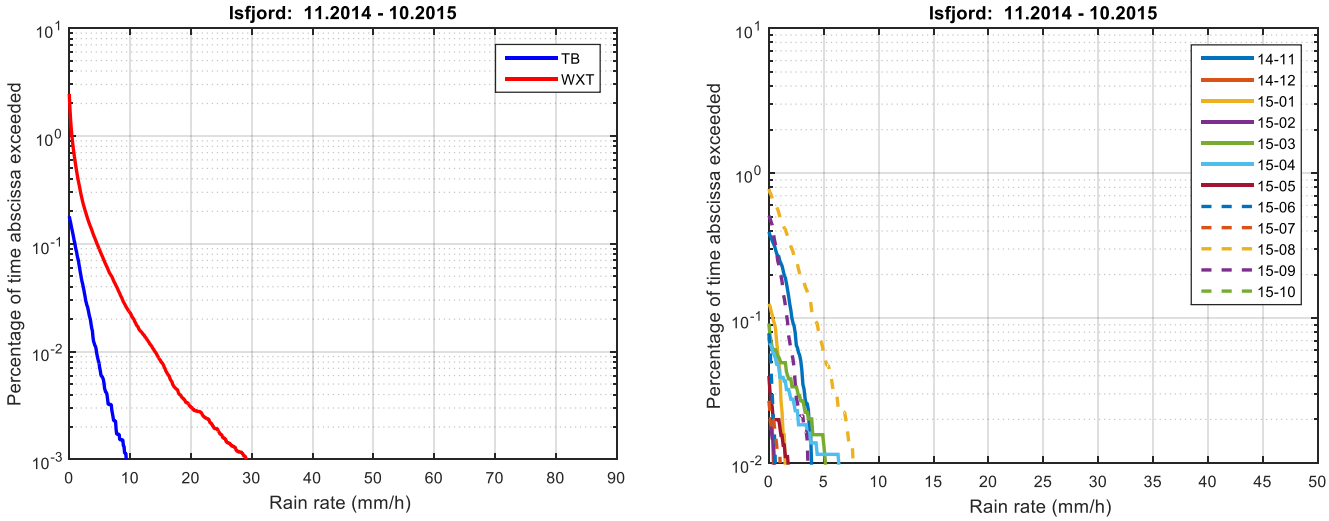

CoFigure 5-48. ***CCDF of rain for the period 11.2014 – 10.2015 and for each month with valid measurements during the period. Monthly data are from tipping bucket only.***

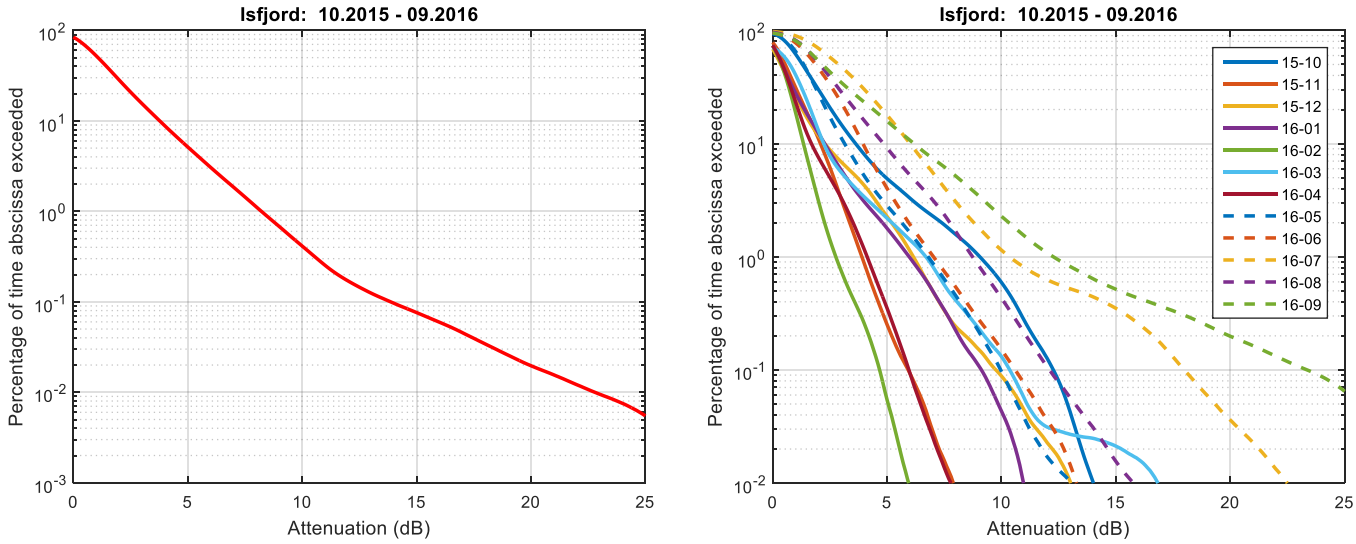

Figure 5-49. ***CCDF of attenuation for the period 10.2015 – 09.2016 and for each month with valid measurements during the period.***

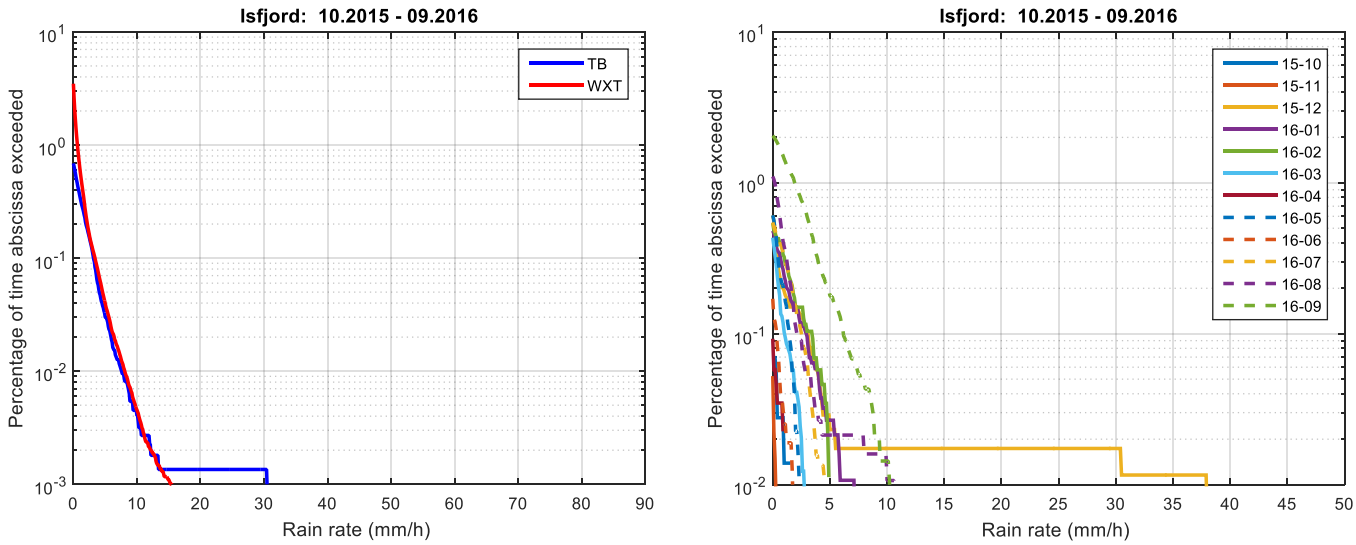

Figure 5-50. ***CCDF of rain for the period 01.2015 – 09.2016 and for each month with valid measurements during the period. Monthly data are from tipping bucket only.***

5.2.1.6 Attenuation and rain Bjørnøya

The attenuation plots in this section show combined water vapour, cloud and rain attenuation as mentioned at the start of the chapter. The actual amount and intensity of precipitation are very low, with little variation through the year. But due to the very low elevation angle the total attenuation from all sources is very high.

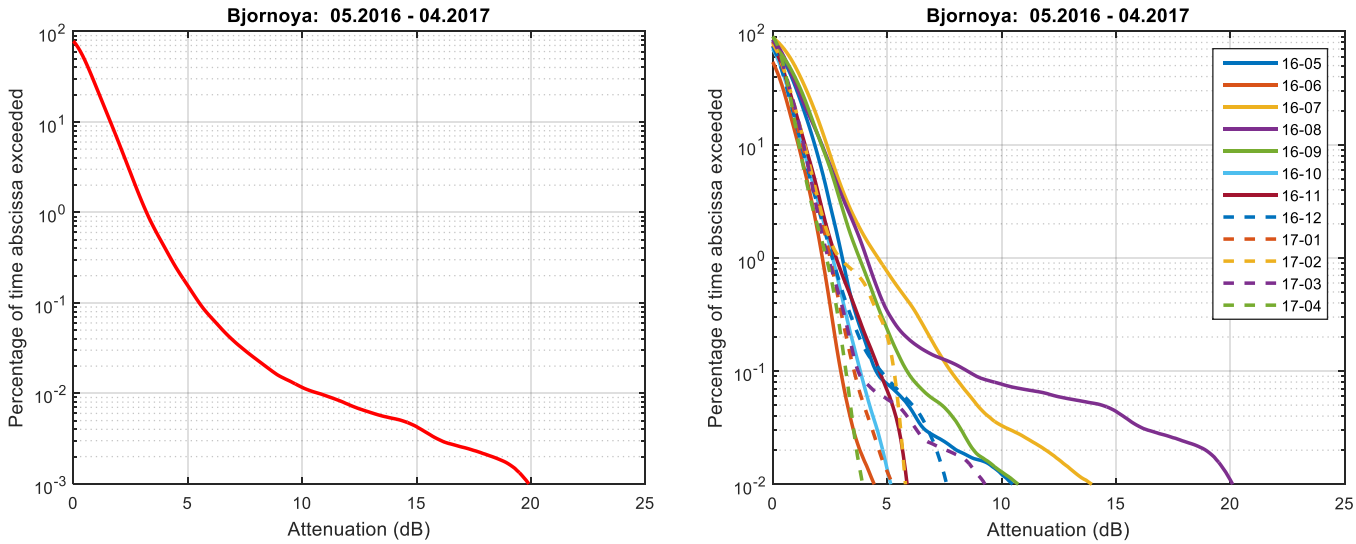

Figure 5-51. ***CCDF of attenuation for the period 05.2016 – 04.2017 and for each month with valid measurements during the period.***

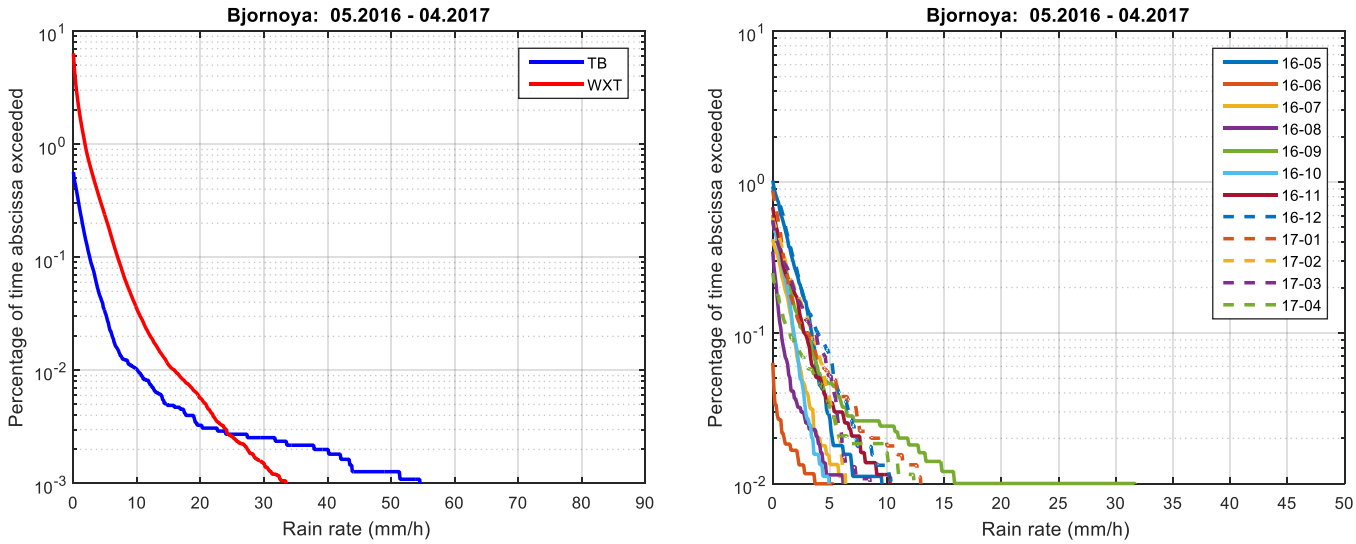

Figure 5-52. ***CCDF of rain rate for the period 05.2016 – 04.2017 and for each month with valid measurements during the period. Monthly data are from tipping bucket only.***

5.2.1.7 Attenuation and rain for all stations over 2 years

The combined plots for all stations in **Figure 5-53** show that even though the rain rates recorded at each of them were quite different the recorded attenuation levels are actually very similar between 10 and 0.1 % of time for all stations except Isfjord radio and Bjørnøya. At Røst there were fewer high-attenuation events and the more frequent rain also causes more frequent low attenuation. The increased path length trough troposphere at lower elevation angles seem to be compensated by the lower amount of rain and colder climate in the north. However, this is not true for Isfjord Radio where the very low elevation angle causes large attenuation levels even for very high percentages of time.

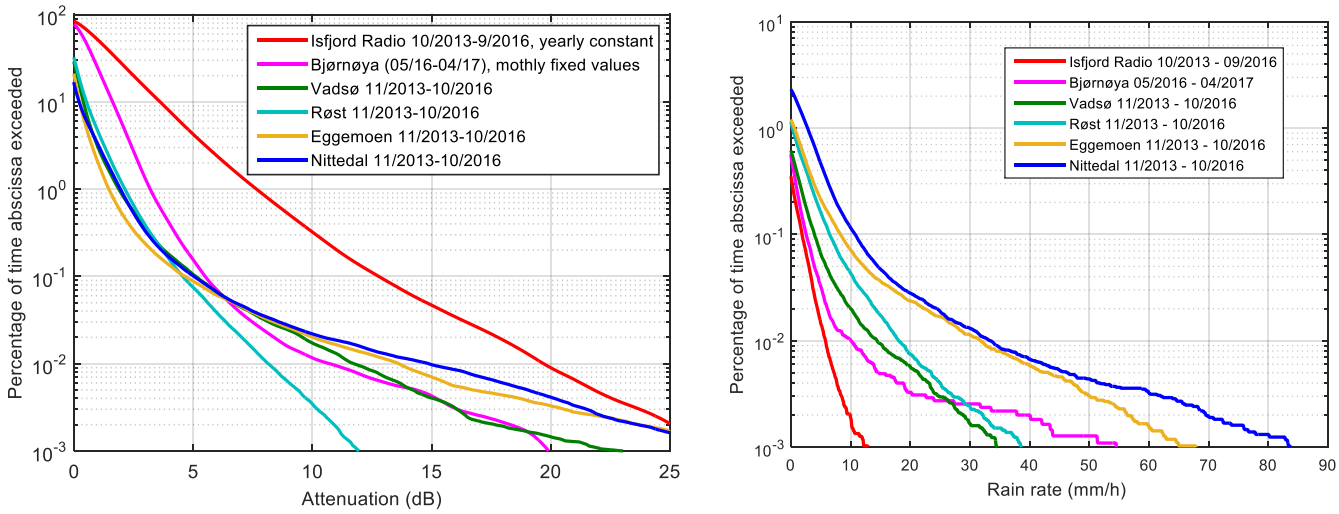

Figure 5-53. ***CCDF of attenuation and rain for all stations for the 3 years (1 year at Bjørnøya).***

Prediction errors in dB are shown in **Figure 5-54**.

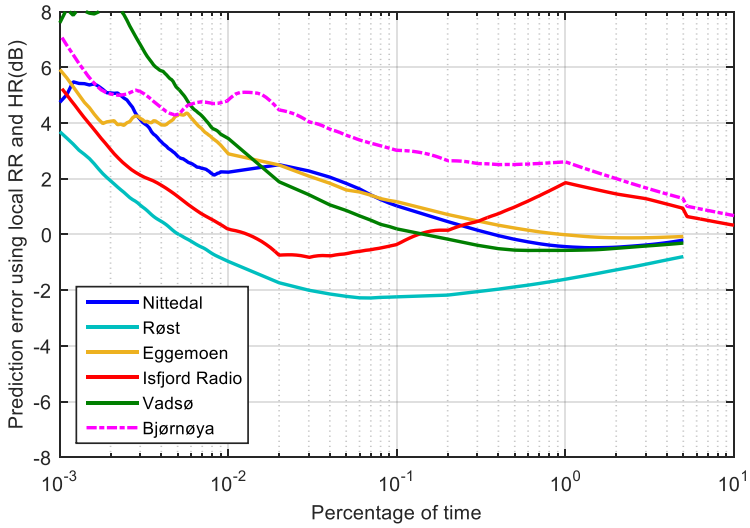

Figure 5-54. ***Prediction error compared with ITU-R prediction using measured rain rate and rain height from ITU-R maps. For Nittedal, Egemoen, Røst and Vadsø only rain attenuation prediction is used. For Isfjord Radio and Bjørnøya water vapour part of gaseous attenuation and cloud attenuation are also added.***

5.2.1.8 Attenuation and rain for Eggemoen – Nittedal diversity combination

Data availability during the first year was quite low due to two long periods without data. At Nittedal the oscillator was faulty during January 2014 and at Eggemoen the weather station was not operating correctly during August of the same year. Even with this low availability the results are not very different from the second year. As can be seen in the figures below significantly lower attenuation levels can be achieved using site separation of just 29.7 km. The reduction is most prominent for high attenuation levels.

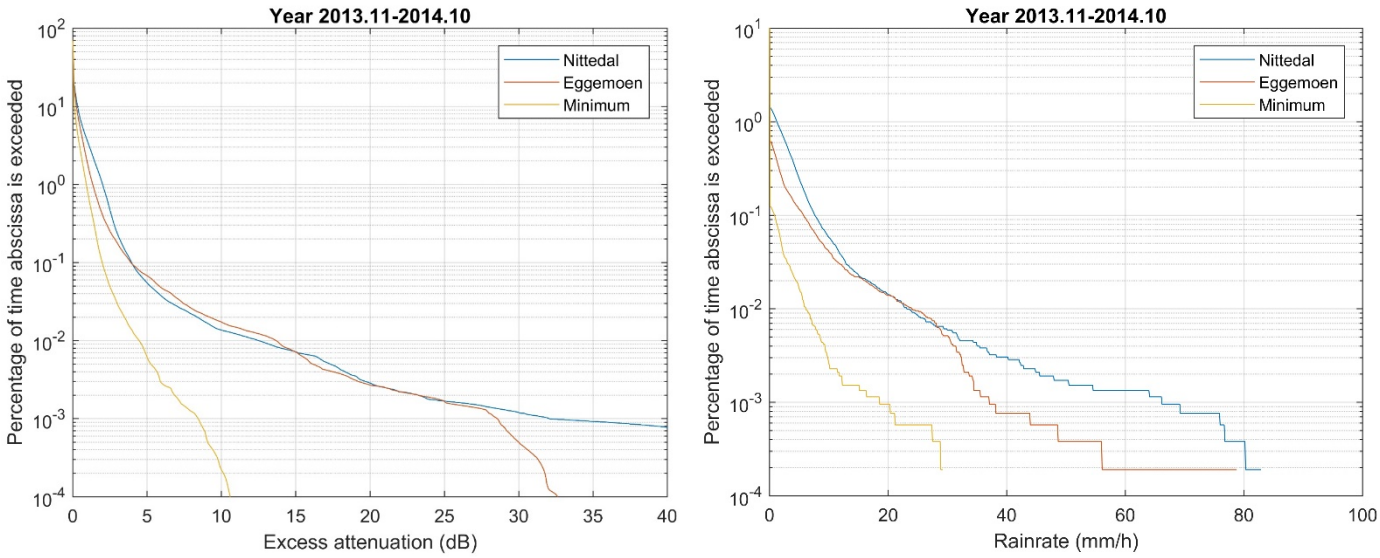

Figure 5-55. ***Attenuation and rain rate with diversity combination of Eggemoen and Nittedal, 2013.11 – 2014.10.***

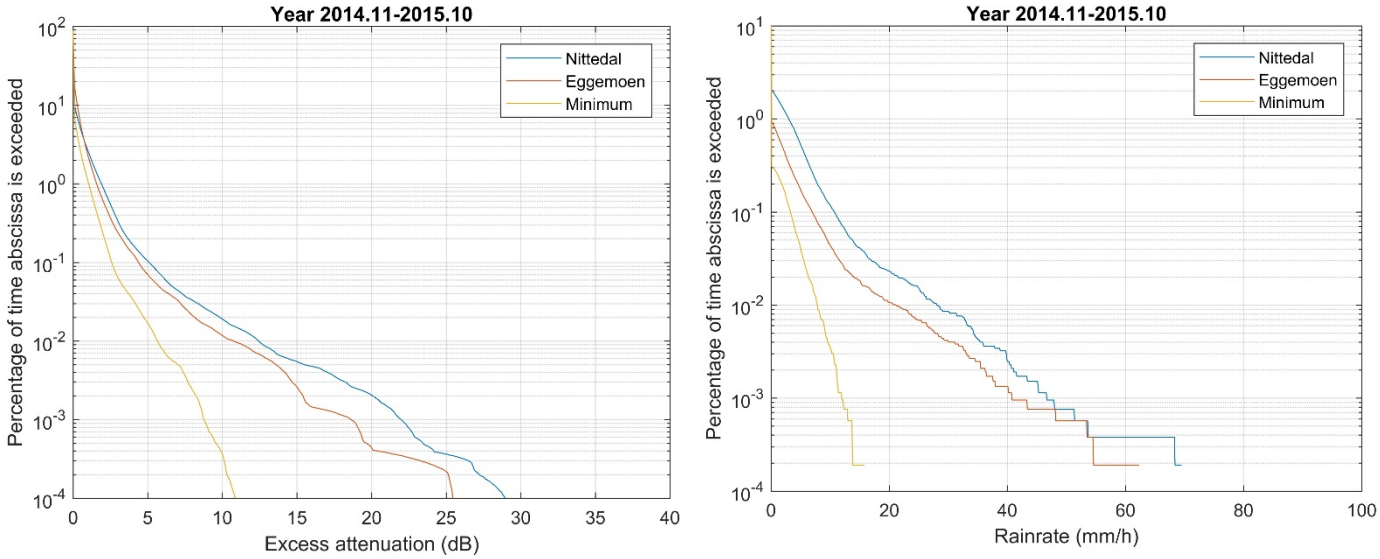

Figure 5-56. ***Attenuation and rain rate with diversity combination of Eggemoen and Nittedal, 2014.11 – 2015.10.***

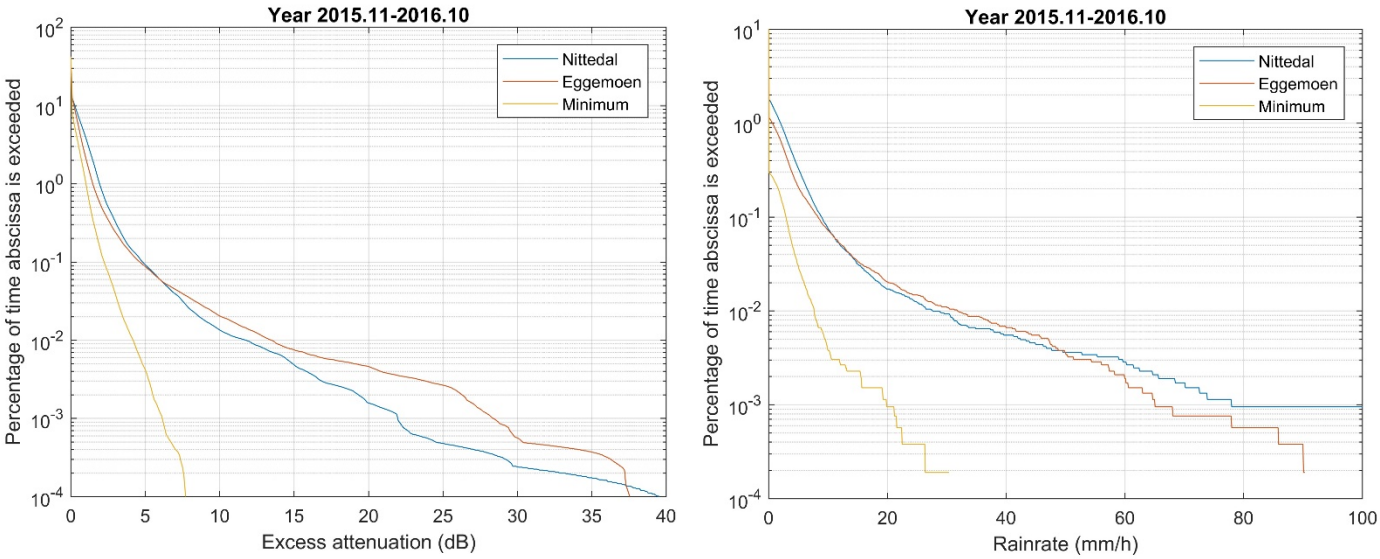

Figure 5-57. ***Attenuation and rain rate with diversity combination of Eggemoen and Nittedal, 2015.11 – 2016.10.***

5.2.2 Second order statistics of rain attenuation

The long-term second order statistical analyses of rain attenuation for the five stations were performed using two years of data. The fade duration and fade slope results where extracted from the measurements.

The fade duration is usually described by two different types of conditional cumulative distributions:

- The probability of occurrence of fades of duration d longer than D (s), given that the attenuation a is greater than A (dB), $P_n(d > D \mid a > A)$. This probability can be estimated from the ratio of the number of fades of duration longer than D to the total number of fades observed, given that the threshold A is exceeded.

- The cumulative exceedance probability, or, equivalently, the total fraction (between 0 and 1) of fade time due to fades of duration d longer than D (s), given that the attenuation a is greater than A (dB), $F(d > D \mid a > A)$. This probability can be estimated from the ratio of the total fading time due to fades of duration longer than D given that the threshold A is exceeded, to the total exceedance.

The fade slope $\zeta(t)$ is calculated as the difference of two rain attenuation values, $A(t)$, divided by the time interval Δt between them at different attenuation levels as:

$$\zeta(t) = \frac{A(t + \Delta t) - A(t)}{\Delta t} \qquad \text{(dB/s)}$$

Time interval used was 60s for all stations except Isfjord Radio and Bjørnøya, where 200 and 120s were used instead. Figs 4.2.1 to 4.2.10 show yearly fade duration statistic $P_n(d > D \mid a > A)$ and $F(d > D \mid a > A)$ for the six stations utilizing measurement data for the 3 years of measurement (1 year for Bjørnøya). For the same period, fade slope probability density function (PDF) as well as the cumulative distribution function (CDF) for the absolute fade slope values for all five stations are shown in Figs. 4.2.11 to 4.2.20.

5.2.2.1 Fade duration Nittedal

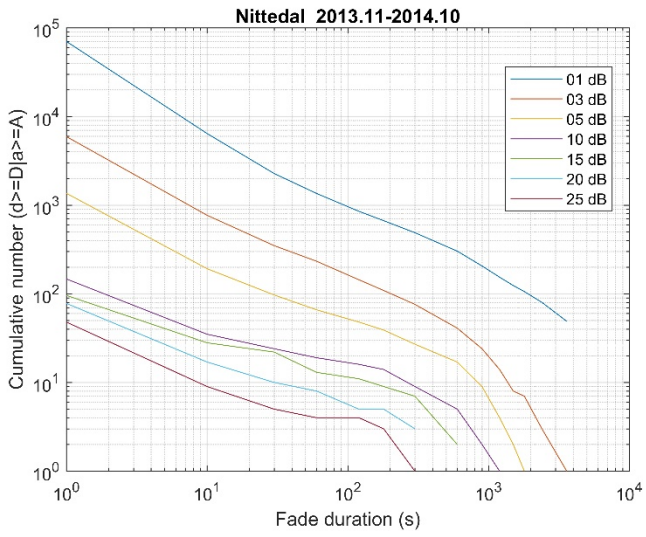

a)

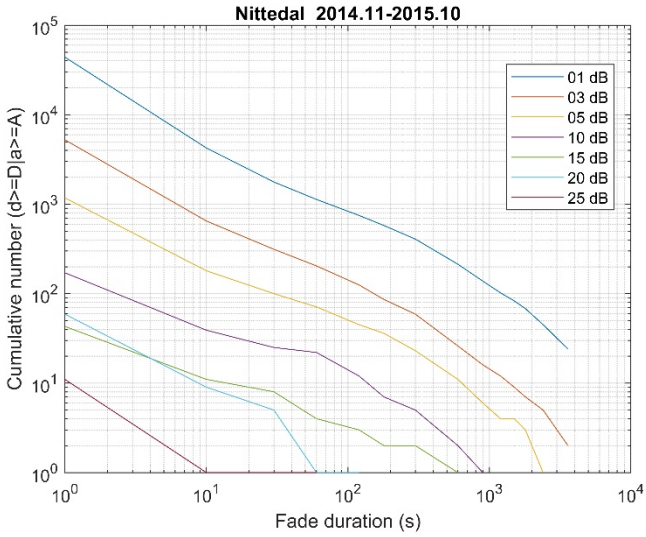

b)

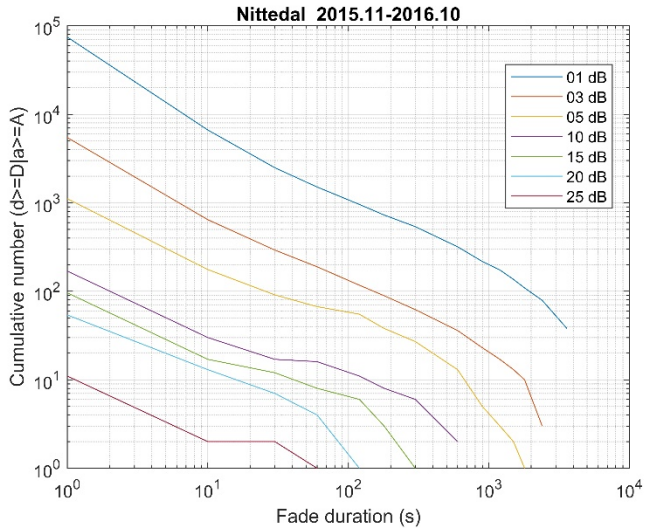

c)

Figure 5-58. Cumulative distributions of fade durations for Nittedal, *d > D | a > A: a) Year 2013.11-2014.10, b) Year 2014.11-2015.10, and c) Year 2015.11-2016.10*.

5.2.2.2 Fade duration Eggemoen

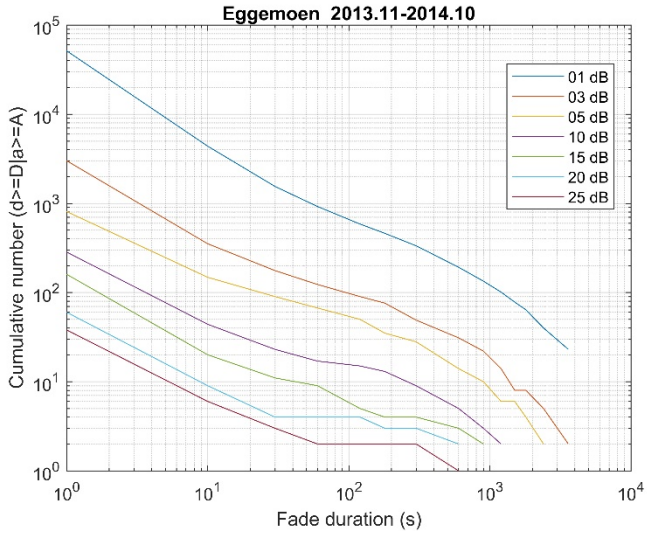

a)

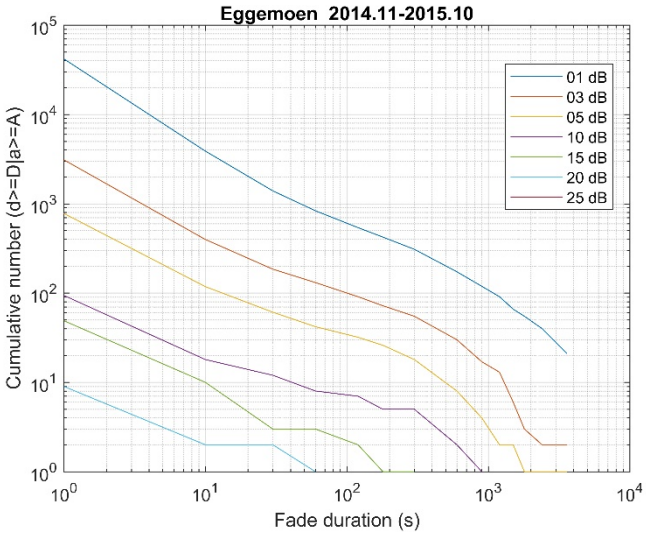

b)

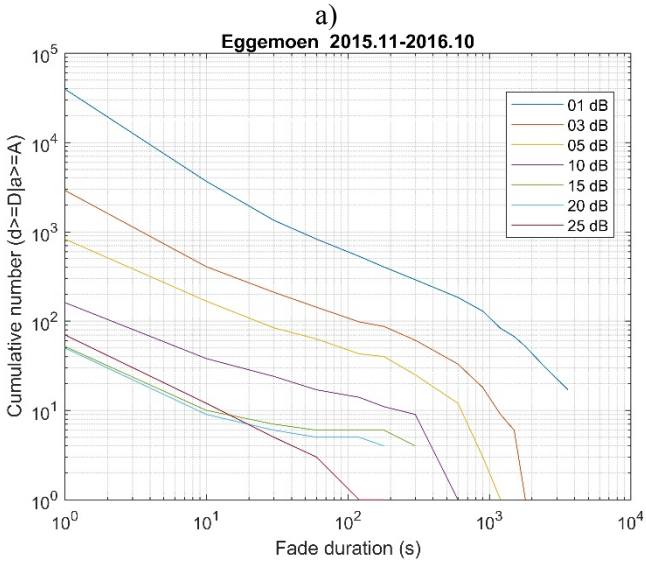

c)

Figure 5-59. Cumulative distributions of fade durations for Eggemoen, *d > D | a > A: a) Year 2013.11-2014.10, b) Year 2014.11-2015.10, and c) Year 2015.11-2016.10*.

5.2.2.3 Fade duration Røst

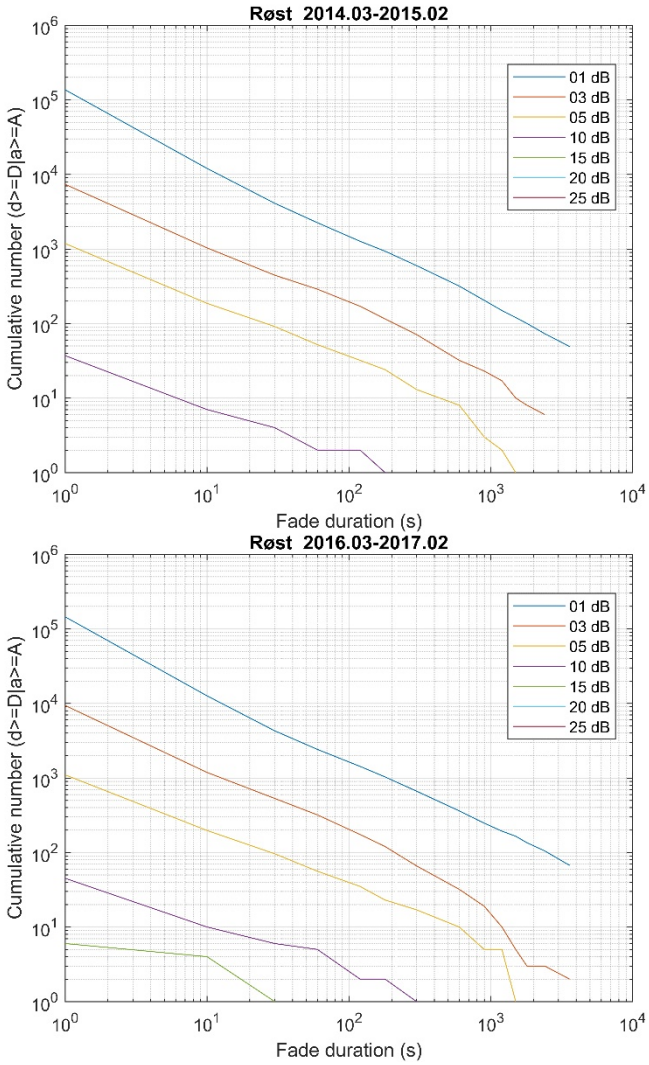

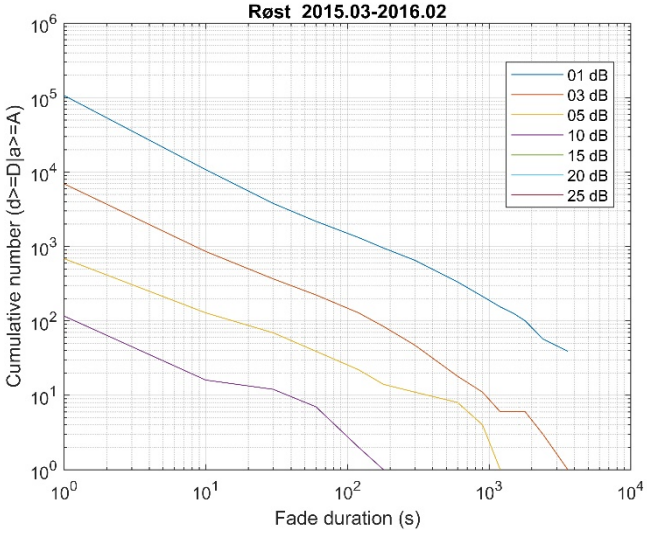

Figure 5-60. Cumulative distributions of fade durations for Røst, *d > D | a > A: a) Year 2014.03-2015.02, b) Year 2015.03-2016.02, and c) Year 2016.03-2017.02*.

5.2.2.4 Fade duration Vadsø

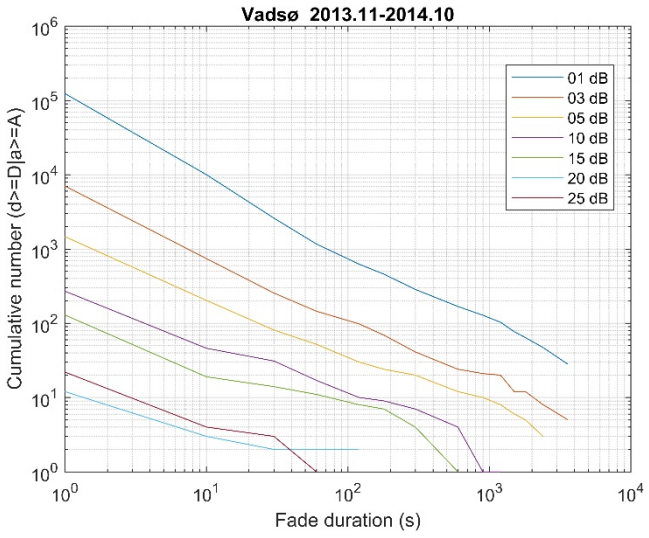

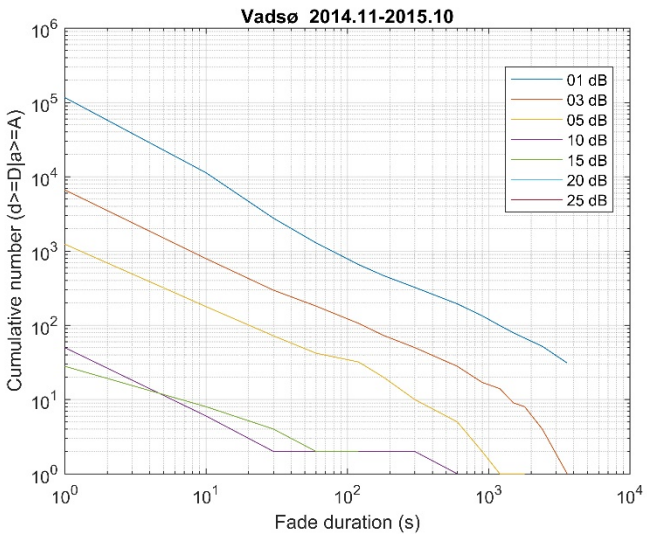

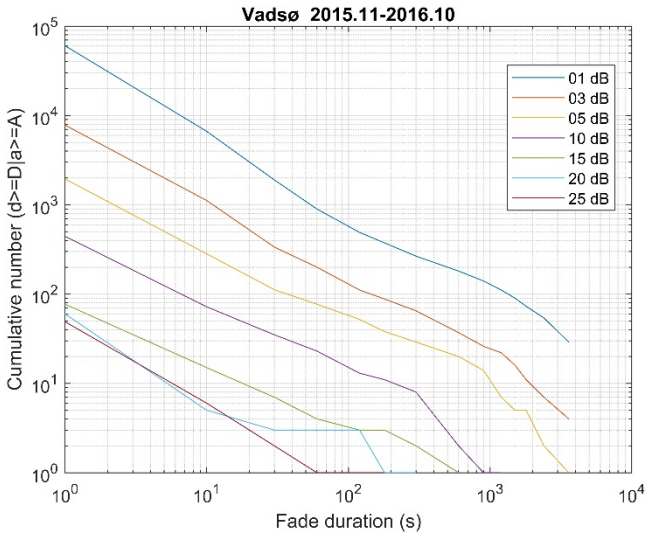

Figure 5-61. Cumulative distributions of fade durations for Vadsø, *d > D | a > A: a) Year 2013.11-2014.10, b) Year 2014.11-2015.10, and c) Year 2015.11-2016.10*.

5.2.2.5 Fade duration Isfjord Radio

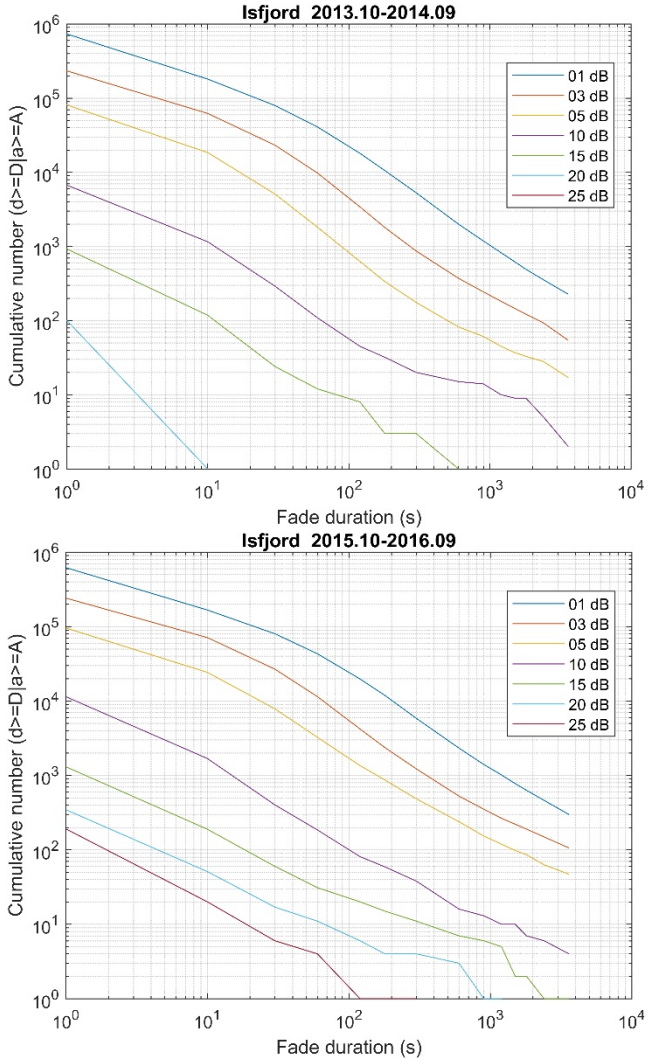

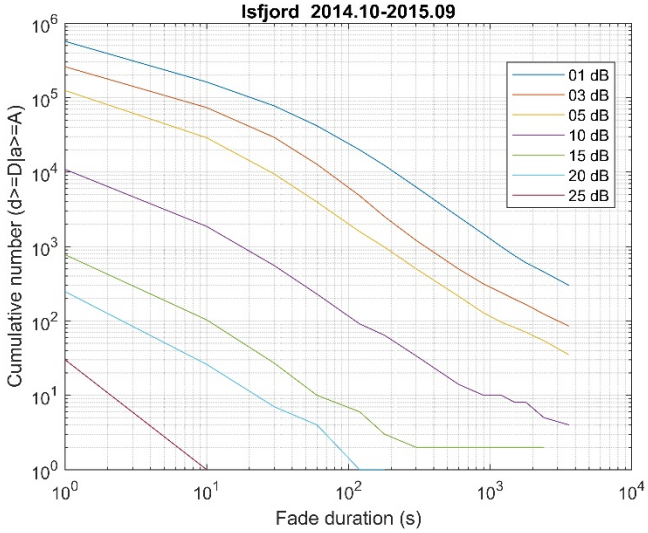

Figure 5-62. Cumulative distributions of fade durations for Isfjord Radio, *d > D | a > A: a) Year 2013.10-2014.09, b) Year 2014.10-2015.09, and c) Year 2015.10-2016.09*.
Distributions are derived from unfiltered beacon data.

5.2.2.6 Fade duration Bjørnøya

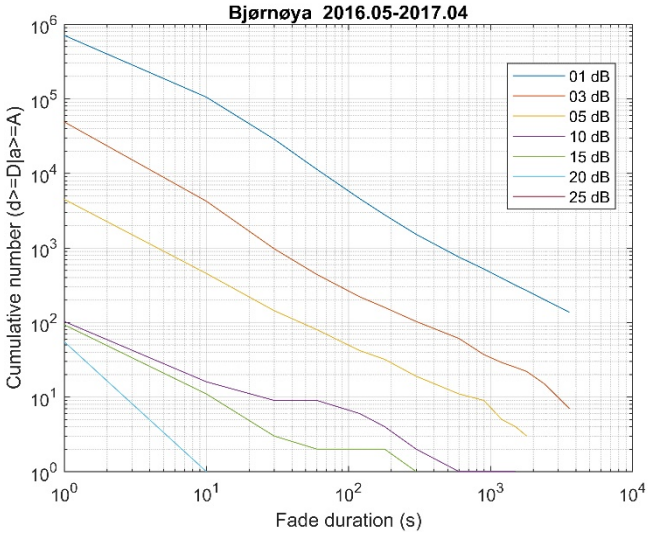

Figure 5-63. Cumulative distributions of fade durations for Bjørnøya, *Year 2016.05-2017.04*.

5.2.2.7 Fade slope Nittedal

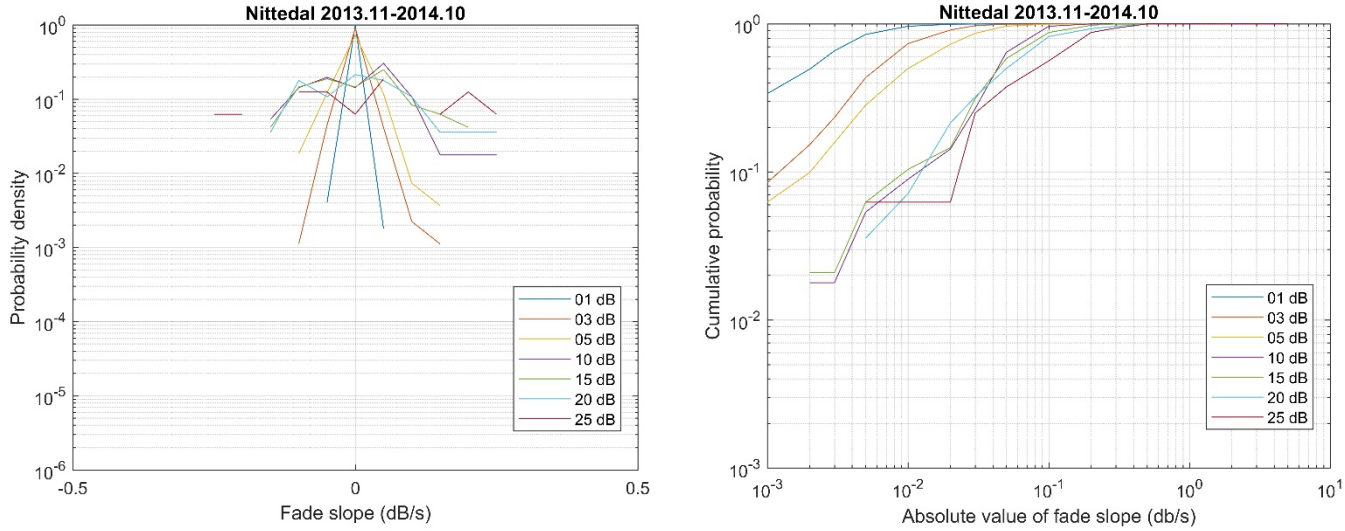

Figure 5-64. ***PDF of fade slope and CDF of absolute fade slope values derived from filtered beacon data collected from the Nittedal station for the period 11.2013 – 10.2014.***

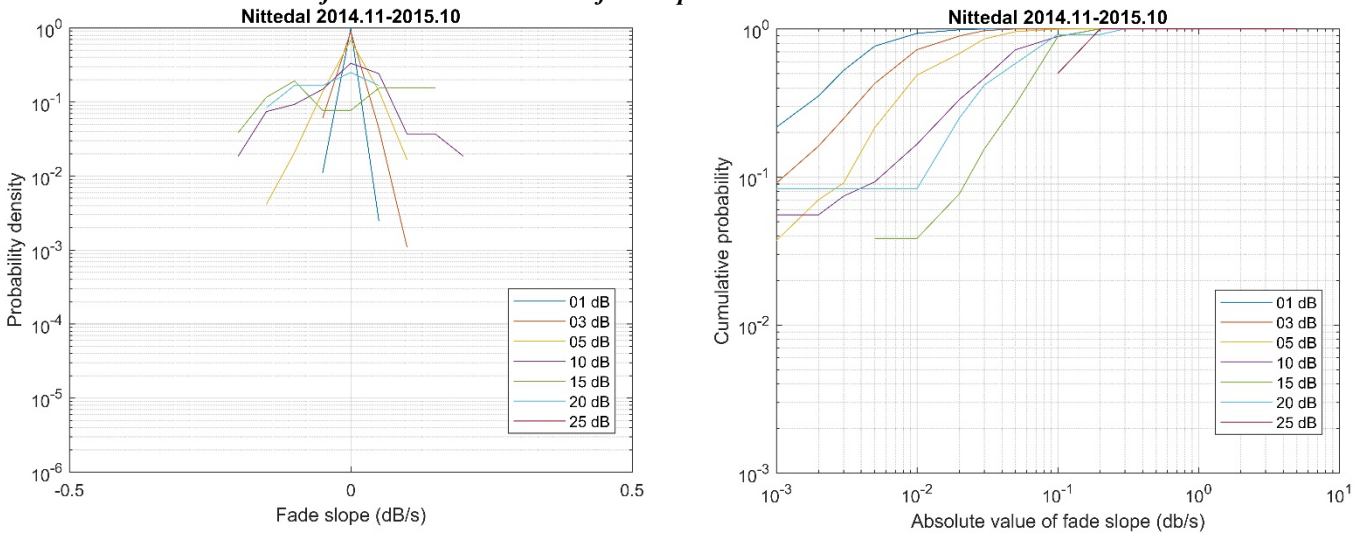

Figure 5-65. ***PDF of fade slope and CDF of absolute fade slope values derived from filtered beacon data collected from the Nittedal station for the period 11.2014 – 10.2015.***

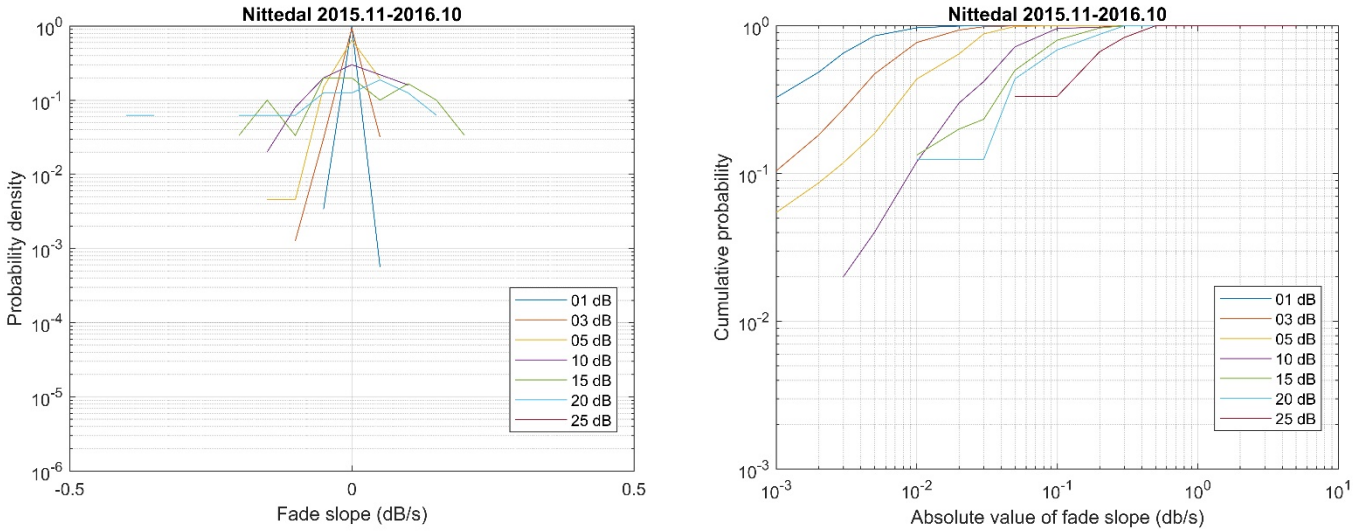

Figure 5-66. ***PDF of fade slope and CDF of absolute fade slope values derived from filtered beacon data collected from the Nittedal station for the period 11.2015 – 10.2016.***

5.2.2.8 Fade slope Eggemoen

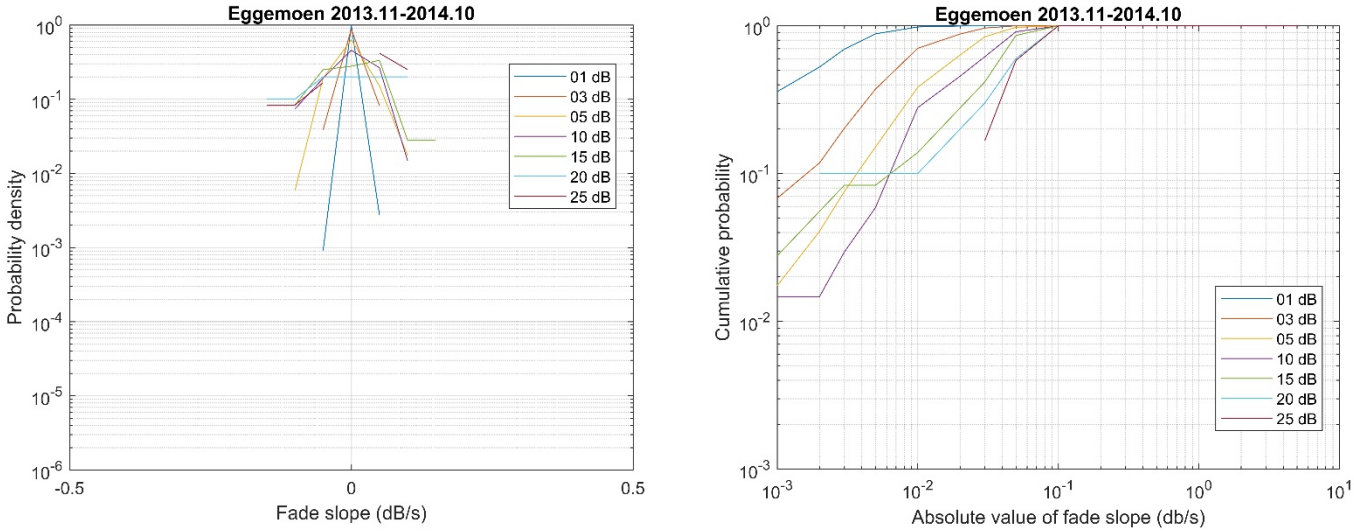

Figure 5-67. ***PDF of fade slope and CDF of absolute fade slope values derived from filtered beacon data collected from the Eggemoen station for the period 11.2013 – 10.2014.***

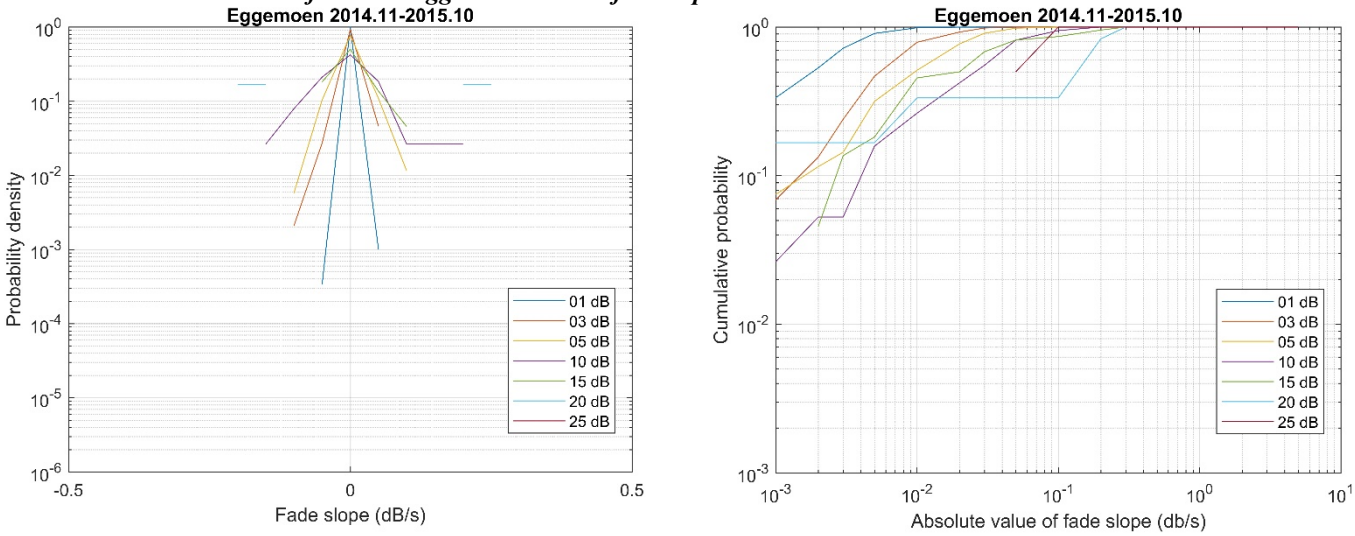

Figure 5-68. ***PDF of fade slope and CDF of absolute fade slope values derived from filtered beacon data collected from the Eggemoen station for the period 11.2014 – 10.2015.***

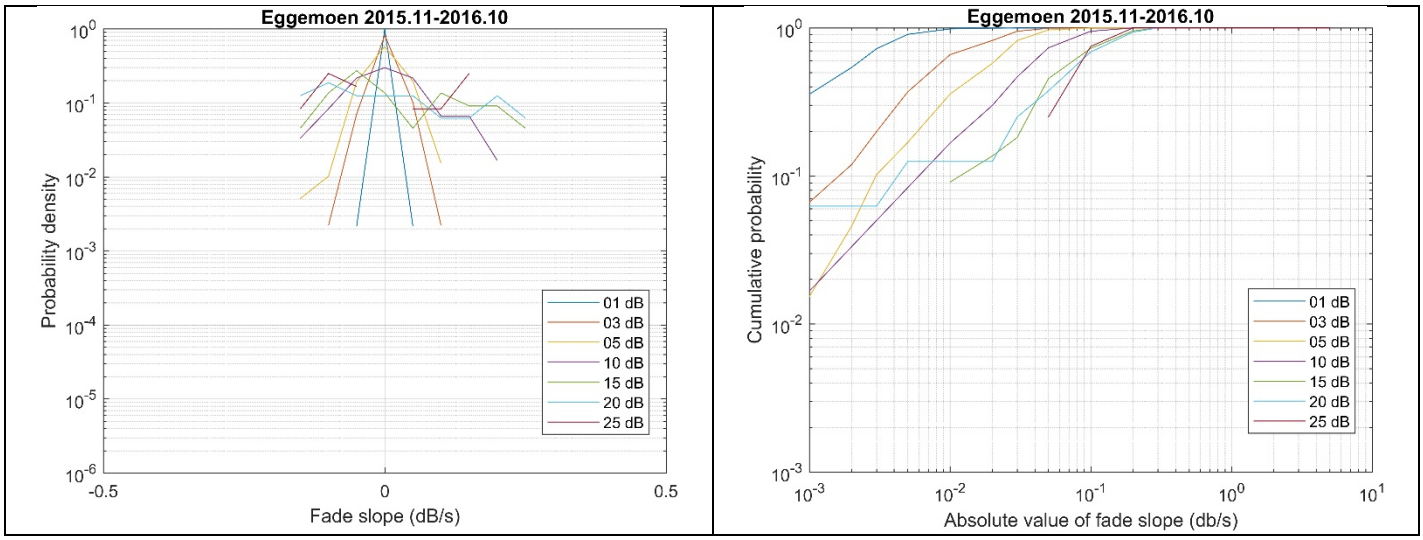

Figure 5-699. ***PDF of fade slope and CDF of absolute fade slope values derived from filtered beacon data collected from the Eggemoen station for the period 11.2015 – 10.2016.***

5.2.2.9 Fade slope Røst

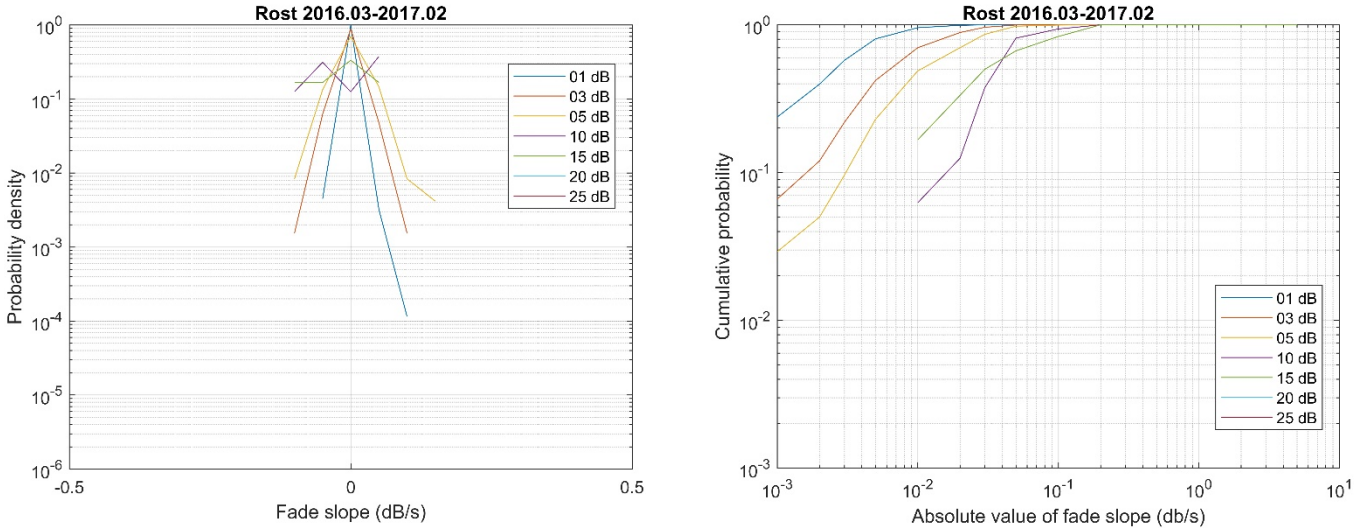

Figure 5-70. ***PDF of fade slope and CDF of absolute fade slope values derived from filtered beacon data collected from the Røst station for the period 03.2014-02.2015.***

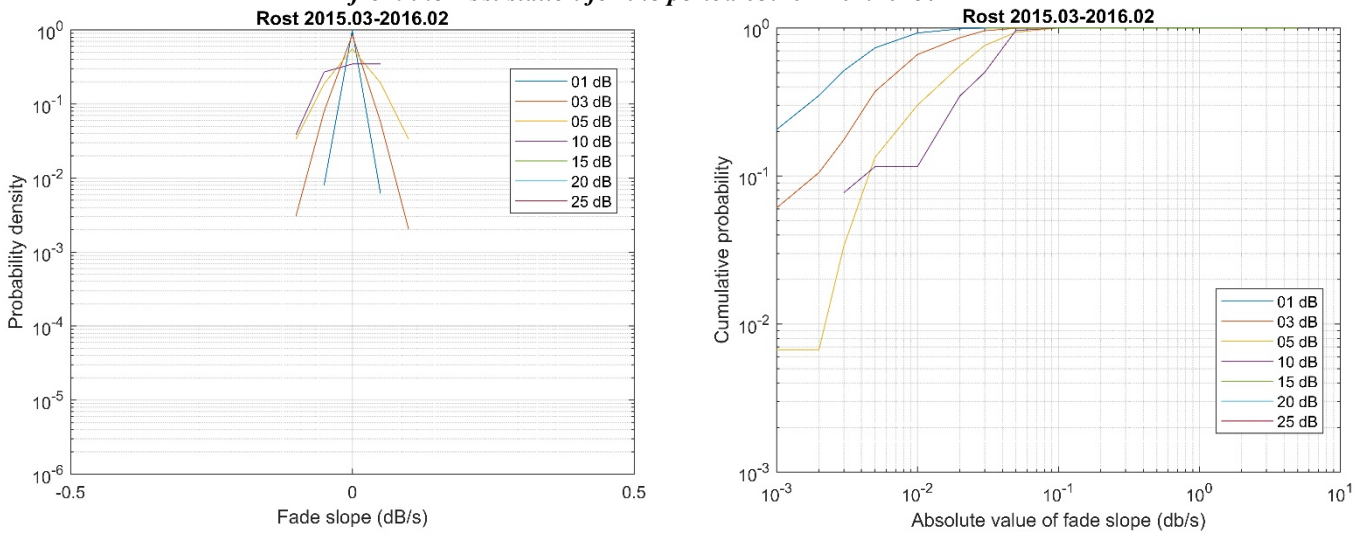

Figure 5-71. ***PDF of fade slope and CDF of absolute fade slope values derived from filtered beacon data collected from the Røst station for the period 03.2015 – 02.2016.***

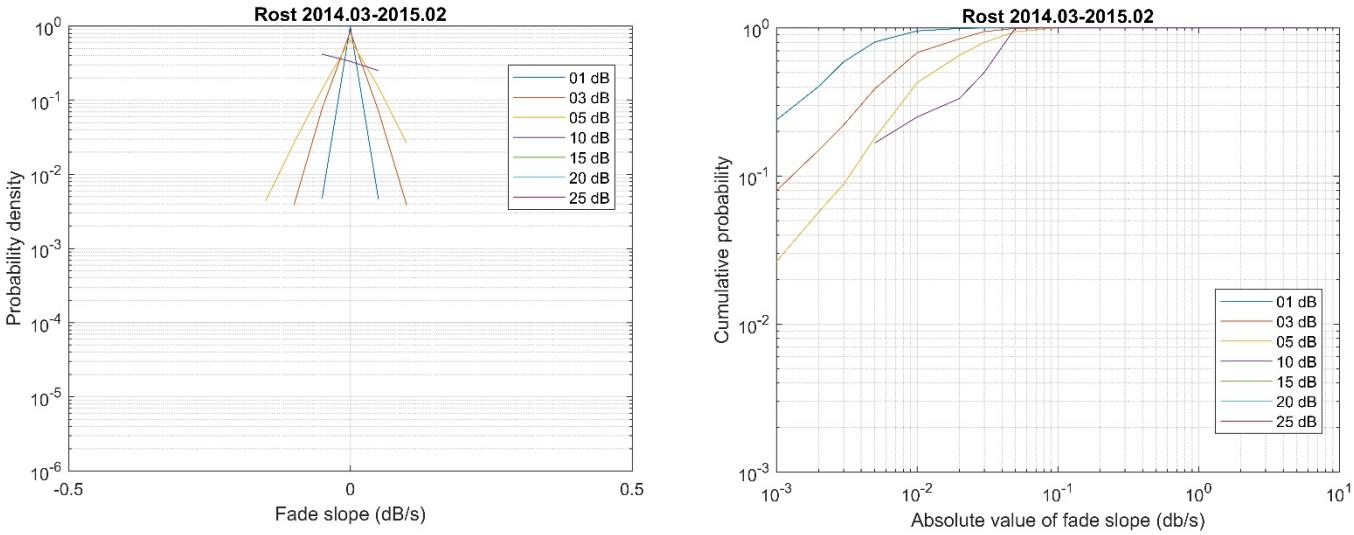

Figure 5-72. ***PDF of fade slope and CDF of absolute fade slope values derived from filtered beacon data collected from the Røst station for the period 03.2016 – 02.2017.***

5.2.2.10 Fade slope Vadsø

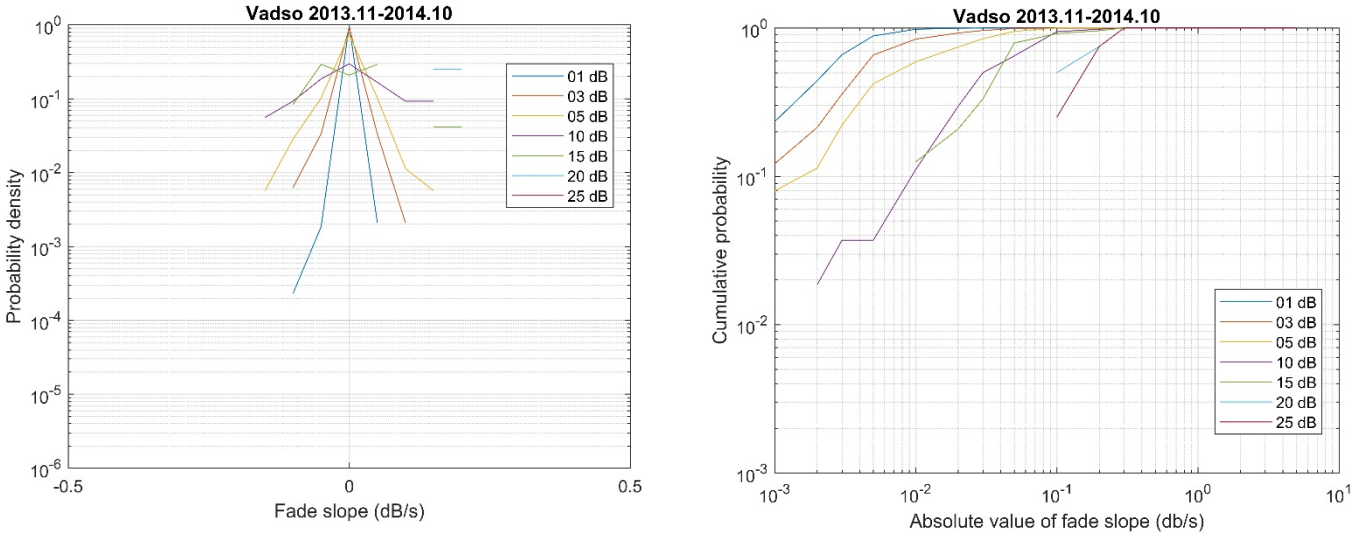

Figure 5-73. ***PDF of fade slope and CDF of absolute fade slope values derived from filtered beacon data collected from the Vadsø station for the period 11.2013 – 10.2014.***

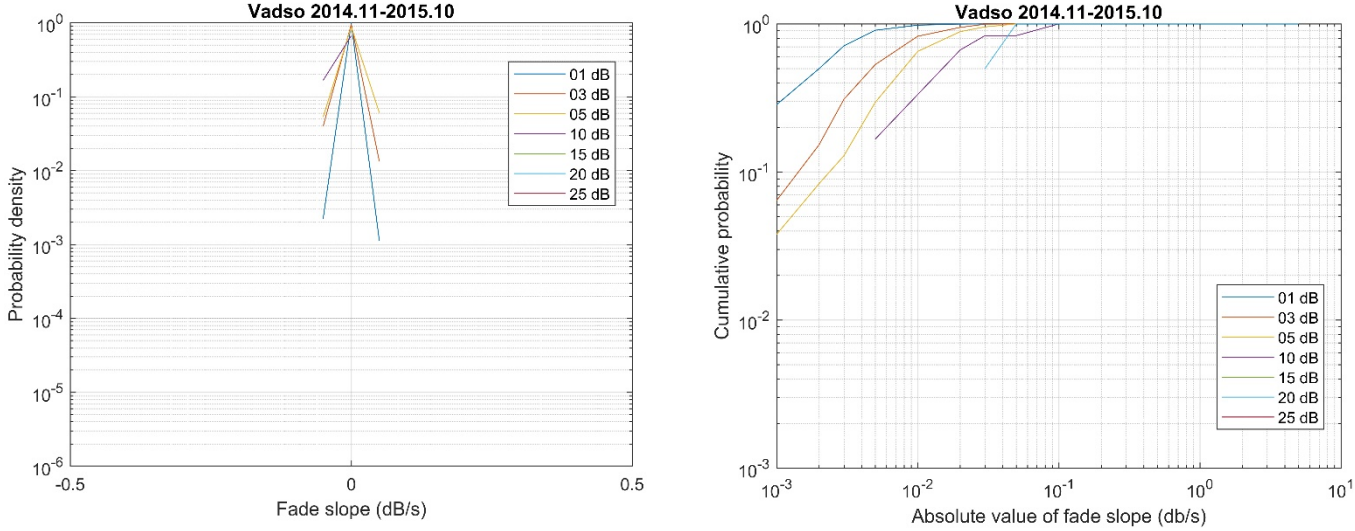

Figure 5-74. ***PDF of fade slope and CDF of absolute fade slope values derived from filtered beacon data collected from the Vadsø station for the period 11.2014 – 10.2015.***

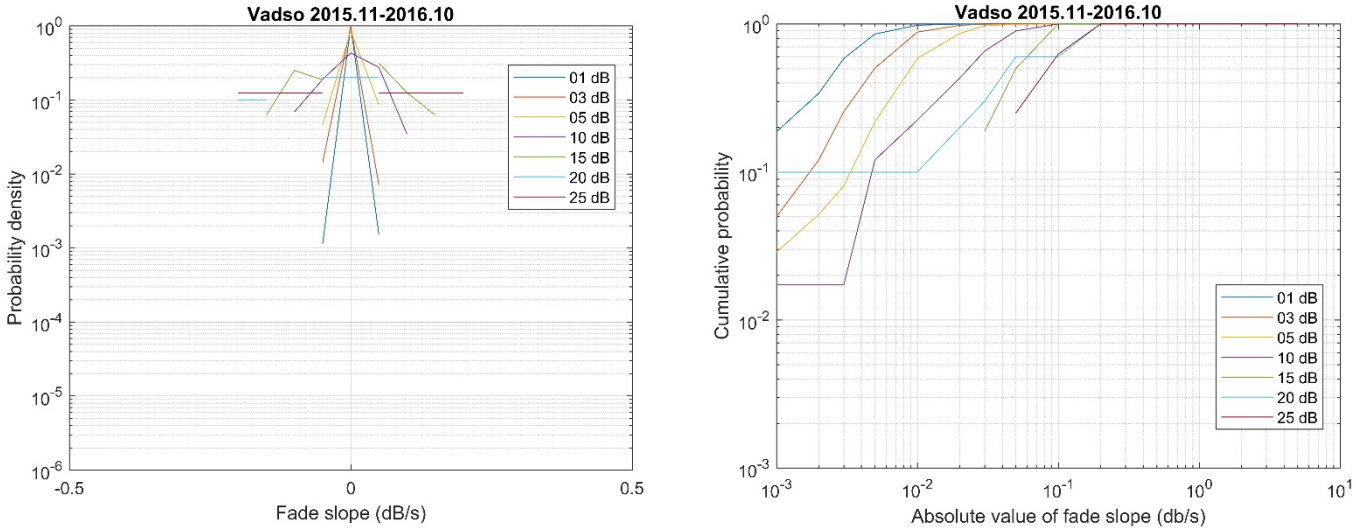

Figure 5-85. ***PDF of fade slope and CDF of absolute fade slope values derived from filtered beacon data collected from the Vadsø station for the period 11.2015 – 10.2016.***

5.2.2.11 Fade slope Isfjord Radio

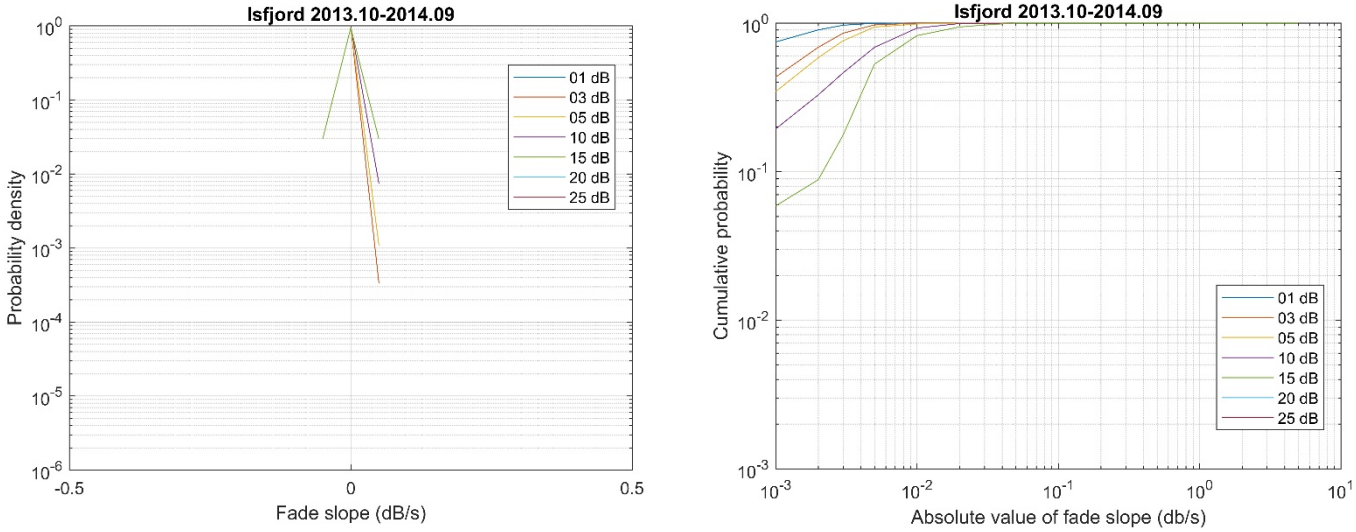

Figure 5-75. ***PDF of fade slope and CDF of absolute fade slope values derived from filtered beacon data collected from the Isfjord Radio station for the period 10.2013 – 09.2014.***

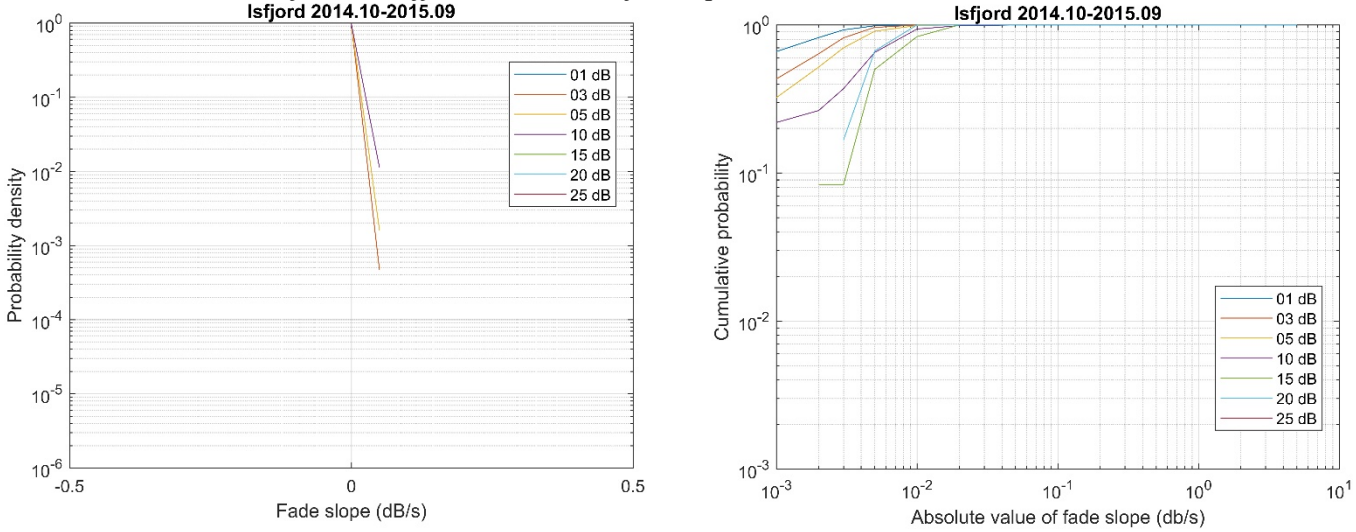

Figure 5-76. ***PDF of fade slope and CDF of absolute fade slope values derived from filtered beacon data collected from the Isfjord station for the period 10.2014 – 09.2015.***

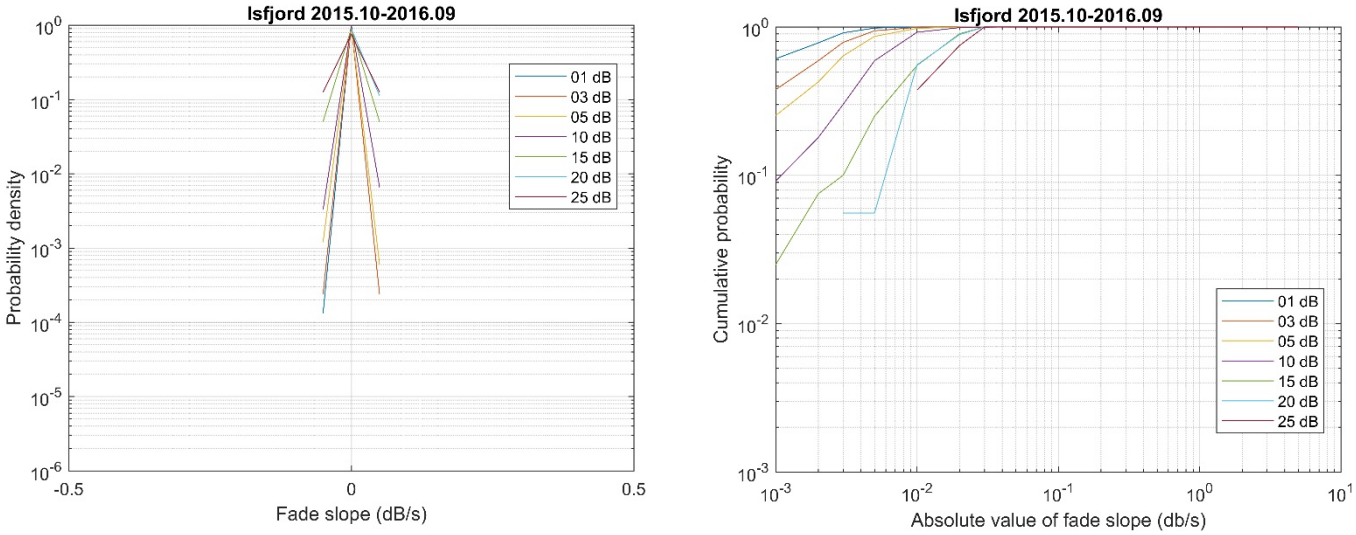

Figure 5-77. ***PDF of fade slope and CDF of absolute fade slope values derived from filtered beacon data collected from the Isfjord Radio station for the period 10.2015 – 09.2016.***

5.2.2.12 Fade slope Bjørnøya

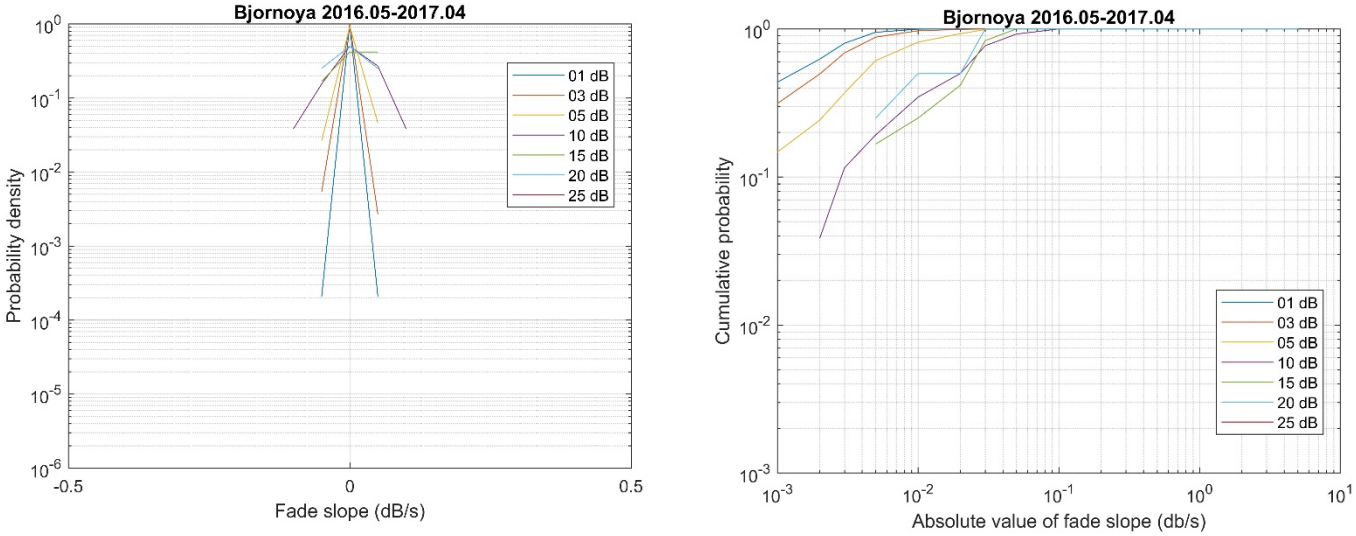

Figure 5-78. ***PDF of fade slope and CDF of absolute fade slope values derived from filtered beacon data collected from the Bjørnøya station for the period 05.2016 – 04.2017.***

5.2.3 Scintillation

The resampled signal was filtered using a 6th order Butterworth filter in order to separate slow-varying attenuation from fast signal changes due to scintillation and noise. The cutoff frequency of this filter is different for each location and a different value is also used for clear-sky and attenuation conditions (as identified using the classification tool). The frequencies used based on spectral analysis of numerous events through the year at each station and are given in Table 4.5.

Location	Isfjord Radio	Vadsø	Røst	Eggemoen	Nittedal
Clear-air cutoff [mHz]	1	8	10	12	12
Attenuation cutoff [mHz]	4	11	15	20	20

Table 5-9. ***Filter Cutoff frequencies.***

Data plotted in the following figures were not scaled as scintillation is relatively evenly distributed and there is always some scintillation present. This is in contrast with rain attenuation which is concentrated in events and is zero outside of these. Scintillation has also zero average (for weak scintillation) and scaling with availability

would cause it to be skewed. It should be noted that the stations at Eggemoen and Isfjord Radio used larger antennas (1.8 m vs 1.2 m on others) this effectively reduces scintillation severity due to aperture averaging. The results from the different stations are therefore not precisely comparable, though the effect is relatively small.

5.2.3.1 Scintillation amplitude Nittedal

For Nittedal the scintillation amplitude is low and while showing large relative changes through the year stays low even in the summer months. The distribution is also close to normal.

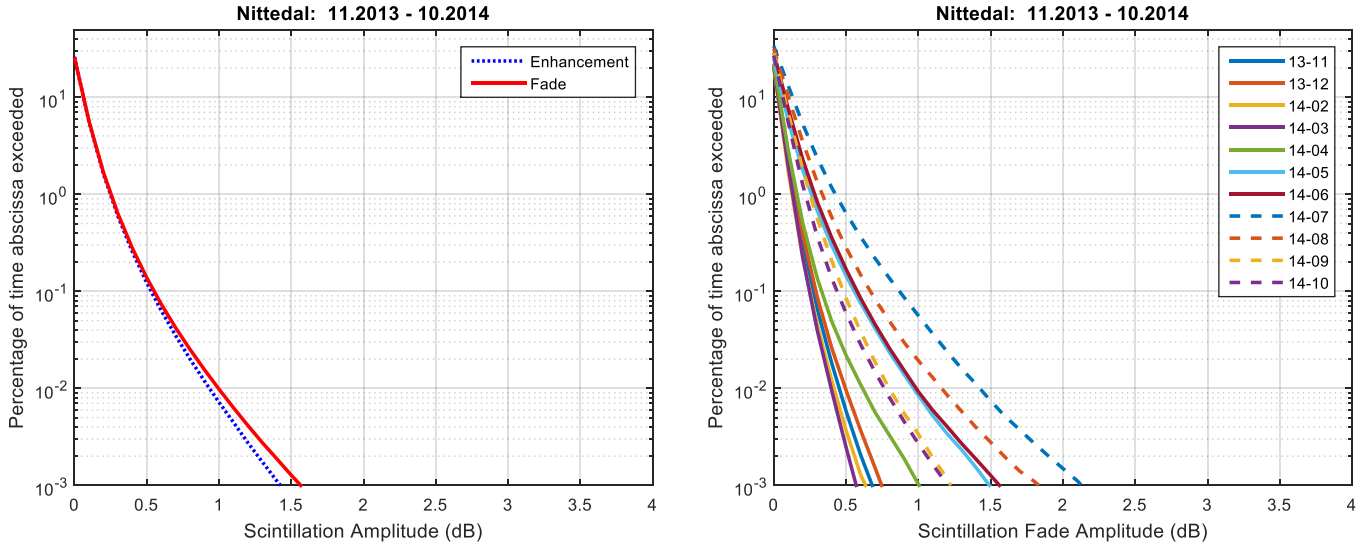

Figure 5-79. ***CCDF of scintillation amplitude for the period 11.2013 - 10.2014 and for each month with valid measurements during the period.***

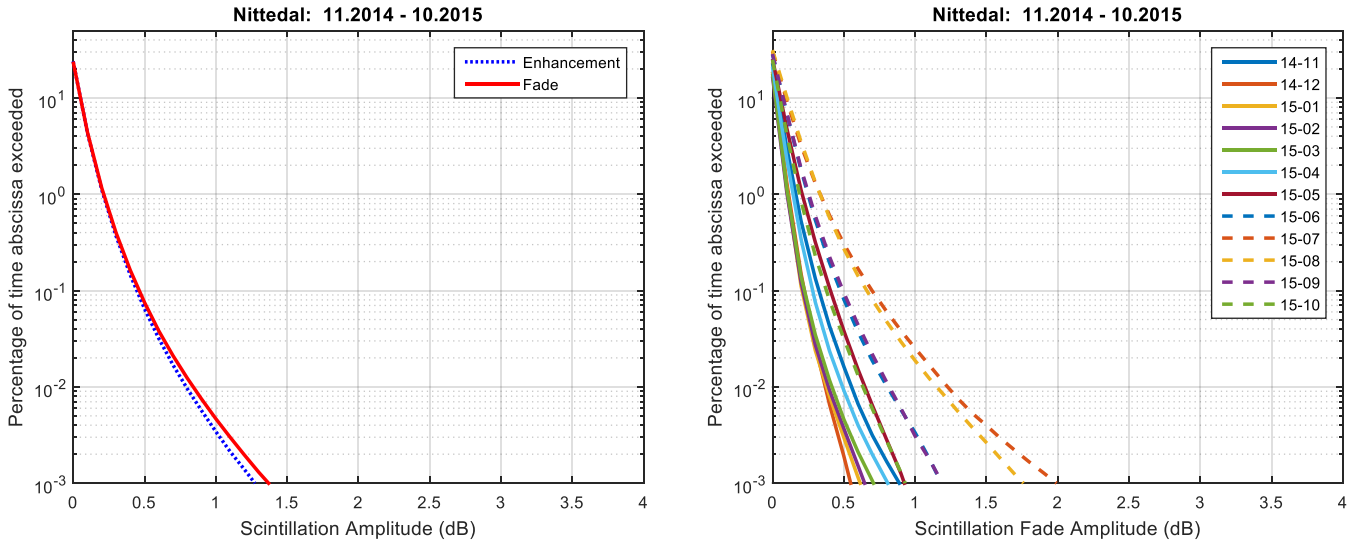

Figure 5-80. ***CCDF of scintillation amplitude for the period 11.2014 - 10.2015 and for each month with valid measurements during the period.***

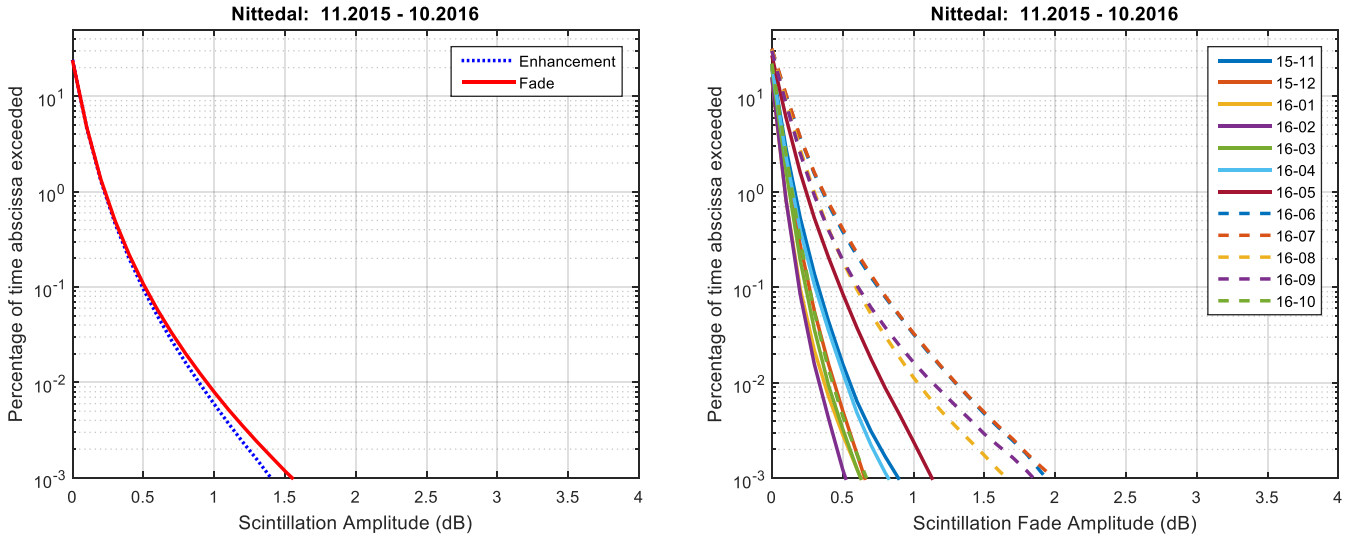

Figure 5-81. ***CCDF of scintillation amplitude for the period 11.2015 - 10.2016 and for each month with valid measurements during the period***

5.2.3.2 Scintillation amplitude Eggemoen

Eggemoen shows larger variations that Nittedal, most likely due to slightly drier climate during winter. The overall scintillation is slightly lower, partly due to larger antenna aperture.

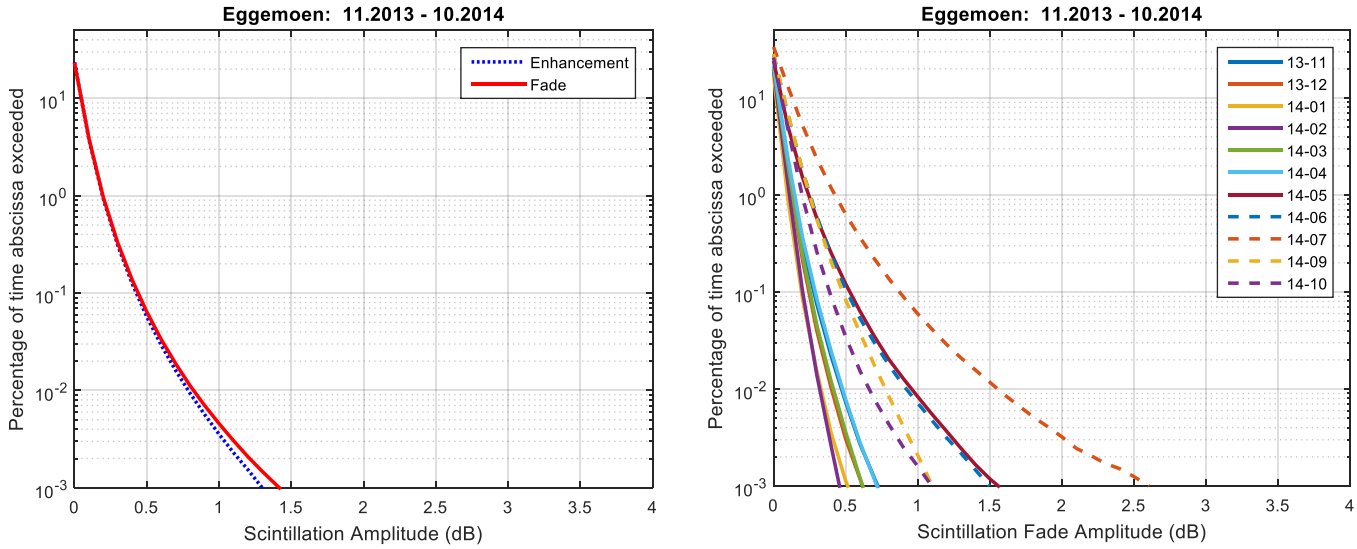

Figure 5-82. ***CCDF of scintillation amplitude for the period 11.2013 - 10.2014 and for each month with valid measurements during the period.***

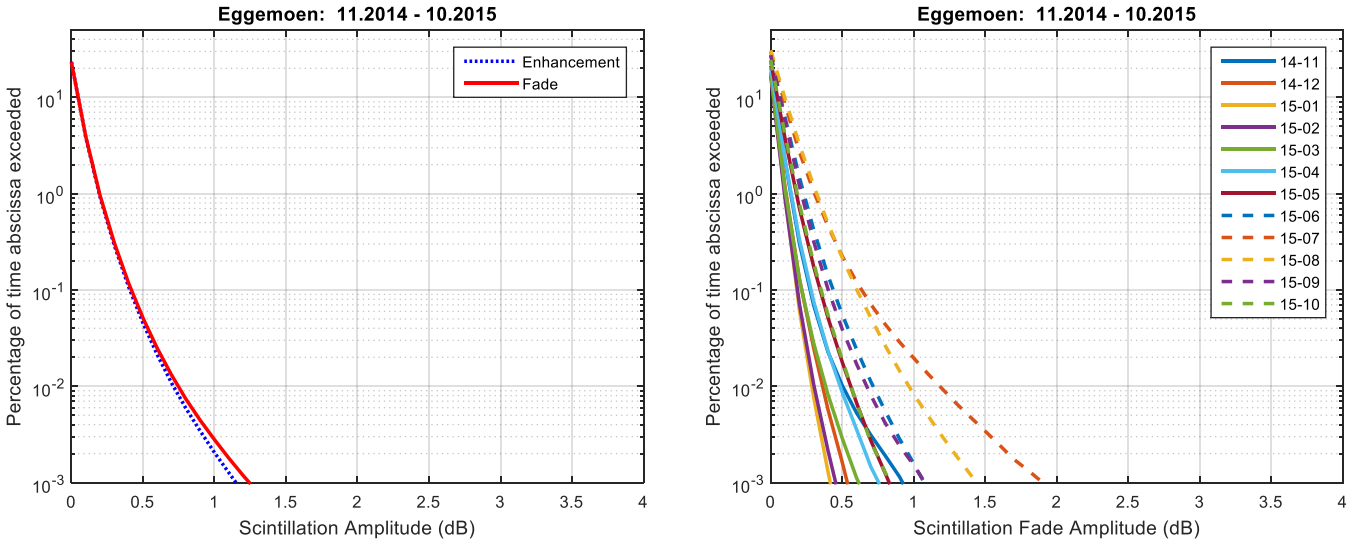

Figure 5-83. ***CCDF of scintillation amplitude for the period 11.2014 - 10.2015 and for each month with valid measurements during the period.***

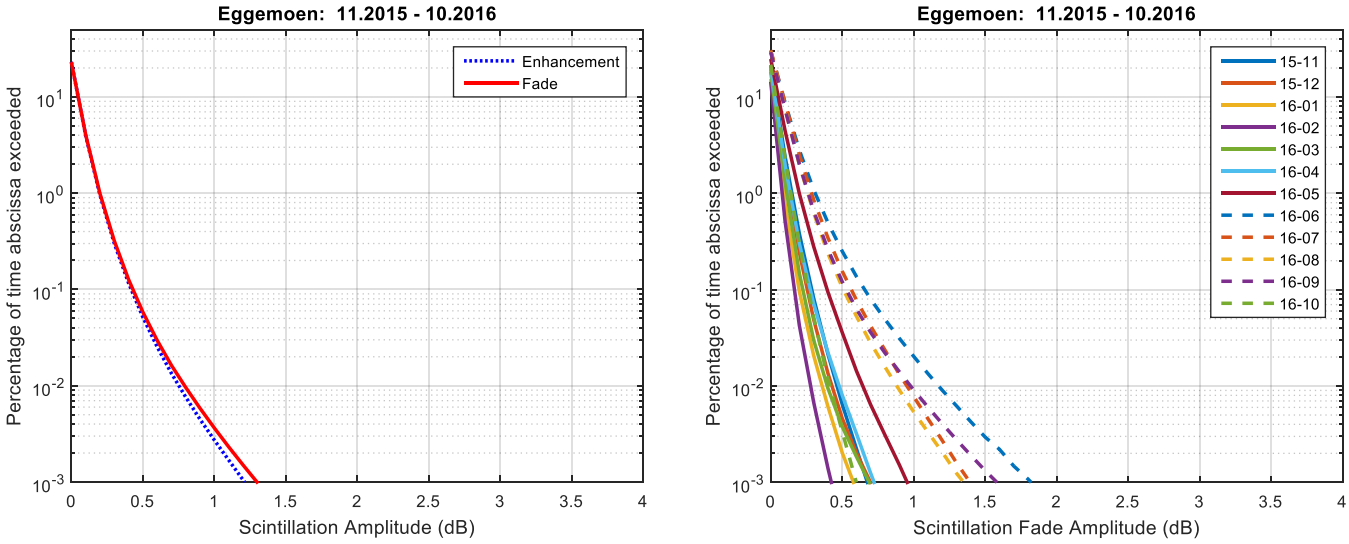

Figure 5-84. ***CCDF of scintillation amplitude for the period 11.2015 - 10.2016 and for each month with valid measurements during the period.***

5.2.3.3 Scintillation amplitude Røst

At Røst the difference between summer and winter scintillation is much lower due to the stable ocean climate. Overall amplitude is also quite low, especially taking into account the longer path through the atmosphere.

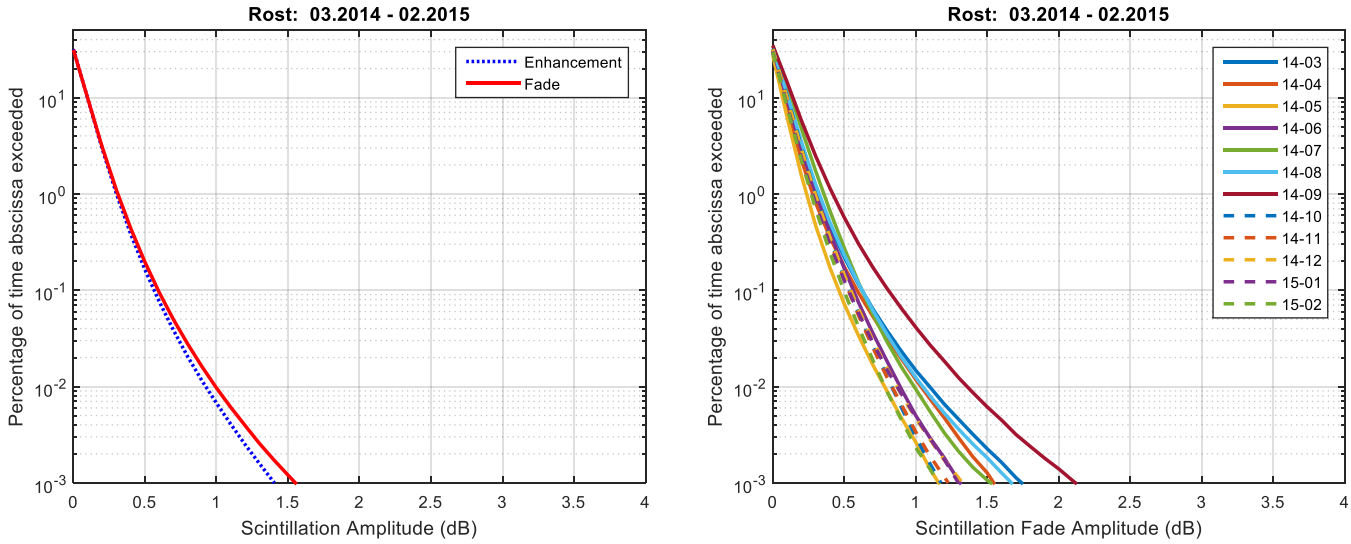

Figure 5-85. ***CCDF of scintillation amplitude for the period 03.2014 - 02.2015 and for each month with valid measurements during the period.***

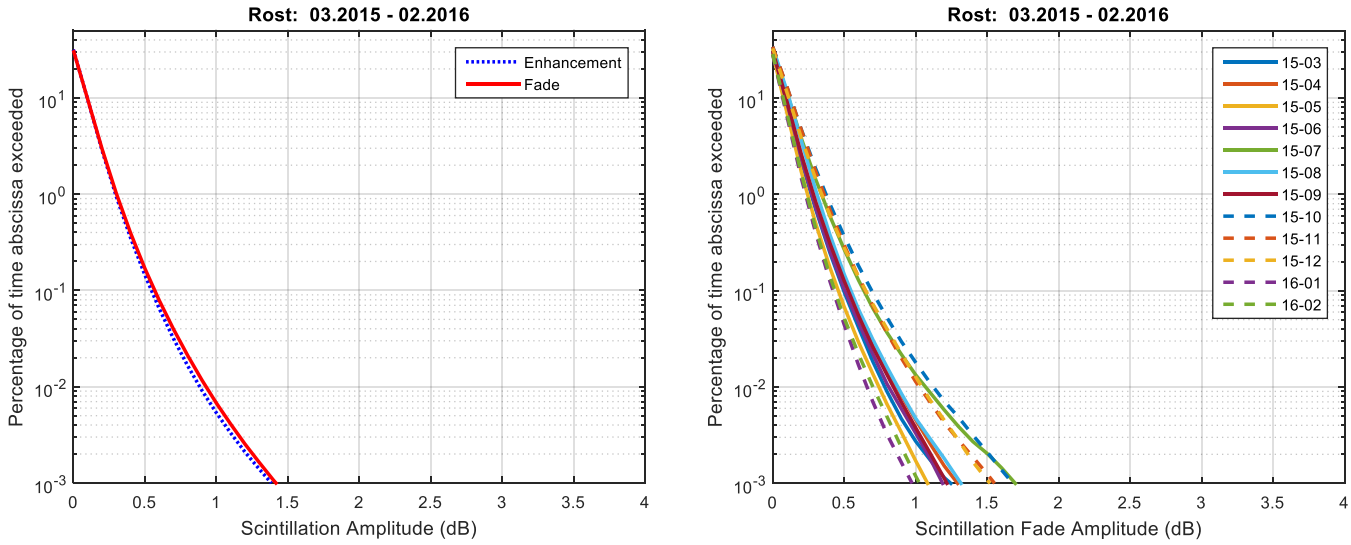

Figure 5-86. ***CCDF of scintillation amplitude for the period 03.2015 - 10.2016 and for each month with valid measurements during the period.***

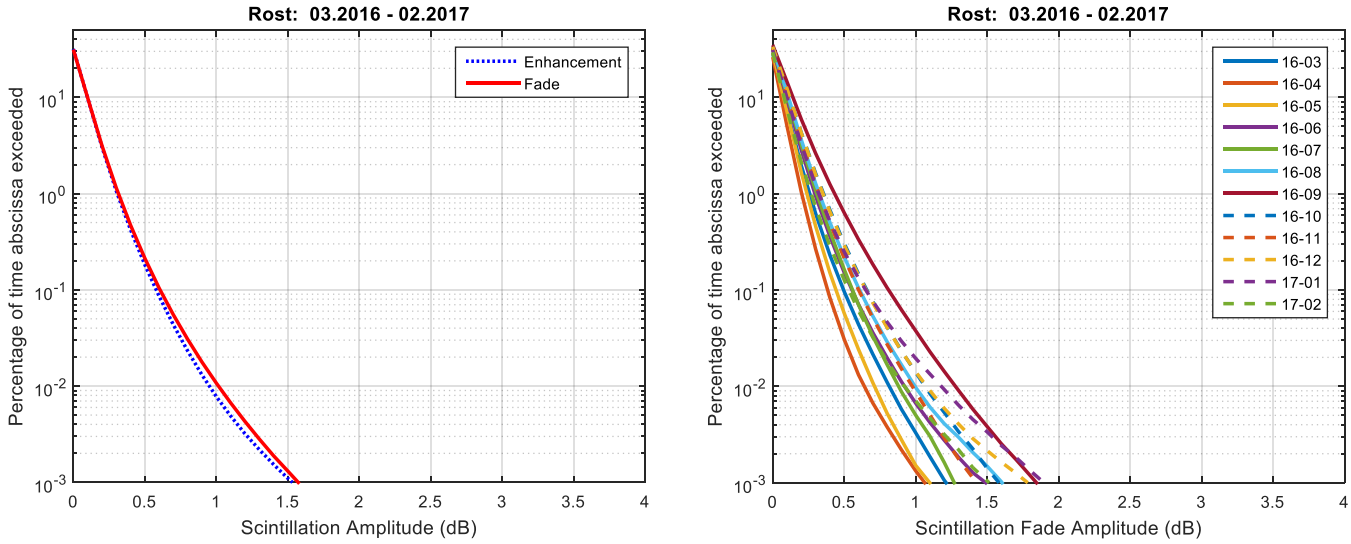

Figure 5-87. ***CCDF of scintillation amplitude for the period 03.2016 - 02.2017 and for each month with valid measurements during the period.***

5.2.3.4 Scintillation amplitude Vadsø

Vadsø combines lower elevation with land-heating related effects and large changes in temperature through the year resulting in big differences between summer and winter scintillation levels as well as high levels overall.

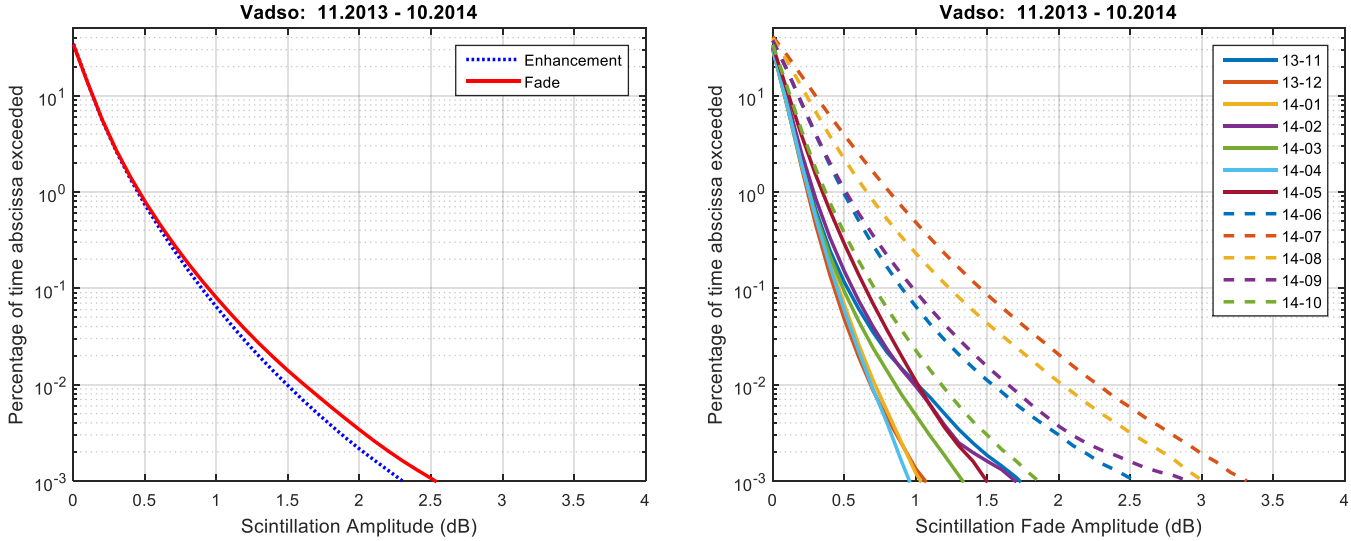

Figure 5-88. ***CCDF of scintillation amplitude for the period 11.2013 - 10.2014 and for each month with valid measurements during the period.***

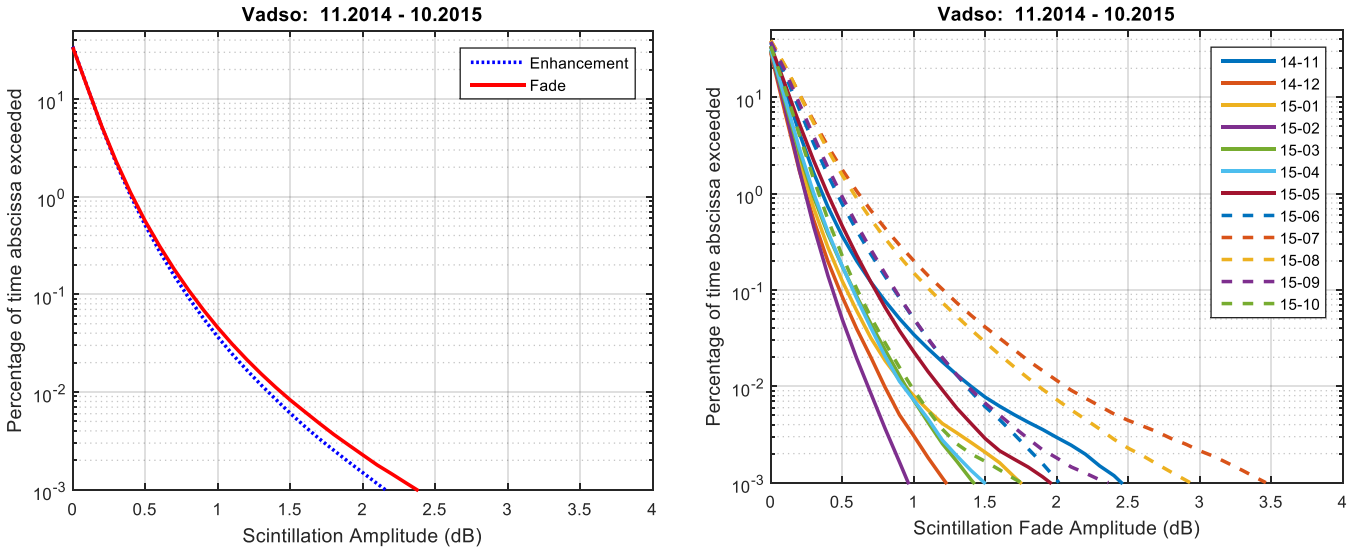

Figure 5-89. ***CCDF of scintillation amplitude for the period 11.2014 - 10.2015 and for each month with valid measurements during the period.***

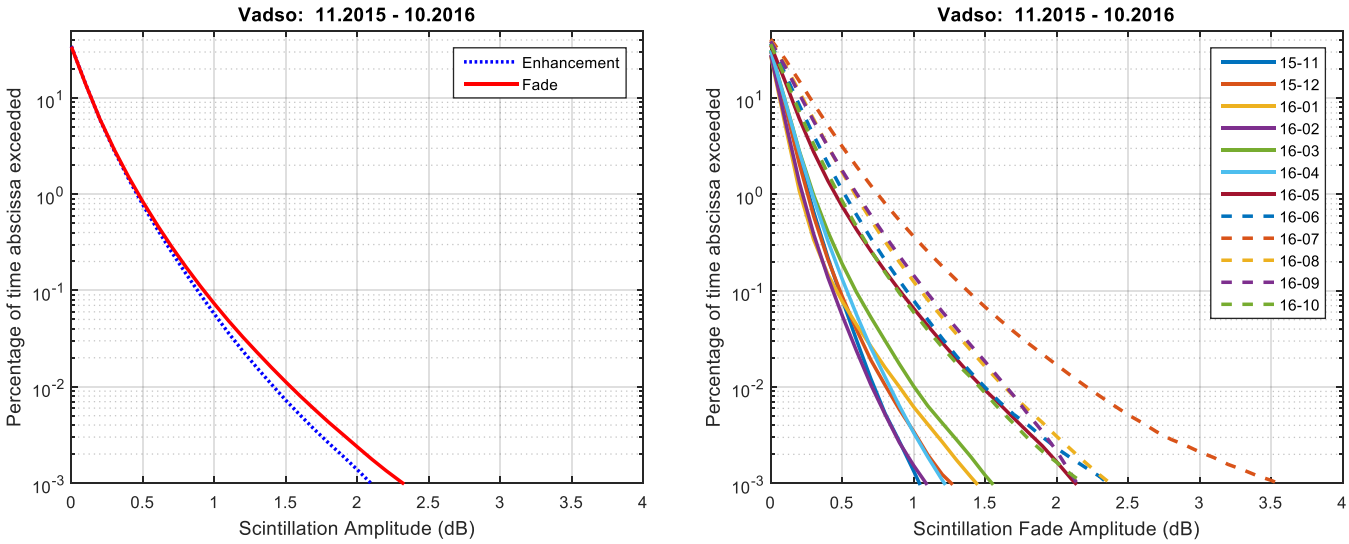

Figure 5-101. ***CCDF of scintillation amplitude for the period 11.2015 - 10.2016 and for each month with valid measurements during the period.***

5.2.3.5 Scintillation amplitude Isfjord Radio

Severe scintillation and Multipath were recorded at Isfjord Radio with very large levels recorded during July-August. The amplitude distribution is highly skewed towards the negative values.

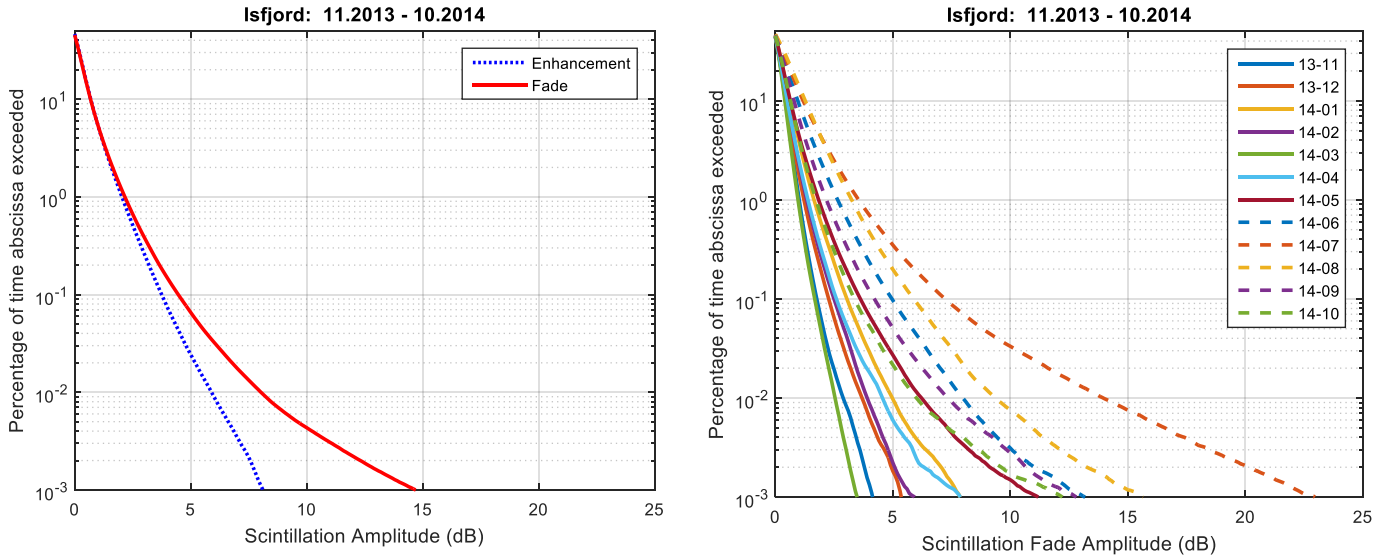

Figure 5-90. ***CCDF of scintillation amplitude for the period 11.2013 - 10.2014 and for each month with valid measurements during the period.***

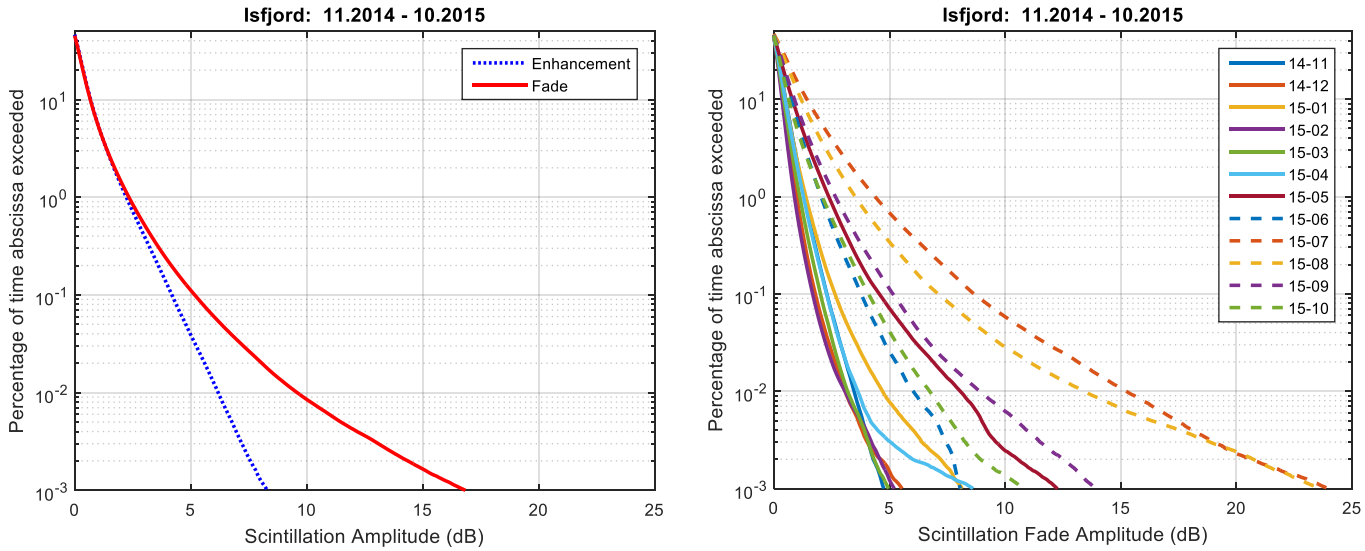

Figure 5-103. ***CCDF of scintillation amplitude for the period 11.2014 - 10.2015 and for each month with valid measurements during the period.***

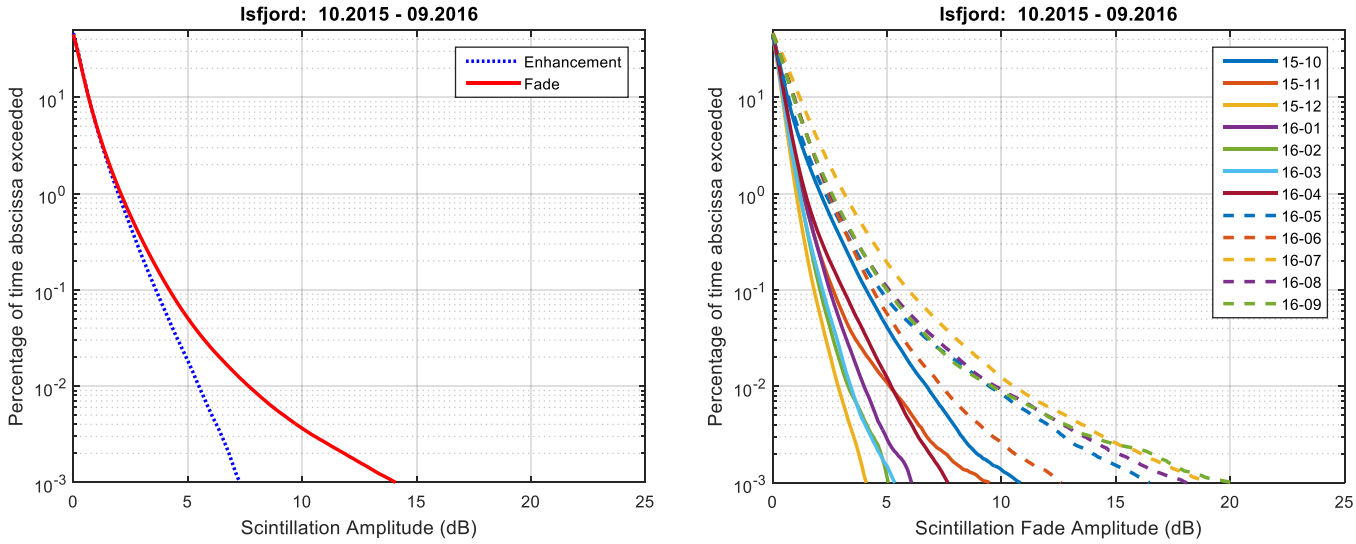

Figure 5-91. ***CCDF of scintillation amplitude for the period 10.2015 - 09.2016 and for each month with valid measurements during the period.***

5.2.3.6 Scintillation amplitude Bjørnøya

The one year of measurement at Bjørnøya revealed higher scintillation levels than at Vadsø, but still significantly lower than at Isfjord Radio. Since the link crosses the majority of the island mass some land-induced monthly variations are visible, but not as large as in Vadsø.

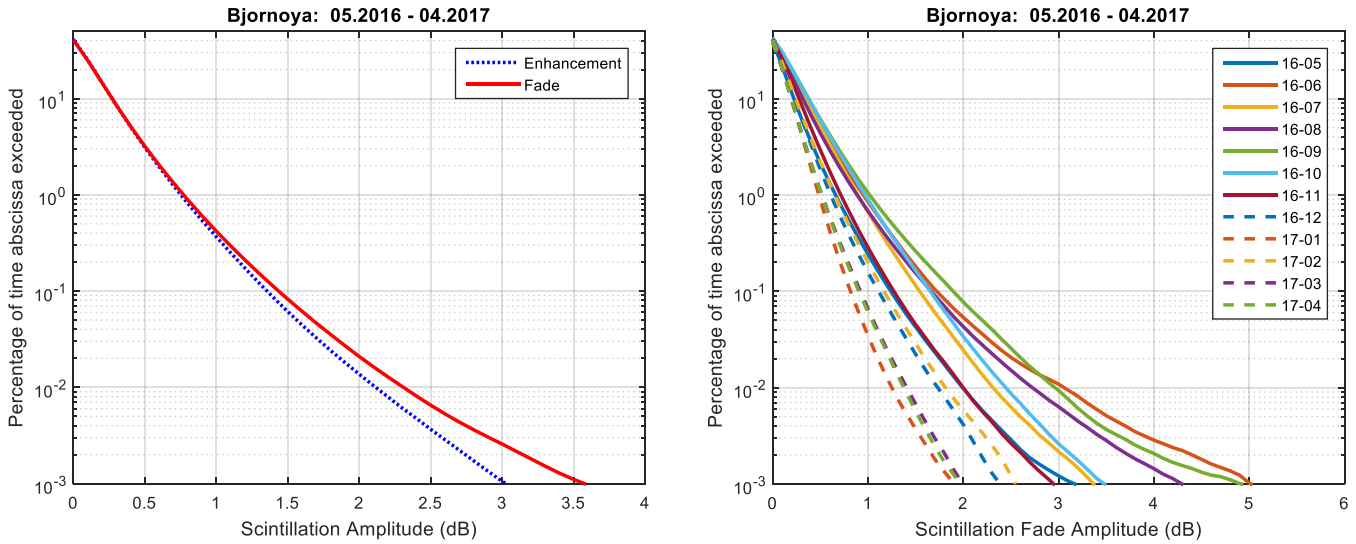

Figure 5-92. ***CCDF of scintillation amplitude for the period 05.2016 - 04.2017 and for each month with valid measurements during the period.***

5.2.3.7 Scintillation for all stations over 3 years

Plot combining all stations clearly shows how much higher the scintillation levels at Isfjord Radio are compared with others. Bjønøya and Vadsø also have slightly increased scintillation levels, though nowhere near Isfjord. Perhaps surprisingly, scintillation at Røst is actually comparable with the two southern stations despite the much lower elevation angle, as explained previously this is quite likely due to the stable and mild oceanic climate. The slightly lower scintillation levels measured at Eggemoen are due to a combination of dryer climate and larger antenna aperture.

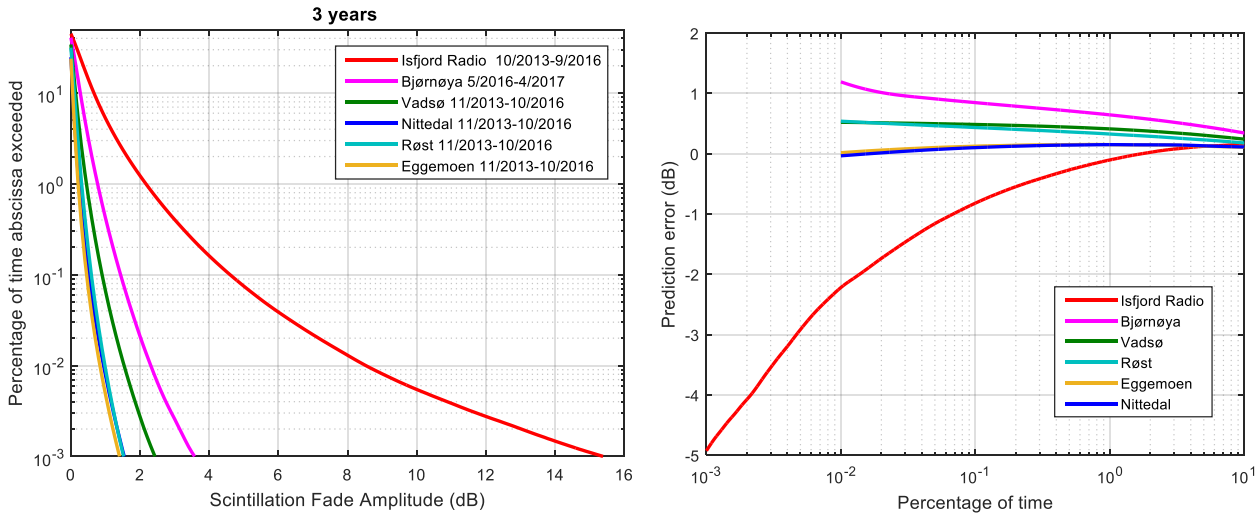

Figure 5-93. ***CCDF of scintillation all stations for 3 years (Bjørnøya 1 year) on the left and errors compared with ITU-R Rec. P.614-12 model predictions using local weather data.***

6 Telecom experiment

The telecom experiment was executed from 02.07.2015 to 02.01.2016 in Vadsø.

6.1 Experiment set-up

The telecom experiment was set-up in Vadsø and the installation was co-located at the same site as the propagation terminal. The main concept with the telecom experiment was to have a satellite terminal connected on two-way link on Ka-band, analyse propagation effects on a broadband spectrum and monitor impact on modem performance. Figure 6-1 shows the Ka-band coverage of Thor 7, Telenor Satellite's high throughput satellite located in $1^{o}W$ orbital location. The aggregated wide-coverage shown in the figure consists of multiple spot beams, where one of the beams in particular is covering Vadsø.

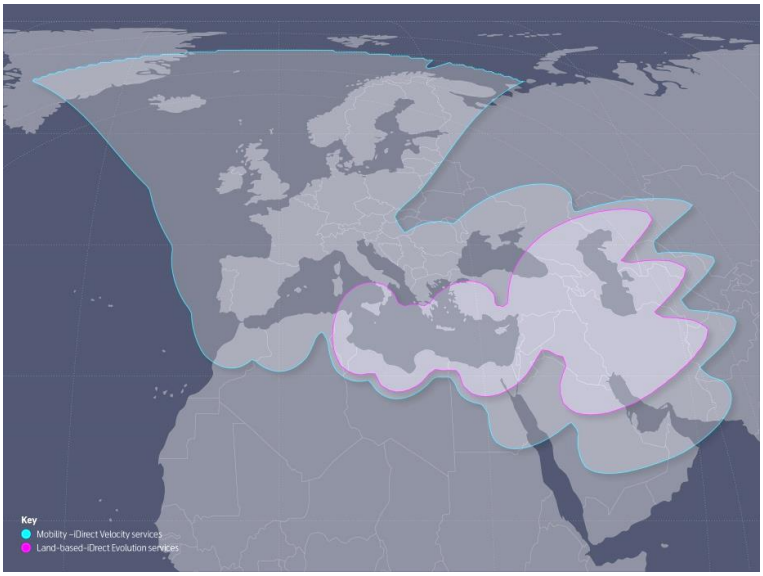

Figure 6-1. Thor 7 Ka-band coverage.

The iDirect Velocity platform is a shared access platform using a TDM carrier on the forward (outbound) link and multi-frequency TDMA on the return link (inbound). Forward link is DVB-S2, while return link format is proprietary iDirect.

Every spot beam on Thor 7 has minimum one outbound carrier to handle the forward traffic, and a set of inbound carriers to handle the return traffic optimum depending on terminal traffic profile, location and antenna size. Telenor Satellite is targeting typically two antenna sizes for the maritime services, ca 1m. and 0.6m reflectors.

The forward link utilises ACM with MODCODs ranging from QPSK ¼ to 16APSK 8/9, while the return link is operated in an adaptive TMDA, where the terminal is moved around on different frequency slot to use the optimum carrier size and modulation scheme for the current conditions. The return link modulation schemes are QPSK and 8PSK, and the FEC rates vary from ½ to 6/7.

Thor 7 has one GW beam covering partly Scandinavia with beam centre right North of Oslo. The network topology on Thor 7 is a star and all traffic in all spots is anchored in the GW, located at Nittedal.
The telecom set-up had two parallel measurements going:

1. Continuous logging of the broadband spectrum on Ka-band downlink (45 Msps over 54 MHz)
2. An on-line Ka-band terminal providing access to physical layer statistics from the iDirect Velocity VSAT HUB.

The overall idea was to monitor the broadband spectrum and identify the impact of frequency selective propagation effects e.g., multipath over low elevation angles over sea. And if such events were present, the modem data could be used to address the impact of multipath on a communication link. Modem statistics like estimated C/N, physical layer CRC and operating MODCOD could have been used to verify the impact of such propagation effects.

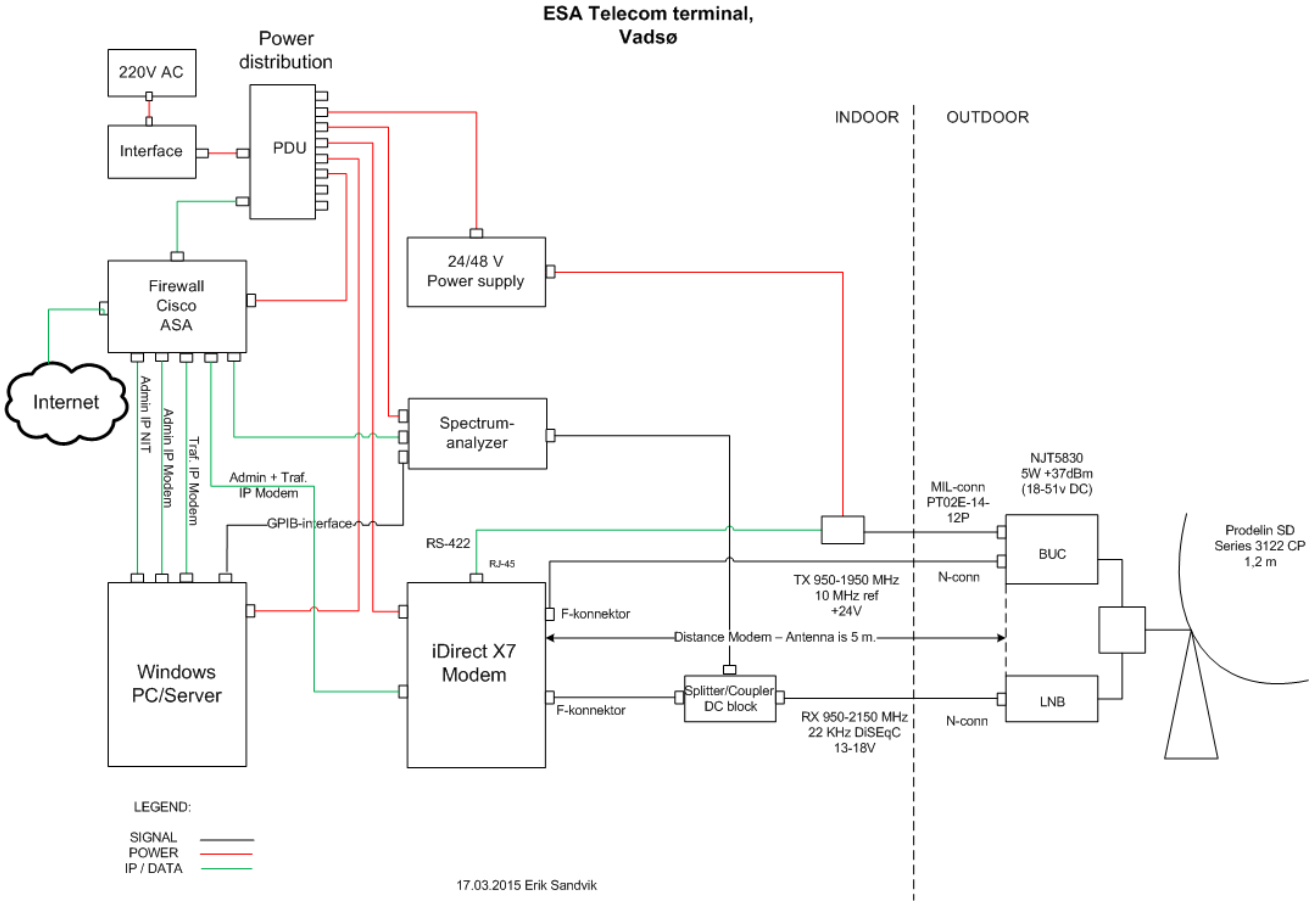

Figure 6-2. Block schematic of telecom terminal set-up.

Figure 6-2 of the telecom terminal. The fixed terminal installation was provided by iDirect as a package and consisted of X7 modem, BUC and LNB assembly and antenna dish. Modem was powering the LNB, while the BUC was powered from an external power supply. There was installed a server at site to store measured data and to provide console access to the modem. A local internet access point was needed for remote control and monitoring of the equipment.

The continuous broad band carrier received from the Thor 7 satellite was split after the LNB on the intermediate frequency, one path going to the receive port on the modem for downlink path, while the other path was going to the spectrum analyser for spectrum tracing. A Matlab application was running on the Spectrum Analyser where the received signal level was measured at 131 frequencies between 1.45 GHz and 1.5145 GHz. The telecom signal was a modulated carrier at 45 Msps with 1.2 roll-off factor resulting in a total bandwidth of 54 MHz.

Figure 6-3and Figure 6-4 show the installation in Vadsø, in-door and out-door, respectively.

Figure 6-3. Telecom – in-door installation.

Figure 6-4. Telecom – out-door installation.

During the period of the telecom experiment in this campaign, the Velocity platform on Thor 7 was still in beta test phase. The commercial service on Thor 7 was kicked-off May 2016.

6.2 Experiment data analyses

6.2.1 Measurements

Telecom measurements of Thor 7 Ka-band signals started at Vadsø 2 June 2015. This section contains examples of identified events affecting the spectrum occurring during the subsequent six months.

The Ka-band signal from Thor 7 has a signal bandwidth of 45 MHz with roll-off factor 0.2. The signal level is measured at intermediate frequency (IF) in the ground receiver. The signal level is measured at 131 frequencies between 1.45 GHz and 1.5145 GHz. The spacing between the frequencies is 496.18 kHz, and the total measured bandwidth is 64.5 MHz. As the telecom signal bandwidth is considerably smaller than the overall measured bandwidth, the measured spectrum is divided into an in-band spectrum and out-of-band spectrum, as illustrated in Figure 6-5. In-band spectrum is defined as the 44 MHz in the middle of the spectrum, and the out-of-band spectrum is the 4.5 MHz bands on each edge of the measured spectrum.

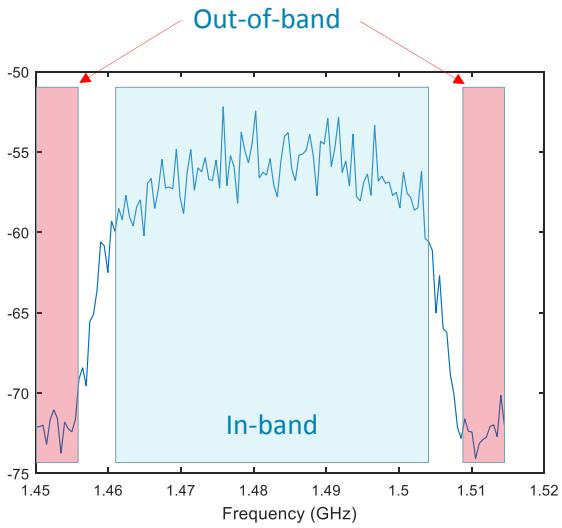

Figure 6-5. Shape of spectrum.

The spectrum is measured at a sampling frequency of 8 Hz. Figure 6-6 shows a 30-minute snapshot of how the measured spectrum looks like under normal conditions.

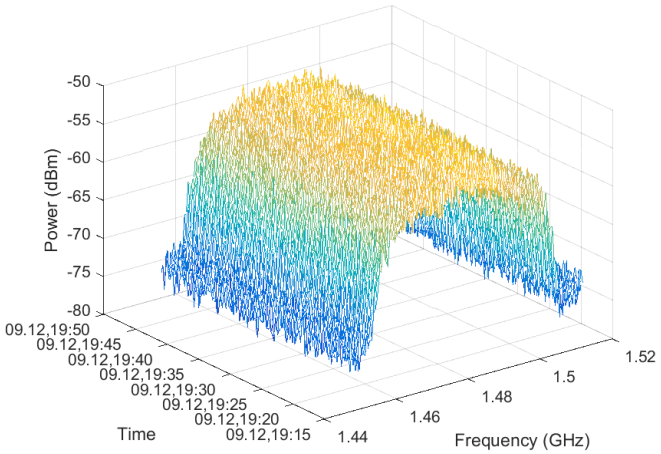

Figure 6-6. Mesh plot of 30 minutes of measurements.

6.2.2 Pre-processing of the data

For a measurement period of several months, the amount of data becomes significant. In order to be able to assess the data in an efficient and convenient way, some preliminary processing is done to visualise the quality and characteristics of the data in form of day plots containing three subplots:

- Subplot 1: The mean power of the in-band spectrum and the out-of-band power are calculated. This subplot shows any malfunction of the equipment causing no signal reception or increased out-of-band noise. In addition, signal attenuation over the entire signal bandwidth caused by precipitation becomes very apparent.
- Subplot 2: The in-band spectrum is divided into 10 bins, and the mean signal power within each bin is calculated. The difference in level in dB between the first bin and the last bin give information about the tilt of the spectrum. If the tilt varies or is far from zero, it may be an indication of frequency selective fading.
- Subplot 3: The difference in signal power in dB between the edge bins and the one bin among the eight remaining bins with lowest power gives an estimate of the shape of the spectrum. Under normal conditions, the spectrum has a shape as a 'U' turned upside down so that the result is negative. If the result is positive, there is a dip somewhere within the signal bandwidth, indicating frequency selective

fading.

An example of a day plot is included in Figure 6-7. The first subplot shows the mean in-band signal power and the mean out-of-band noise power. The second sub-plot shows the tilt of the spectrum. The third sub-plot shows the shape of the spectrum. The three sub-plots also contain smoothed curves to better visualize the trends. The length of the smoothing filter is 100, corresponding to 12.5 seconds. This length is considered as a good trade-off between removing white noise and keeping the dynamics of the signal.

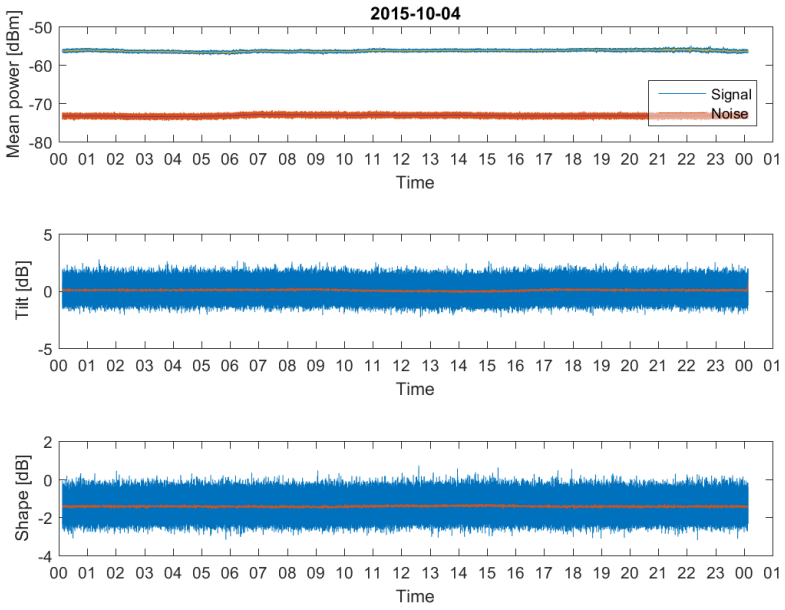

Figure 6-7. Example of a day plot showing signal and noise level, tilt of the spectrum, and the shape of the spectrum for one day.

Measurement period	2 July to 1 September 2015
Mean in-band received power	-57.0 dBm
Mean out-of-band received power	-72.3 dBm
Mean SNR	15.3 dBm
Percentage of invalid data	0.27%
Time without recorded data	0.2%

Table 6-1. Parameters from the spectrum measurements.

Table 6-1 includes the average signal and noise power during the first two months of measurements and the percentage of invalid data. Visual inspection of the day plots indicates however that the signal and noise levels are similar, and that the percentage of invalid data seems to be reduced.

6.2.3 Frequency flat fading

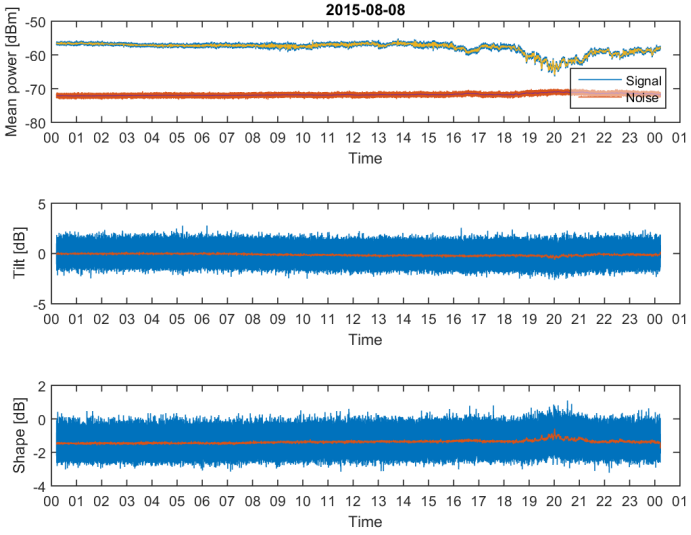

Figure 6-8. Day plot containing a rain event.

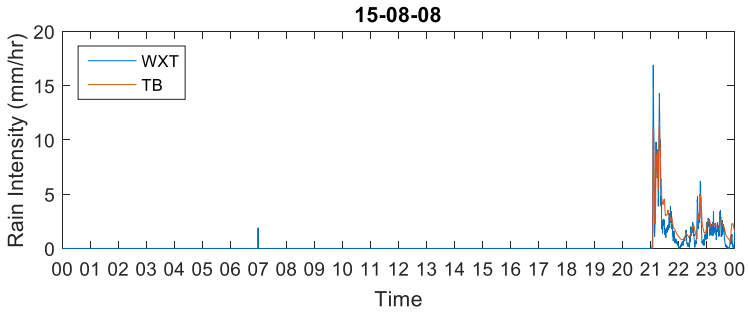

Figure 6-9. Rain measurements at Vadsø.

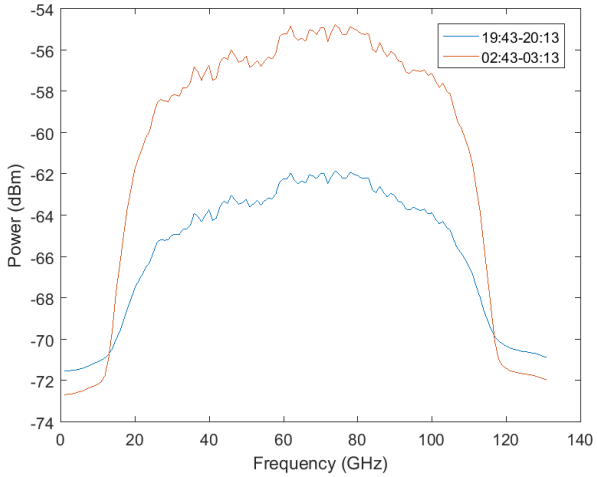

Figure 6-10. Mean spectrum over two 30-minute periods August 8 2015.

Figure 6-8 contains an example of the effect of heavy rain on the signal. The signal attenuations in the evening is about 8-10 dB. Registration of rain intensities higher than 10 mm/hr around 21h at Vadsø that particular day confirms that heavy rain caused the deep attenuation. The noise level increased slightly during the same time interval, the tilt remained approximately zero, while the shape of the spectrum was slightly modified.
Figure 6-10 illustrates how the attenuation is flat over the signal bandwidth and how the noise level is slightly increased.

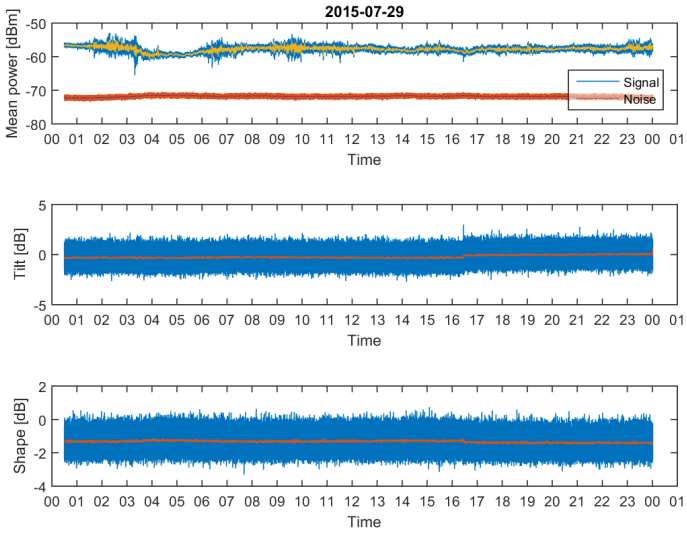

Figure 6-11. Example of rapid fluctuating signal level.

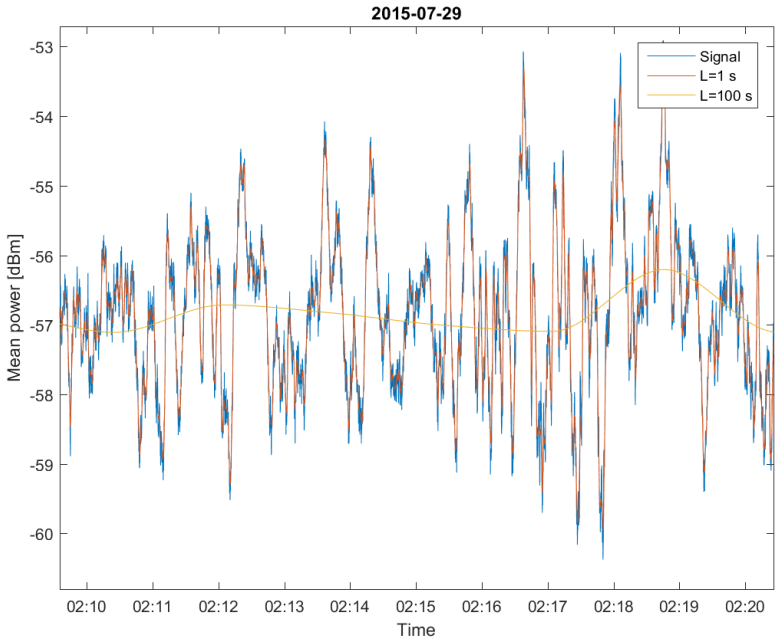

Figure 6-12. Snapshot of signal without smoothing filter, with filter length 1 second and with filter length 1 minute.

Rain attenuation varies slowly over minutes and hours as seen in Figure 6-8. There are also examples of incidents where the signal varies rapidly. Figure 6-11 shows one such example. Both the blue and the smoother yellow curve in the upper sub-plot experiences rapid fluctuations, while the average signal level is quite constant. Only insignificant rain intensities were measured during this day, so these variations must be due to other atmospheric conditions. Figure 6-12 shows the results when modifying the smoothing filter length to 8 samples and 800 samples, corresponding to filter lengths of 1 second and 100 seconds. The curves show that most of the fluctuations have frequencies between 0.01 Hz and 1 Hz.

6.2.4 Frequency selective fading

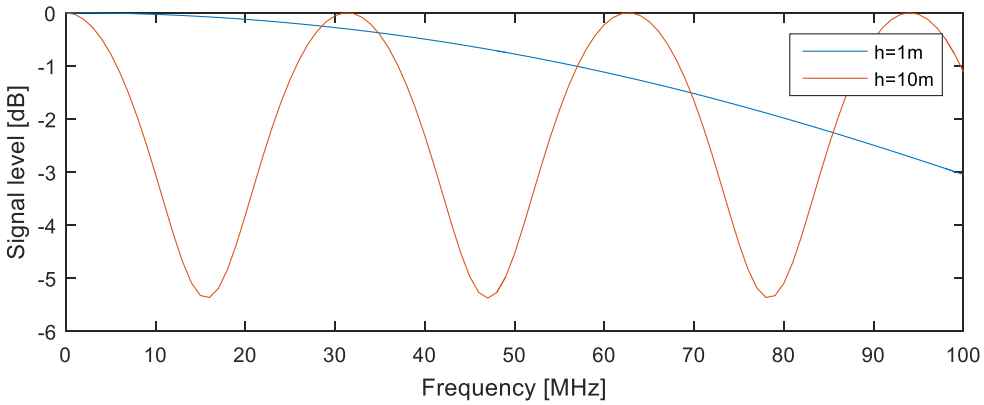

Figure 6-13. Channel spectrum of a 2-ray channel with reflection coefficient equal to 0.3 and two different delays between taps.

There was no clear indication of frequency selective propagation in the measurements. Below is a short justification of why this is as expected.

The telecom signal frequencies are between 19.7 and 20.2 GHz and the signal is continuous in time. The antenna has a diameter of 1.2 meter. A corresponding uniform antenna pattern is shown in Figure 6-14, with an elevation in the order of 8.4 degrees. The two-sided 3 dB polar angle width is $0.73°$.

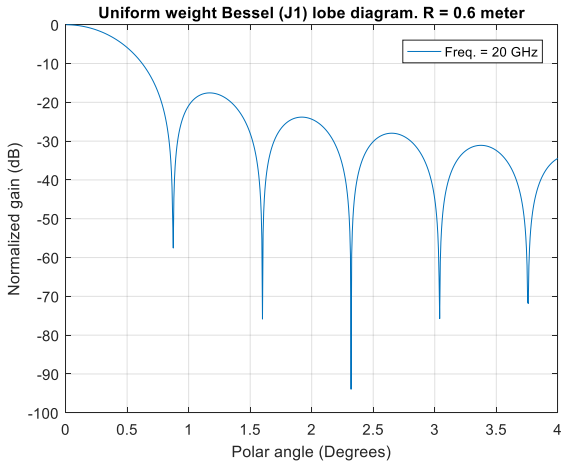

Figure 6-14. Antenna diagram with uniform weighting. Diameter =1.2 meter.

Frequency selective fading is generally due to multipath propagation. A potential source of frequency selectivity is a ground reflected signal component adding to the line-of-sight component. At Vadsø, the elevation angle towards Thor 7 is about 8.4°. The time difference between the line-of-sight component and the reflected component depends on the height of the antenna compared to the reflecting surface. Assuming a height between one and ten meters, this corresponds to a time difference between 3 ns and 30 ns. For a 20 GHz signal, that leads to the channel spectrum included in Figure 6-13. The curves indicate that there is a potential for frequency selectivity with a signal bandwidth of 45 MHz. One reason why there is no trace of frequency selectivity is the directive antenna. The beam width is considerably lower than 8.7° and any ground reflection component will be attenuated before entering the receiver chain. In addition, the antenna is located and mounted in a way that optimises the propagation conditions and hence minimises the multipath propagation adverse effects.

Effects of atmospheric turbulence on radio-wave propagation in the form of ducting and other atmospheric layers have been studied extensively in the literature for several decades. It might cause multipath propagation for Ka-band satellite communication for very low elevation angles. No conclusive results on the frequency selectivity, and on what coherence bandwidth that can be expected, is however found during the course of this

project. From terrestrial radio links, delay spreads of 6-12 ns over 50 km distance are reported. Translating this to a satellite link with 8.4° elevation angle and rain height 3 km, a delay spread of 3-5 ns could be expected. This would lead to a coherence bandwidth of 100-200 MHz, considerably wider than the signal bandwidth of the telecom measurements in this project.

6.2.5 Modem effects

Telenor Satellite has used the telecom experiment to optimise the return efficiency and return peak rate in the Thor 7 network by including the Vadsø site in a cluster of terminal locations in the total coverage. Understanding propagation effects for mobile terminals in a multi-spot beam satellite system is important. It is significant to understand in which areas of the coverage the transmission is limited by propagation effects and which are not. Even though propagation cannot be overlooked from a total system throughput perspective, it is more adequate to correctly estimate the throughput of the system in clear sky conditions. Based on input from the experiment the nominal forward and return spectral efficiencies were increased. The experiment was used to trade overall return spectral efficiency with terminal peak-rate, and an increase in terminal peak-rate (1m antenna) of up to 50 % was observed.

If the spectrum analysis had shown a non- negligible impact due to frequency selective fading, such degradation would have been a great challenge to quantify using a high-end satellite modem. The high-end DVB-S2 receivers used in both low cost VSAT and high-end SCPC equipment have advanced embedded processing to mitigate linear and non-linear channel distortions like compression, slope and group delay variations. These techniques would limit the impact of frequency selective propagation effects on broad traffic carrier.

6.3 Summary

The telecom measurements performed in Vadsø did not detect any clear incidents of multipath fading. This is as expected due to the elevation angle of 8.4° and the antenna directivity and geometry of the surroundings. Multipath propagation will most likely occur further north as the elevation angle decreases. The effects on the modem performance may however still be low due to signal processing algorithms in modern wideband receivers efficiently counteracting such channel degradations.

6.4 Further work

For future telecom experiments, the elevation angle should be reduced down to elevation angles of 3-5 degrees, on the edge of typically commercial GSO coverages.

To quantify the effects of multi-path fading on a high-end modem platform is very challenging. An alternative test is to define a user scenario, e.g., continues video streaming up and/or down, and detect which MODCODs and/or bandwidth profiles that give a reasonable QoS for the end-user in areas with low elevation angle.

7 Conclusion and recommendation

The project has successfully collected three years propagation data from five sites, one year from one site, and six months of telecom data from one site. All sites are located in Norway, with elevation angles ranging from 21.8° to 3.2°, where the four most Northern stations are all in maritime climates. With the new data of 19.7 GHz along with con-current and co-located meteorological data a highly valuable data bases have been assembled. Three year tabulated data of first and second order signal statistics have been submitted to the ITU-R. The telecom results were used to check possible spectrum degradation caused by propagation effects.

Rain attenuation is one major concern at this frequency and must be considered for any link budget evaluation. However, as the elevation angle reduced other effects becomes important such as scintillation. With the longer path through the atmosphere also atmospheric gases and clouds become more important, relatively more than the non-homogenous rainfall. Therefore, non-precipitation effects and combination of propagation effects become increasingly important with smaller elevation angles which also mean increase in latitude.

Measured rain attenuation distributions compare well with the ITU-R prediction model, given that local rain

rate data are used. However, for availability in the range of three nines (99.9) combination of effects play a major role where gaseous absorption, scintillation and cloud attenuation must be considered. At the most northern stations scintillation and ducting effects clearly dominates the deep fading range. At Bjørnøya, the station in between Vadsø and Isfjord Radio, the scintillation is not very strong, perhaps even less that what could be expected.

Another conclusion is that the link availability can be high at all sites, but the availability is reduced at the lowest elevation angle site, Isfjord radio, dominated by scintillation and perhaps multipath effects. At elevation angles below 5° the ITU-R recommendations provide unclear and in fact limited guidance. Therefore, the prediction methods for scintillation and multipath, gaseous absorption, and cloud attenuation need a revision to satisfactory cover these regions.

8 Future work

The project results suggest improving modelling of very low elevation angle propagation and also provide or refine prediction methods for links with elevation angles below 5°. Maritime, but coastal stations were used in the High North. It is still of interest to understand the influence of land at these sites, compared to what might be the case for a purely maritime station on a vessel. For example, the scintillation results observed from Isfjord Radio, at Bjørnøya, and then Røst, invites to further studies. What is the dependency on elevation angle and to what degree does the mixture of land and sea influence the results. The small scale to large scale phenomena covered in this project might offer results that can be further analysed to improve diversity schemes.

Acknowledgements

The project partners were Telenor Satellite (project manager), Norwegian Defence Research Establishment (FFI), Norwegian Defence Logistics Organisation (NDLO), University Graduate Centre – Kjeller (UNIK), with support from Gjøvik University College, and SINTEF ICT. The authors of the final report wish to acknowledge a lot of good contributions through various parts of the project from Josef Noll, Michael Ciecko, Terje Mjelde, Terje Medby, Jostein Sander, Vegard Arneson, Herman Hansen, and Trond Henning Johansen, and Bjørnar Dragsnes.

References

[1] Contract, Statement of Work, ARTES 5.1 Workplan 2011 3B.027, 5/12/2011
[2] J. Mamen and T. Tjelta, “New Norwegian hydrometeor precipitation rate maps derived from long term measurements,” Submitted to 7th European Conf. Ant. and Prop. (EuCap), Gothenburg, Sweden, 8-12 April 2013.
[3] ITU-R, Recommendation P.837-6, "Characteristics of precipitation for propagation modelling," International Telecommunication Union, Geneva, 2012.
[4] T. Tjelta, J. Sander, M. Rytir, P. A. Grotthing, J., Noll, K. Grythe, T. H. Johansen, M. Ciecko, M. Cheffena, T. M. Mjelde, “Experimental campaign with first results for determining high north 20 GHz satellite links propagation conditions,” In proceedings of 9th European Conference on Antennas and Propagation (EuCAP), Lisbon, Portugal, 13-17 April 2015.
[5] L. E. Bråten, J. Sander and T. Mjelde, “Satellite-Earth K-band Beacon Measurements at Kjeller, Norway; Measurement setup and initial results,” In proceedings of 7th European Conf. Ant. and Prop. (EuCAP), Gothenburg, Sweden, 8-12 April 2013.

Appendix A: Abbreviations

ACM	Adaptive coding and modulation
APSK	Amplitude PSK
AWGN	Additive white Gaussian noise
BUC	Block up-converter
C/N	Carrier over noise
CCDF	Complementary CDF
CDF	Cumulative distribution function
CRC	Cyclic redundancy check
CW	Carrier wave
DC	Direct current
DDR	Double data rate
EIRP	Effective isotopically radiated power
FEC	Forward error coding
FFT	Fast Fourier transform
HPBW	Half power bandwidth
LNB	Low noise block converter
MODCOD	Modulation and code
MUX	Multiplex
OCXO	Oven stabilised crystal oscillators
OMT	Orthomode transducer
PDF	Probability density function
PLL	Phase locked loop
PSK	Phase shift keying
RAID	Redundant array of independent disks
RAM	Random access memory
RF	Radio frequency
RMS	Root mean square
SNR	Signal to noise ratio
TDM	Time division multiplex
TDMA	TDM access
UPS	Uninterruptible power supply